

**THE USE OF HIGH FIELD STRENGTH
MAGNETIC RESONANCE IMAGING IN
PROSTATE CANCER STAGING AND
LOCALISATION**

A thesis submitted to the
University of Hull for the degree

Doctor of Medicine

By

Bachar Zelhof

MRCS

May 2012

Table of contents

1. Introduction	1
1.1. Incidence	1
1.1.1. Trends in prostate cancer incidence	4
1.1.2. Geographic variation in prostate cancer incidence	6
1.2. Mortality	7
1.3. Natural history of prostate cancer	9
1.4. Prostate Specific Antigen.....	11
1.4.1. Introduction of PSA.....	11
1.4.2. PSA modalities	12
1.4.3. PSA screening	14
1.4.4. Trans rectal Ultrasound biopsy	16
1.5. Anatomy of the prostate.....	16
1.5.1. Prostate arterial supply and venous drainage.....	20
1.5.2. Prostatic innervation:	21
1.6. Prostate histology:	21
1.7. Physiology of prostate:	22
1.8. Pathology of Prostate Cancer.....	22
1.8.1. Prostatic Intraepithelial Neoplasia (PIN)	23
1.8.2. Atypical and suspicious small acinar proliferations (ASAP)	25
1.8.3. Grading system:.....	26
1.8.4. Staging of prostate cancer:	28
1.9. Radical prostatectomy	31
1.9.1. Preoperative clinical staging and prediction.....	31
1.9.2. Anatomic open radical retropubic prostatectomy (nerve sparing procedure)	35
1.9.3. Rationale for radical prostatectomy	38
1.9.4. Complications of radical prostatectomy:	42
1.9.5. Radical prostatectomy with positive surgical margins:	43

1.10.	Pathology reporting of radical prostatectomy specimens.....	45
2.	Imaging of prostate cancer	47
2.2.	Trans-rectal ultrasound scanning (TRUS)	47
2.3.	Computer Tomography (CT).....	48
2.4.	Positron emission tomography (PET)	48
2.5.	Evolution of Magnetic Resonance Imaging (MRI):.....	49
2.6.	Basic MR Principles.....	53
2.6.1.	MRI components:.....	53
2.6.2.	Basic physics:	55
2.6.3.	T1, T2, TR and TE	58
2.6.4.	Contrast agents and dynamic contrast enhanced MRI (DCE-MRI)	65
2.6.5.	Diffusion weighted imaging:	72
3.	The clinical accuracy of multi-sequence MRI at 3 tesla in localising and staging prostate cancer	77
3.1.	Objective.....	77
3.2.	Methods.....	77
3.2.1.	Patients selection.....	77
3.2.2.	Patients preparation.....	78
3.2.3.	MR examination.....	81
3.2.4.	MR image evaluation	83
3.2.5.	Histologic evaluation	86
3.2.6.	Statistical analysis	90
3.3.	Results.....	91
3.3.1.	Patients demographic data	91
3.3.2.	Localisation data.....	92
3.3.3.	Staging data.....	103
3.4.	Discussion	110

3.5. Conclusion:.....	118
4. Correlation of apparent diffusion coefficient with cell density in prostate cancer	120
4.1. Objective.....	120
4.2. Methods.....	121
4.3. Results.....	125
4.4. Discussion	132
4.5. Conclusion.....	137
5. Description of MR derived enhancement parameters in pathologically confirmed prostate cancer and normal peripheral zone regions	139
5.1. Objective.....	139
5.2. Methods.....	140
5.2.1. Patients.....	140
5.2.2. Image Acquisition	141
5.2.3. Histological study	142
5.2.4. Histology and DCE-MRI correlation	142
5.2.5. Data analysis	143
5.3. Results.....	148
5.4. Discussion	153
5.5. Conclusion:.....	158
6. The potential role of 3 tesla MRI in patients with rising PSA but negative prostatic biopsies	160
6.1. Introduction.....	160

6.2.	Methods.....	161
6.2.1.	Patients recruitment.....	161
6.2.2.	MR examination.....	162
6.2.3.	TRUS biopsy.....	163
6.3.	Results.....	167
6.4.	Discussion	168
6.5.	Conclusion.....	172

7. Visualisation of prostate cancer foci and prostate capsule using endorectal coil compared to pelvic-phased array coil at 3 tesla MRI 174

7.1.	Introduction.....	174
7.2.	Methods.....	175
7.2.1.	Patient characteristics.....	175
7.2.2.	MR technique.....	176
7.2.3.	MR image evaluation	177
7.2.4.	Statistical analysis	178
7.3.	Results:.....	179
7.4.	Discussion:	186
7.5.	Conclusion:.....	190

8. Future applications of prostate MRI 192

8.1.	Predicting tumour aggressiveness and relation to Gleason score. 192	
8.1.1.	Correlation between Gleason score and ADC values	193
8.1.2.	Assessment of cancer aggressiveness using spectroscopic prostate MR Imaging.....	194
8.1.3.	Assessment of cancer aggressiveness using DCE-MR Imaging 195	
8.2.	The role of prostate MRI in treatment selection for organ confined prostate cancer.....	196

8.3. MRI guided prostate biopsy	198
8.4. Summary	201
9. References	204

Index of tables

Table 1. Outlines normal age-specific PSA (data from Cancer Research UK)	12
Table 2. PPV of PSA for cancer detection in patients with positive findings on DRE. The higher the PSA, the more likely that its elevation is due to cancer. (European Association of Urology Guidelines, 2011).....	32
Table 3. Prostate cancer risk stratification (from D’Amico et al [70]).....	34
Table 4. List of foremost studies looking at outcome following radical prostatectomy	39
Table 5. Complications of radical prostatectomy (European Association of Urology guidelines, 2007)	42
Table 6. Detection of extracapsular tumour extension on T2 weighted imaging at 1.5T (Rouvier et al).....	52
Table 7. Pre-operative TRUS prostate biopsy results. The majority of cases that were suitable for RP were Gleason Grade 6 or 7.	91
Table 8. Mapping tumour presence on pathology slides showed that the peripheral zone is most commonly affected by cancer compared to central gland, base and apex.....	92
Table 9. The number of cases, for each anatomical region, with T2 weighted features suspicious of cancer presence.....	93
Table 10. Represents the number of cases for each anatomical region that showed high signal intensity following administration of contrast for readers 1 and 2.....	94
Table 11. The number of normal and suspicious cases at the apex for both readers identified on T2 weighted imaging.	95
Table 12. The number of normal and suspicious cases at the base for both readers identified on T2 weighted imaging.	95
Table 13. The number of normal and suspicious cases at the anterior middle region (central gland) for both readers identified on T2 weighted imaging.	95
Table 14. The number of normal and suspicious cases at the posterior middle region (peripheral zone) for both readers identified on T2 weighted imaging.	96
Table 15. The number of normal and suspicious cases at the apex for both readers identified on DCE-MRI.....	96
Table 16. The number of normal and suspicious cases at the base for both readers identified on DCE-MRI.....	97
Table 17. The number of normal and suspicious cases at the central gland for both readers identified on DCE-MRI.....	97
Table 18. The number of normal and suspicious cases at the peripheral zones for both readers identified on DCE-MRI.	97
Table 19. Sensitivity, specificity, positive predictive value, negative predictive value, and accuracy of tumour localisation on T2 weighted imaging. Results from reader 1 / reader 2 are provided for each parameter.	100
Table 20. Sensitivity, specificity, positive predictive value, negative predictive value and accuracy for tumour localisation by DCE-MRI. Results from reader 1 / reader 2 provided for each parameter.	101
Table 21. Sensitivity, specificity, positive predictive value, negative predictive value and accuracy for tumour localisation in the whole	

gland. Results from reader 1 / reader 2 detailed. An improvement in all parameters was noted for DCE-MRI compared to T2 weighted imaging.	102
Table 22. Staging descriptive analysis for detection of ECE from T2 weighted imaging for reader 1 / reader 2, using a pelvic phased array coil. Sensitivity, specificity, positive predictive value, negative predictive value, and accuracy for two cutoff points. 95% confidence intervals shown in parenthesis.	108
Table 23. Staging descriptive analysis for detection of ECE from T2 weighted imaging for reader 1 over reader 2 using an endorectal coil. Sensitivity, specificity, positive predictive value, negative predictive value, and accuracy shown for two cutoff points. 95% confidence intervals in parenthesis.	108
Table 24. Sensitivity, specificity, positive and negative predictive values for prediction of ECE according to the D'Amico risk classification.	112
Table 25. The mean values for tumour and PZ ADC and CD are shown. Tumour regions have lower ADC and higher cell density.	126
Table 26. Mean \pm standard deviation values for all DCE parameters for cancer lesions and normal PZ. Statistically significant p value when tested utilizing paired T-test.	148
Table 27. AUC values for all enhancement parameters with the resulted sensitivity, specificity, positive predictive value (PPV), negative predictive value (NPV) and accuracy for tumour identification based on the pre-determined cut-off values. 95% confidence intervals are shown in parenthesis. (<i>MaxEI: maximum enhancement index (arbitrary unit); TMax: time to maximum enhancement (in minutes); EI: enhancement index (arbitrary unit); Initial and final slopes (arbitrary unit); nAUC :normalised area under SI-time curve (arbitrary unit)</i>)	150
Table 28. Logistic regression analysis results including all enhancement parameters (2 nd row) and after excluding the non-significant parameters (3 rd row). 95% confidence intervals are shown in parenthesis.	151
Table 29. By selecting cases with type 2 SI time curves only, the mean \pm standard deviation values for all DCE parameters in cancer lesions and normal PZ remains statistically significant. A paired T-test was used to evaluate differences.....	152
Table 30. This shows the site of suspicious lesion on MRI, if cancer was detected in this biopsy round, its site and pathological findings for the suspicious MRI focus for each patient.	167
Table 31. A review of papers on the use of MR spectroscopy in patients with prior negative biopsy. (<i>Patient number (Pt No), Sensitivity (SEN), Specificity (SPEC), Positive predictive value (PPV), Negative predictive value (NPV), Accuracy (ACC)</i>).....	170
Table 32. Visual assessment of image quality by reader A according to specific criteria using PPA surface coil and ERC. (<i>* Mean value of assessment on a scale 1 to 4 quoted with SD in parentheses.</i>).....	179
Table 33. Visual assessment of image quality by reader B according to specific criteria using PPA surface coil and ERC. (<i>* Mean value of assessment on a scale 1 to 4 quoted with SD in parentheses.</i>).....	180
Table 34. Discrimination between PZ and CG. Number and percentage of patients in each category detailed for both readers.	180

Table 35. Visibility of PZ, the number and percentage of patients in each category for both readers.....	182
Table 36. Degree of tumour identification according to reader.	183
Table 37. Extracapsular cancer extension as seen on T2w images (comparison between surface coil and ER coil imaging for reader A / reader B).....	184

Index of figures

Figure 1. Distribution of male cancer types in the UK in 2009 (data from Cancer Research UK).....	2
Figure 2. Numbers of new cases and age-specific incidence rates of prostate cancer, UK 2009 (data from Cancer Research UK).....	3
Figure 3. Increasing incidence of prostate cancer in Great Britain from 1993 to 2008 (data from Cancer Research UK).....	4
Figure 4. Age-adjusted cancer incidence rates for men in the United States. Noted the sharp increase in rate of prostate cancer detection in early 1990s. The later decline in incidence may represent the effect of screening anticipation as cases that were bound to present have already been diagnosed at screening. (Data obtained from The National Cancer Data Base report on prostate carcinoma, The American College of Surgeons Commission on Cancer and the American Cancer Society [8]).	5
Figure 5. Prostate cancer incidence and mortality rates around the world in 2006 (data from Cancer Research UK).	6
Figure 6. Incidence rate and age-standardized mortality rate for prostate cancer, Great Britain, 1975-2008 (Data from Cancer Research UK). Note the stable mortality rate between 1975 and 2008 despite the dramatic increase in incidence rate.	8
Figure 7. Sagittal section of the anatomy of the male pelvis showing the location and relationship of the prostate and seminal vesicles (image obtained from the introduction to urology course, Sheffield).	17
Figure 8. Axial and sagittal views of the prostate showing normal zonal anatomy (obtained from www.aboutcancer.com/prostate anatomy).	19
Figure 9. Haematoxylin and eosin section of normal prostate tissue at low magnification (X200), showing glandular units (stained blue/purple) surrounded by stroma elements rich in smooth muscle (stained pink).	22
Figure 10. Gleason grading system for prostate cancer. Grades 1 to 5 are defined as detailed below: Grade 1 tumours consist of small, uniform glands with minimal nuclear changes. Grade 2 tumours have medium sized acini, still separated by stromal tissue. Grade 3 tumours show marked variation in glandular size and organization, and infiltrating stroma. Grade 4 tumours show marked cytologic atypia and extensive infiltration. Grade 5 tumours are characterized by sheets of undifferentiated cancer cells.	27
Figure 11. Kattan’s nomogram for predicting prostate cancer recurrence after radical prostatectomy. Adapted from Kattan MW <i>et al.</i> A preoperative nomogram for disease recurrence following radical prostatectomy for prostate cancer. <i>J Natl Cancer Inst</i> 1998;90:768.....	34
Figure 12. Normal prostate anatomy in a young man, detailing prominent peripheral zones (PZ) and small central gland (CG).	50
Figure 13. Benign prostatic hypertrophy involving the central gland and compressing the peripheral zones in a man over 60.	50
Figure 14. Normal looking seminal vesicles.	51
Figure 15. Prostate MR Image using integrated endorectal-pelvic phased-array coil. The endorectal coil is seen in the rectum and filled with air to	

stabilize it. Axial image (a) and coronal image (b) showing great anatomical details.	55
Figure 16. : Longitudinal magnetic vector (a) at B ₀ , a new transverse magnetic vector is formed and decrease in longitudinal vector when applying RF pulse (b), longitudinal vector may disappear depending on RF pulse (c). Modified from original Source: MRI from A to Z: A Definitive Guide for Medical Professionals by Gary Liney [103].	57
Figure 17. Spin echo pulse sequence showing the time to repetition (TR) between two radio frequency pulses giving two signals, and time to echo (TE) between the initial 90 degree RF pulse and the signal received after 180 degree RF pulse.	59
Figure 18. T2 weighted image of prostate using the pelvic phased array coil (a) and the endorectal coil (b). This shows a normal left peripheral zone (bright) and a malignant lesion in the right peripheral zone (dark). Brightness flare occurs in the peripheral zones of the gland due to the proximity of the coil to the gland and signal decrease in the anterior part of the gland.	61
Figure 19. T2 weighted images using the pelvic phased array coil, showing an area of low signal intensity in the left peripheral zone (a). Same lesion is seen on endorectal imaging (b). T1 weighted image showing the corresponding location with an area of haemorrhage seen as a “bright” area in the left peripheral zone (c).	62
Figure 20. Low resolution pelvic image (a) is useful for detecting pelvic lymph node disease and bony disease, whereas high resolution image (b) is mainly to look at the prostate anatomy and pathology.	64
Figure 21. T1 weighted images of the prostate. Pre (a) and post (b) contrast administration. The area suspicious of malignancy on the left PZ, takes up contrast and looks bright on T1 weighted image post-contrast. Also note the enhancement of the vessels.	66
Figure 22. Showing the enhancement of malignant tissue in the prostate gland, which is not otherwise seen on T2 weighted imaging. On the left is a T2 weighted image showing a slightly darker right peripheral zone compared to the left but not diagnostic of cancer. On the right is the contrast enhanced image showing the increased uptake (demonstrated by the red areas) in both peripheral zones. Histology confirmed cancer in the areas highlighted in red.	67
Figure 23. Signal intensity – time curve for a typical malignant lesion: The enhancement curve consists of an early upslope to reach peak intensity and a wash-out phase. The figure shows the time point at which contrast reaches the prostate (a) and the maximum enhancement (b) achieved. Time to maximum enhancement (a-b), initial and final slopes can be obtained as shown.	68
Figure 24. Shapes of signal intensity curves as demonstrated by Kuhl <i>et al.</i> Type I shows continuous enhancement throughout the dynamic study, either as a straight line Ia or curved line Ib. Type II is a plateau curve following an upstroke. Type III is a rapid washout time course.	70
Figure 25. PK map (right) showing an area of increase permeability which correlates with low signal intensity on the corresponding T2 weighted image (left).	71

Figure 26. Diffusion weighted image of prostate gland (a) showing an area of low signal intensity in the right peripheral zone representing a malignant lesion. Corresponding ADC map reflecting low ADC in right peripheral zone using b -values of 0 and 500 s/mm ² (b).....	73
Figure 27. A 3 Tesla 8 channel torso phased-array coil. The figure shows the anterior and posterior elements connected with Velcro straps. The plastic inner bridge can be positioned over the patient to support the anterior elements if the weight of the device is uncomfortable.....	80
Figure 28. Endorectal coil with inflatable balloon to ensure retention which can be integrated with pelvic phased array coil.	82
Figure 29. The proforma used by each reader to evaluate each series independently. The area of tumour was drawn on the prostate illustration.....	84
Figure 30. H&E slide of whole mount prostate specimen with cancer foci outlined in red.	87
Figure 31. Sections obtained from prostatic apex (first 3 on left), base (middle 3) and seminal vesicles (last 2 on right). Evidence of cancer was noted in the apical sections (black dotted areas).	87
Figure 32. The proforma that was used to document pathology details including localisation, staging and surgical margins.	89
Figure 33. T2 weighted image (left) demonstrating low signal intensity in the left peripheral zone (black arrow). This correlates with high contrast uptake on DCE image (middle). The correlation with H&E stained histopathology slide (right) is also noted. There is an additional small area of uptake in the right peripheral zone seen on DCE image (white arrow) which correlated with scattered islands of malignant cells seen histologically.	99
Figure 34. The ROC curve for tumour localisation using T2 weighted imaging and DCE-MRI for reader 1 and 2. AUC for T2 w imaging is 76 and 67 for reader 1 and 2 respectively. AUC for DCE-MRI is 81 and 79 for reader 1 and 2 respectively.	103
Figure 35. Demonstrate the number and percentage of cases according to pathological stage.....	104
Figure 36. T2 weighted image (left) demonstrates a tumour involving the left peripheral zone with an area suggestive of extracapsular extension (white arrow). This corresponds with tumour extracapsular extension on H&E histology slide (x10 and x20 magnification).	105
Figure 37. ROC curves for T2 weighted detection of ECE using PPA coil for readers 1 and 2.....	106
Figure 38. ROC curves for T2 weighted detection of ECE using an endorectal coil for readers 1 and 2.	107
Figure 39. An example of seminal vesicle involvement. Low intensity areas seen in both seminal vesicles (left) with high contrast uptake on DCE-MRI (middle). These findings correlated with tumour involvement pathologically.	109
Figure 40. Images of H&E stained prostatic carcinoma at x200 magnification, before (a) and after processing (b) using MATLAB software. Cell nuclei are highlighted in blue and connective stroma in pink.	123
Figure 41. a) Diffusion weighted image of the prostate showing area of low signal intensity in the right PZ. b) ADC map demonstrating the low	

diffusivity in the right PZ indicated by the blue pixels. c) The corresponding H&E pathology slide showing the presence of tumour area on the right PZ as marked.	124
Figure 42 Boxplot showing the differences in mean CD and ADC between the PZ and cancer areas. There is a degree of overlap between the 2 tissues.	127
Figure 43. The differences in ADC values and cell density between tumour and normal PZ for all cases. Although there is a noticeable overlap in values between individuals, all cancer lesions demonstrated lower ADC values and higher CD values than normal PZ tissue.	129
Figure 44. The blue line shows the ROC curve for ADC data. The AUC for tumour detection accuracy is 0.86.	130
Figure 45. Scatter plot of the estimated CD (expressed as a percentage of surface area occupied by nuclei per high power field) with ADC value. A significant correlation ($p < 0.0001$) is obtained between the ADC value and the percentage CD for both tissue types (normal PZ and tumour).	131
Figure 46. Using a cutoff ADC value of $1.62 \times 10^{-3} \text{ mm}^2/\text{s}$, a good separation is noted between tumour and normal PZ ADC values.	135
Figure 47. The cancer regions are outlined on the H&E stained pathology slide of the whole mounted prostatectomy specimen (left). T2 weighted image shows a low signal intensity area in the right peripheral zone (middle). The positive enhancement integral image (right) shows the corresponding area of tumour (outlined in red) and an area of normal peripheral zone (outlined in grey). The high contrast uptake seen in the central gland on the positive enhancement integral image reflects the presence of hypervascular benign prostatic hypertrophy in most cases.	142
Figure 48. Signal intensity time curve for a typical malignant lesion (type 3 curve). X-axis shows time in seconds, and y-axis shows signal intensity (arbitrary unit). This illustrates the time when the contrast reached the prostate (a), maximum enhancement achieved (b), the time to maximum enhancement (b-a), initial and final slopes.....	144
Figure 49. Types of SI time curve: Type 1 curve demonstrates slow SI rise with no subsequent washout (top); type 2 curve demonstrates rapid rise in SI and subsequent plateau with no rapid washout (middle); type 3 curve demonstrates rapid uptake in SI and rapid washout (bottom). ...	146
Figure 50. Suspicious area of low signal intensity seen in the right postero-medial PZ on T2 weighted imaging using PPA (left) and ER coils (middle). This correlates with an area (shown in red) of increased contrast uptake seen on DCE-MRI (right).	163
Figure 51. Trans-rectal ultrasound scan. Axial view on the left and sagittal view on the right. This allows measurement of the prostate gland in 3 dimensions to get the prostatic volume.....	164
Figure 52. 12 core biopsy scheme. This was adjusted to include one biopsy from the suspicious area detected on MR imaging.	165
Figure 53. Hypoechoic lesion imaged during TRUS in an area highly suspicious of cancer on MRI (white arrow). Biopsy revealed adenocarcinoma.	166

Figure 54. Organisation chart detailing all the pathological findings for the suspicious MR lesions.	168
Figure 55. An example of PPA coil image (a) compared with ECR image (b). Noticeable improvement in CG and PZ discrimination by using ERC.	181
Figure 56. Better PZ visualization seen on ERC image (b) compared to PPA coil image (a).	182
Figure 57. A 63 year old man with PSA of 8.0 and biopsy proven prostate cancer with Gleason score of 7. T2 weighted image using PPA (a) does not show any abnormalities. By using ERC (b) a low signal intensity area is seen in the right PZ.	183
Figure 58. Low signal intensity area was seen in the left PZ and the cancer was staged as T2 (organ confined) on PPA coil image (a). ERC image shows the same low signal intensity area, causing irregularity of the prostatic capsule (b) suspicious of extraprostatic cancer extension (T3a).	185
Figure 59. The prostatic capsule over the left PZ is not clearly seen using PPA coil (a). A better identification of the capsule allowed the reader to stage the disease as T2.	185

Acknowledgements

I would like to express my gratitude to all those people who have assisted me during the period of my research which has led to the production of this thesis. In particular I would like to thank the following colleagues:

Professor Lindsay Turnbull for her invaluable supervision and advice during the 2 ½ years of my research and thereafter. This thesis would not be completed without her support.

Mr Sigurd Kraus for his significant encouragement and career advice during the research period

Dr Peter Gibbs for his assistance and guidance in writing this thesis, analysing the data and publishing papers.

Dr Martin Pickles for his constant input into this work and for sharing his radiographic experience to optimise MR sequences.

Dr Gary Liney and Dr Martin Lowry for their numerous recommendations in analysing the data, and improving sequences.

Dr Daniel Siddons and Mrs Julie Ponder for their help in scanning patients and operating the imaging system.

Dr Greta Rodrigues for her valuable guidance in analysing the prostate histopathology specimens, and her assistance in localising tumour foci and counting cell density.

Mr John Hetherington for his career guidance and his supervision in the urology theatre and clinic.

Mr Graeme Cooksey, Mr Matthew Simms and Mr David Almond for their continuous support and help in recruiting patients from the urology department.

The Yorkshire Cancer Research and the University of Hull for funding this study.

My Wife, Zena, for her support and encouragement over the period of my research, and for creating the atmosphere where I succeeded in studying my project and writing my thesis.

Declaration

The work detailed in this thesis was carried out at the University of Hull Centre for Magnetic Resonance Investigations which is located at Hull Royal Infirmary.

Patients were recruited from the Urology department at Castle Hill Hospital, Cottingham.

The work is original and is my own. The enhancement parameters modeling software used in this thesis was developed by Dr Martin Lowry at the University of Hull Centre for Magnetic Resonance Investigations.

The model for automatic cell density counting was developed by Dr Gary Liney at the University of Hull Centre for Magnetic Resonance Investigations.

The histopathologic analysis was performed by Dr Greta Rodrigues, consultant pathologist at Hull & East Yorkshire NHS Trust.

The text was written by me and I have referenced all literature quoted. This work has not been submitted before by me for any other degree at any other institution.

Bachar Zelhof

MRCS

Hull 2012

List of publications

- 1) Description of MR derived enhancement parameters in pathologically confirmed prostate cancer and normal peripheral zone regions**
Zelhof B, Lowry M, Rodrigues G, Kraus S, Turnbull LW
British Journal of Urology International (BJUI). 2009 Sep;104(5):621-7.
PMID: 19281464
- 2) Correlation of diffusion-weighted magnetic resonance data with cellularity in prostate cancer**
Zelhof B, Pickles M, Liney G, Gibbs P, Rodrigues G, Kraus S, Turnbull LW
British Journal of Urology International (BJUI), 2009 Apr;103(7):883-8.
PMID: 19007373.
- 3) Correlation of ADC and T2 measurements with cell density in prostate cancer at 3.0 Tesla.**
Gibbs P, Liney GP, Pickles MD, Zelhof B, Rodrigues G, Turnbull LW
Investigative Radiology. 2009 Sep;44(9):572-6. PMID: 19692841
- 4) Analysis of prostate DCE-MRI: comparison of fast exchange limit and fast exchange regimen pharmacokinetic models in the discrimination of malignant from normal tissue.**
Lowry M, Zelhof B, Liney GP, Gibbs P, Pickles MD, Turnbull LW.
Investigative Radiology. 2009 Sep;44(9):577-84. PMID: 19668002

Abbreviations

ADC:	Apparent diffusion coefficient
AUC:	Area under curve
CD:	Cell density
CG:	Central gland
CI:	Confidence interval
DCE:	Dynamic contrast enhanced
DRE:	Digital rectal examination
DWI:	Diffusion weighted imaging
ECE:	Extracapsular extension
EI:	Enhancement index
ERC:	Endo rectal coil
FOV:	Field of view
FSA:	Fast spin echo
FSPGR:	Fast Spoiled Gradient Recalled
Gd:	Gadopentetate dimeglumine
GE:	General electric
H&E:	Haematoxylin and Eosin
HGPIN	High grade prostate intraepithelial neoplasia
LRA:	Logistic regression analysis
MAXEI:	Maximum enhancement index
MRI:	Magnetic resonance imaging
NBV	Neurovascular bundle
PCa	Prostate cancer

PK:	Pharmacokinetic
PPA:	Pelvic phase array
PSA:	Prostate specific antigen
PZ:	Peripheral zone
ROC:	Receiver operating characteristic
ROI:	Region of interest
RP:	Radical prostatectomy
RRP	Radical retropubic prostatectomy
SD:	Standard deviation
SI:	Signal intensity
SNR:	Signal to noise ratio
SVI:	Seminal vesicle involvement
TE:	Time to echo
Tmax:	Time to maximum enhancement
TNM:	Tumour Node Metastasis
TR:	Time to repeat
TRUS:	Transrectal ultrasound
TURP:	Trans-urethral resection of prostate

Chapter one

1. INTRODUCTION

Brief overview of prostate cancer

Prostate cancer (PCa) is a high-profile disease due to its incidence, the large number of men dying yearly from the disease, the considerable debate surrounding the benefit and risks of early detection, and the amount of research currently ongoing in its detection, diagnosis and management. PCa is now recognized as one of the most important medical problems facing the male population.

The first chapter of this thesis outlines the current epidemiology, the natural history, staging, diagnostic tools and management of prostate cancer.

1.1. Incidence

With ageing of the population, the development of the prostate specific antigen (PSA) test, and the continuing decline in other common cancers such as lung and stomach since the mid 1980s, prostate cancer has become the most common cancer among men [Figure 1], accounting for about one in four (24%) of all new male cancers diagnosed in the UK in 2008 [1].

There were 40,841 newly diagnosed PCa cases in the UK in 2009, compared to 22,846 cases of lung cancer and 22,097 cases of colorectal cancer. The cancer statistics in Europe [2] showed that there were 345,900 new cases of prostate cancer diagnosed in 2006.

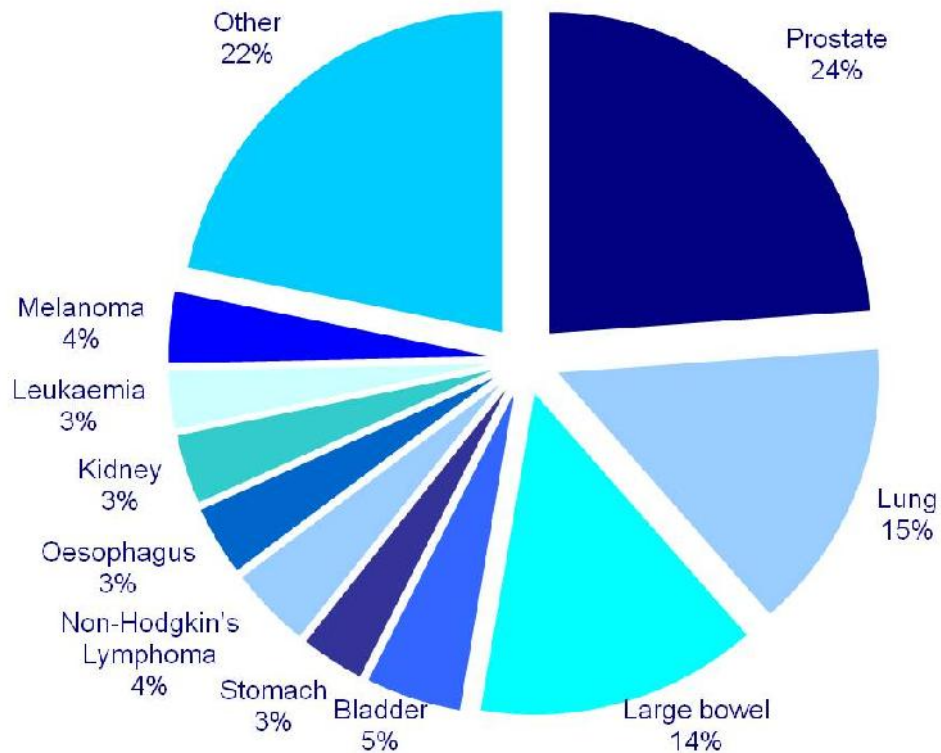


Figure 1. Distribution of male cancer types in the UK in 2009 (data from Cancer Research UK)

The burden of the disease largely occurs among older men, with very few cases registered in men under 50 and more than 60% of cases occurring in men over 70 years old. Incidence rates rise steeply with age, for men aged 55-59 the incidence rate is 155 per 100,000 men; reaching 510 per 100,000 at age 65-69, and by 75-79 the rate is almost five times higher at 751 per 100,000 [Figure 2]. [3]

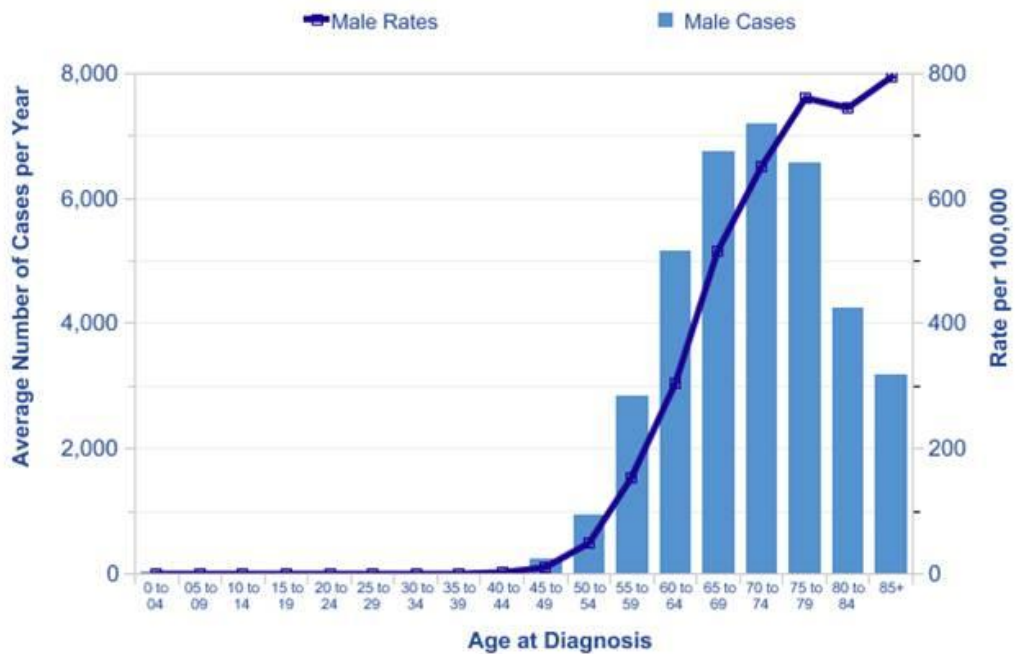


Figure 2. Numbers of new cases and age-specific incidence rates of prostate cancer, UK 2009 (data from Cancer Research UK)

Latent carcinoma of the prostate is found in a large proportion of elderly men with a clinically normal prostate. Autopsy studies have shown that between 15-40% of men aged 50 years and over have small, well differentiated tumours within the peripheral zone of the prostate gland that never presented clinically and would not otherwise have been detected. By the age of 80, microscopically detected prostatic adenocarcinoma is present in 70-80% of all men [4]. In another autopsy study [5], the authors found a 38.8% prevalence of incidental prostate cancer with an increasing age-related incidence, reaching 86.6% in the age group between 81 and 95 years.

1.1.1. Trends in prostate cancer incidence

Substantial increases in prostate cancer incidence have been reported in the last 25 years with an average increase of 4% annually worldwide. From 1993 until 2008, the incident rates have increased by almost 56% with the incidence rate of 62 per 100,000 men in 1993 rising to 98 per 100,000 in 2008 [Figure 3]. This increase was observed in the UK across all age groups, but most markedly in men aged 55-64 years.

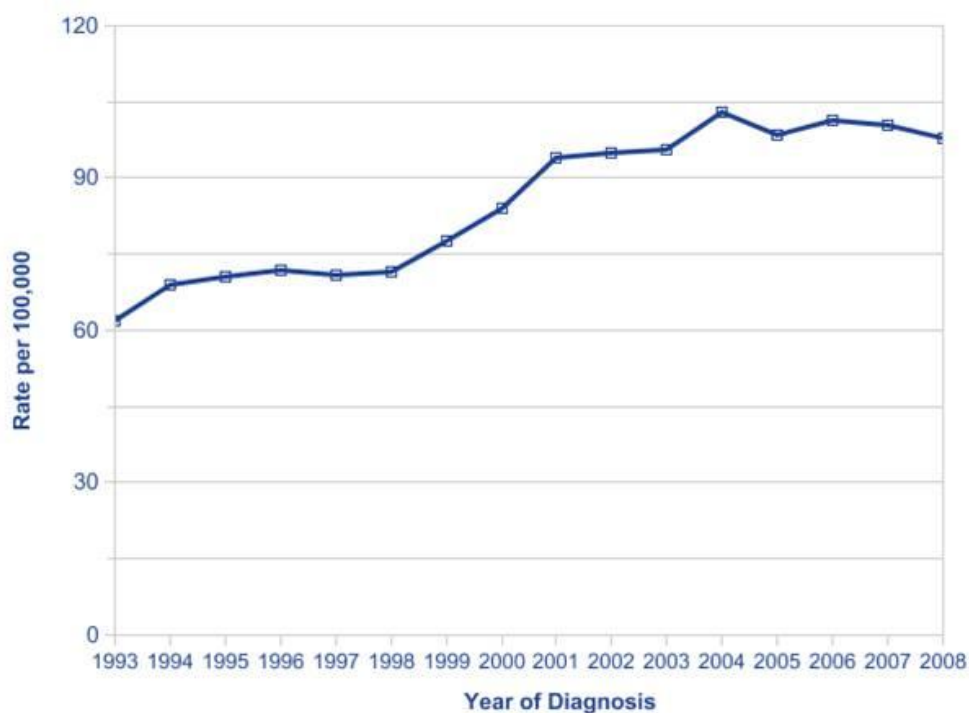


Figure 3. Increasing incidence of prostate cancer in Great Britain from 1993 to 2008 (data from Cancer Research UK)

Some of this increase is due to a real rise in incidence, since the rise in life expectancy causes an increase in the number of men at risk. However, other factors also contribute, namely greater awareness, improved diagnostic techniques, increased reporting of small foci of cancer in pathology specimens [6], as well as the rise in the number of transurethral resections of

the prostate (TURP) performed in the 1980s and the substantial rise in PSA testing in the 1990s [7].

The effect of PSA testing on incidence rates was most noticeable in the United States population following the introduction of PSA screening in the early 1990s [Figure 4].

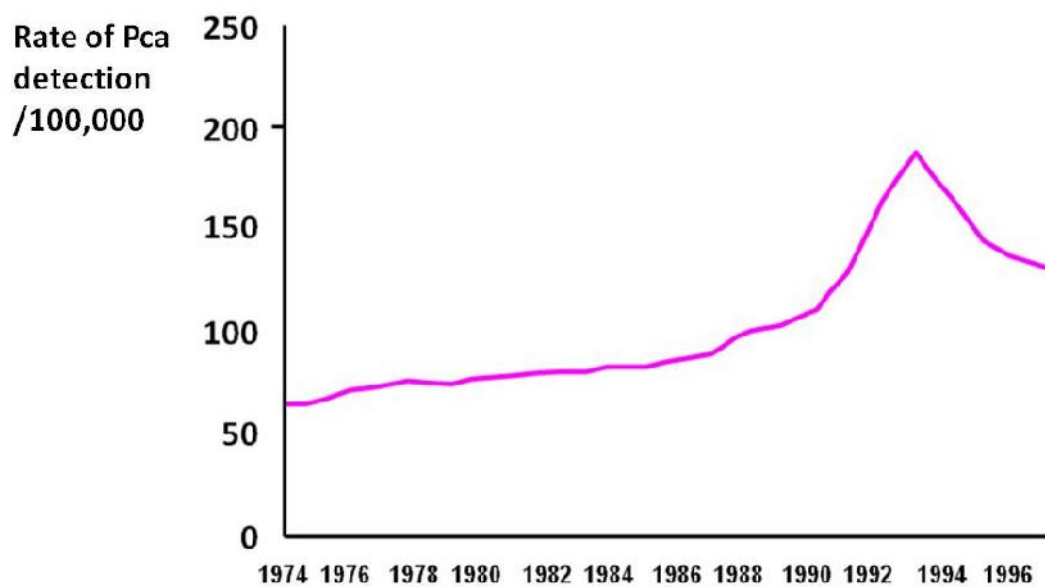


Figure 4. Age-adjusted cancer incidence rates for men in the United States. Noted the sharp increase in rate of prostate cancer detection in early 1990s. The later decline in incidence may represent the effect of screening anticipation as cases that were bound to present have already been diagnosed at screening. (Data obtained from The National Cancer Data Base report on prostate carcinoma, The American College of Surgeons Commission on Cancer and the American Cancer Society [8]).

1.1.2. Geographic variation in prostate cancer incidence

There is a 30-fold variation in prostate cancer incidence rates reported between populations [Figure 5]. The highest reported rates are found in the USA, where the age-standardized rates exceed 120 per 100,000 men. The lowest rates are seen in Asian countries (less than 10 per 100,000 men) [1].

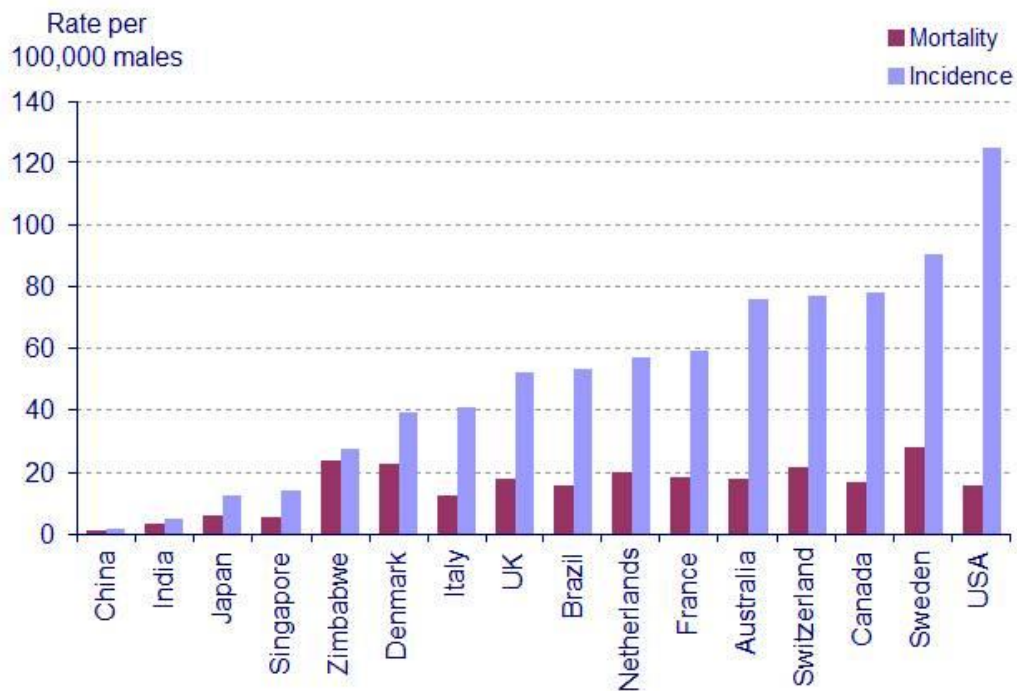


Figure 5. Prostate cancer incidence and mortality rates around the world in 2006 (data from Cancer Research UK).

The large variation in reported incidence rates between countries is partially due to the differences in detection. In Western countries, transurethral resection of the prostate (TURP) is a common procedure carried out for the treatment of obstructive symptoms. The prostatic chippings are routinely sent for histological examination, and in up to 15% of cases, this reveals a small unsuspected prostate cancer, which increases the detection rates [9].

Moreover, the introduction of PSA screening in the USA, Australia and some European countries in health check clinics led to inflation in the detection of small asymptomatic tumours. It is noted that the low incidence rate in Japan is expected to increase by three to four fold when US-based methods of detection are employed. However, the rate will remain 50% lower than that found in men of Japanese ancestry in the USA and 75% lower than that in Caucasian American men. This suggests that both environmental and genetic factors contribute to the variation in incidence rates between countries.

1.2. Mortality

Prostate cancer is the second most common cause of cancer death in men, after lung cancer, accounting for approximately 13% of male deaths from cancer in the UK [1]. In Europe there were 87,400 reported deaths from prostate cancer in 2006, with an estimated age-standardized mortality rate of 22.2 per 100,000 men [2]. Contrary to incidence rates, prostate cancer mortality rates have remained stable in the UK over the last 10 years [Figure 6]. It is not known whether this stability is due to PSA screening and detection of early cancer, to improved treatment or to changes in assigning a cause of death. We are aware that many more men are diagnosed with prostate cancer than die from it.

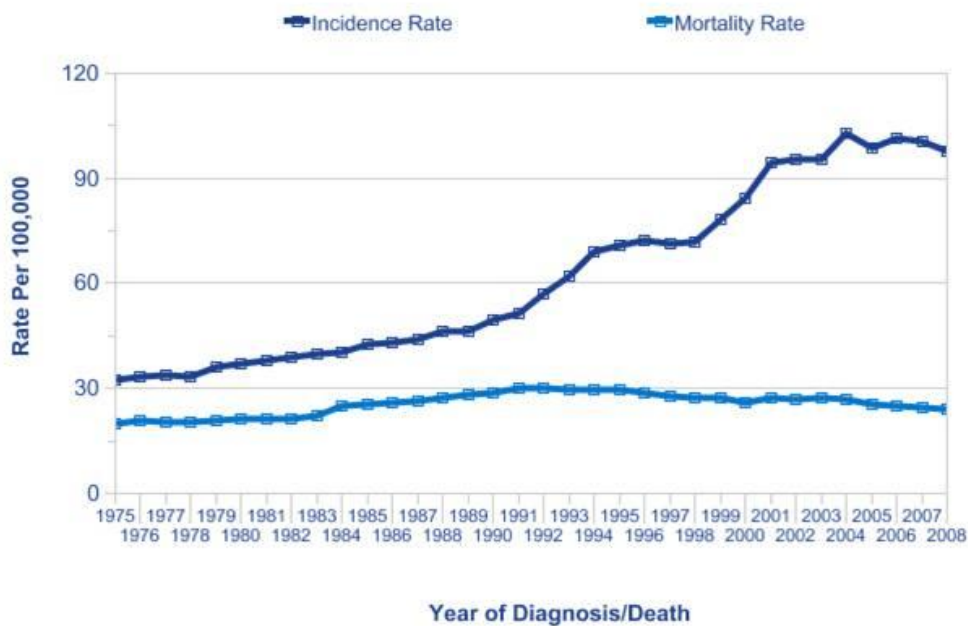


Figure 6. Incidence rate and age-standardized mortality rate for prostate cancer, Great Britain, 1975-2008 (Data from Cancer Research UK). Note the stable mortality rate between 1975 and 2008 despite the dramatic increase in incidence rate.

Data from the Surveillance, Epidemiology and End Result (SEER) program of the National Cancer Institute (NCI) indicated that the 5 year overall survival rate for patients with metastatic disease was 33%. In comparison, men with regional stage disease (T3, T4, N1) had a 98% 5 year survival rate [10].

Overall survival rates for PCa, as opposed to mortality, have increased over the last two decades. This is likely due to the lead time bias with the use of PSA testing. Parker *et al* (2006) demonstrated a 26% 15 year survival benefit from curative treatment compared with conservative management alone for men age 55-59 years with intermediate or high aggressive tumour (Gleason

score >7) [11]. The survival benefit is noted to be less for older patients and for those with low aggressive (Gleason 6) tumours. Further discussion on the rationale of PCa treatment and its effect on mortality are described later in this chapter.

1.3. Natural history of prostate cancer

The natural history of prostate cancer was described years before the advent of PSA testing. The best documented details exist in the data compiled over many years in centres where prostate cancer was treated conservatively. By looking at what happened to men with conservatively managed PCa, we can understand how the disease progresses when it is detectable clinically without the effect of PSA lead-time bias, and left undisturbed until late in its course.

The question that has always been raised by urologists is “How can we distinguish between men who are likely to die from PCa and those with indolent disease?” The first observation of deferred treatment was reported by RW Barnes [12] in the late 1960s. He compiled data on patients between 1930 -1958. His inclusion criteria were: nodule palpable on digital rectal examination, histologically confirmed PCa (by needle biopsy or prostatectomy for BPH), and clinical follow up for between 10 to 15 years. His results showed that at 10 years, 24% of patients died from other causes and 24% of patients died from prostate cancer. At 15 years 38% of patients died from other causes compared to 32% deaths from prostate cancer. He

concluded that competing medical co-morbidity is more likely to cause patient death than prostate cancer.

In 2004, Johansson et al [13] published data on 223 men from Orebro, Sweden, who had received deferred treatment for PCa. This cohort of patients had been followed for an average observation period of 21 years. The patients who had tumour progression were treated with hormone manipulation if they were symptomatic. Most cancers had an indolent course during the first 10 to 15 years. However, follow up from 15 to 20 years showed substantial decrease in progression free survival from 45 to 36 percent and reduction in the prostate cancer specific survival rate from 78.7 to 54.4 percent.

Albertson et al [14], reported an analysis of data from the SEER (Surveillance, Epidemiology and End Results) Trial. The study was designed to estimate survival based on a competing risk analysis stratified by age at diagnosis and Gleason score on histological examination from needle biopsy specimens for men diagnosed as having clinically localised PCa and who were managed conservatively. The study included 767 men diagnosed with PCa between 1971 and 1984 and subsequently followed up for 20 years. The authors showed that men with tumours of Gleason scores 6,7, and 8-10 had a 18-30, 42-70, and 60-87 percent chance, respectively, of dying from the disease within 15 years of diagnosis.

Several points have emerged from PCa natural history studies:

- 1) Early stage, low grade disease can be treated successfully with conservative management in older men with a good outcome of at least 10 and perhaps 15 years of survival.
- 2) Aggressive prostate cancer results in high rate of mortality when left untreated
- 3) Age and co-morbidity are important factors in making decisions about treatment.

1.4. Prostate Specific Antigen

1.4.1. Introduction of PSA

PSA is a protein produced by normal prostate cells. This enzyme participates in the dissolution of the seminal fluid coagulum and plays an important role in fertility. The highest concentration of PSA is found in the seminal fluid, where it was first discovered. Some PSA escapes the prostate and can be found in the serum. PSA was first identified and purified in 1970s. However, its widespread use in clinical urology did not occur until 1980s. The half-life of PSA is about 2.2 to 3.2 days. Because of its relatively long half-life, a minimum of 2-3 weeks is required for the serum PSA to reach its nadir following radical prostatectomy, when it should be undetectable.

PSA testing is minimally invasive, simple and safe. Serum PSA elevation may indicate the presence of prostatic disease (including prostate cancer, benign prostatic hypertrophy, urinary retention and prostatitis) or result from

prostate manipulation such as transrectal biopsy and prostatic massage. Elevation of PSA above 4ng/mL carries a 22% probability of prostate cancer, and a further increase above 10ng/mL raises the cancer risk to 63% [15].

As PSA values rise with age, there is an agreed cut-off level for different age groups [Table 1]. Although this is not universally accepted, as men may harbor PCa despite low levels of serum PSA, the use of an age-specific normal range for PSA values increases the positive predictive value of PSA testing. The following table details the normal range of values according to age.

Age group	Normal PSA value
>60	PSA 3
60-69	PSA 4
>70	PSA 5

Table 1. Outlines normal age-specific PSA (data from Cancer Research UK)

In a study of 1167 men aged 60 with PSA of less than 1 ng/ml [16], Lilja *et al* found that they were unlikely to have clinically relevant prostate cancer (0.5% risk of metastasis by age 85 and 0.2% risk of death from prostate cancer).

1.4.2. PSA modalities

A number of modalities have been proposed to enhance PSA usability such as PSA velocity, PSA density, age-specific PSA and free/total PSA ratio.

PSA velocity

This is defined as the change of PSA value over time; it enhanced the specificity for prostate cancer detection from 42% to 96% when it was studied over a 5 year period [17], compared to a single reading of PSA. In another recent large scale study which involved 4,272 patients [18] and which extended over a 10 year period, men with prostate cancer were found to have significantly greater PSA velocity than those without cancer (0.39 versus 0.03).

PSA velocity as a predictor of tumour stage and grade remains controversial [19, 20]. A more important and established role of PSA velocity is the follow up of patients with prostate cancer who are either on active surveillance strategy, hormone manipulation or post radical treatment [21].

PSA density

This is defined as the serum PSA level divided by the volume of the prostate. It allows adjustments for the PSA component that arise from benign prostatic hypertrophy which arises mainly in the transitional zone [22]. The clinical use of PSA density has been debated. In a study done by Freedland *et al* [23] the additional time and effort required to calculate PSA density was not justified by the minimal improvement in predicting tumour stage, surgical margin and biochemical recurrence after radical prostatectomy. However, more recent studies have shown that PSA density may add additional prognostic value to predict cancer progression. Tosoian *et al*, from John Hopkins Hospital, considered PSA density as an important criterion for patients who opted for an active surveillance strategy [24].

Role of free/total PSA

This parameter has emerged after the discovery that PSA exists in a complexed (bound) form with other proteins and free (unbound) form that can be detected with immunoassays. Stenman *et al* [25] were the first to establish that men with prostate cancer had more complexed PSA (cPSA) than free PSA (fPSA), in contrast to men with benign prostatic hypertrophy, suggesting that the assay of the complex and its proportion to total PSA immunoreactivity can be used to differentiate between PSA elevations caused by benign and malignant prostatic disease. A clinical study done in Egypt showed that men with prostate cancer and a lower free/total PSA ratio had higher Gleason scores than those with higher free/total PSA [26].

1.4.3. PSA screening

Screening to identify organ-confined prostate cancer has provoked much public and scientific attention and there is intense debate about its role in improving men's health. The purpose of screening is to identify a group of asymptomatic men with early stage, organ confined prostate cancer, which would benefit from early radical intervention in terms of prolonged survival and/or improved quality of life. To date, there is no evidence in the literature that these benefits can be obtained by the establishment of mass screening programs.

Two large studies [27, 28] – the US based Prostate, Lung, Colorectal, and Ovarian (PLCO) cancer screening trial, and the European Randomized Study

of Screening for Prostate Cancer (ERSPC)- present the most comprehensive and up-to-date findings on PCa screening.

The PLCO trial recruited 76,693 men from 10 US centres. The screening group consisted of 38,343 men and the control arm included 38,350 men. Men in the screening group received annual PSA screening. The incidence of death per 10,000 person-years was 2.0 in the screening group and 1.7 in the control group with a rate ratio of 1.13 (95% CI, 0.75 – 1.70). These results show that after an average of 7 years of follow-up, mortality did not significantly differ between the screened and the control groups. The contamination in this study selection is that although men the control group were not actively screened, some patients received screening outside of the study.

On the other hand, the ERSPC trial recruited 167,387 men from 7 European centres into a PSA screening trial and showed about 20% reduction in the risk of dying from PCa at 7 years. But this comes at a price, as to prevent 1 cancer death, 1400 men need to be screened in the age group 55-69 years and 48 men need to be treated with all the side effects of treatment.

In conclusion, based on evidence from studies, young patients with long life expectancy have the greatest benefits in PSA testing. However, if PSA is recommended, the pros and cons must be stressed in the discussion, including the anxiety generated by the screening process, as well as the morbidity associated with treatment.

1.4.4. Trans rectal Ultrasound biopsy

Since the initial description of the sextant prostate biopsies by Hodge, very little changes were made until Stamey *et al* [29] extended the standard biopsies to include the lateral areas of peripheral zones. However, even with the extended biopsies, up to 30% of cancers can be missed. At present, most urologists and radiologists use 12 systematic core biopsies including the most lateral anterior horns of the peripheral zones. This increased the detection rate for prostate cancer by 25% [30]. different researchers have demonstrated that saturation biopsy techniques aimed at greatly increasing the number of samples (more than 24 biopsies) and varying the distribution of biopsy sites may provide a higher cancer detection rate up to 41% [31].

In a large systemic review of literature, Scattoni *et al* [32] conclude that it is now reasonable to consider a sampling with 12 cores of the peripheral gland as adequate even if limiting the number of cores to 12 in larger prostate is of concern, and the risk of detecting insignificant tumour should not be neglected. A more invasive saturation or template biopsies should be preserved for repeat biopsies when clinically suspicious cancer was not diagnosed on the initial biopsy.

1.5. Anatomy of the prostate

The prostate gland [Figure 7] extends from the bladder base to the urogenital diaphragm. It envelops the prostatic urethra and the ejaculatory ducts. It measures approximately 4x3x2 cm. The anterior surface lies at the back of the retropubic space and is connected to the pubic bone by the puboprostatic

ligaments. The infero-lateral surface sits on the levator prostatae, a component of levator ani. The posterior surface is in front of the rectum and separated from it by the retrovesical fascia.

The prostatic urethra runs through the centre of the prostate gland and bends anteriorly by approximately 35 degrees at the verumontanum, where the ejaculatory ducts join the prostate.

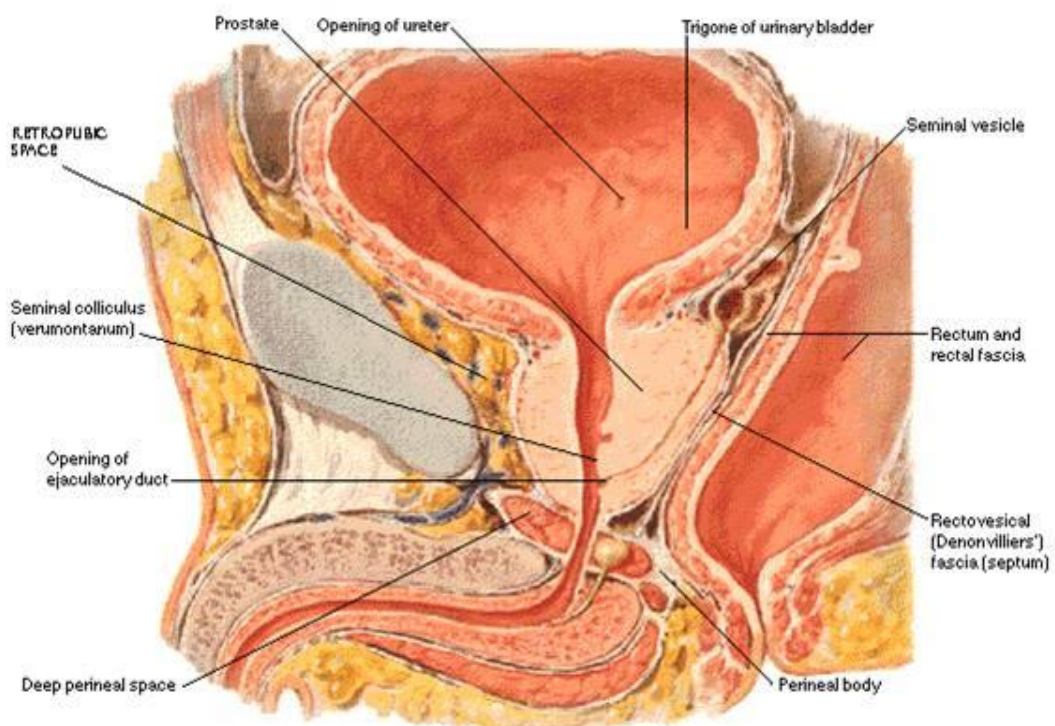


Figure 7. Sagittal section of the anatomy of the male pelvis showing the location and relationship of the prostate and seminal vesicles (image obtained from the introduction to urology course, Sheffield).

The prostate can be divided into 4 zonal components [33] excluding the urethra and periurethral glands [Figure 8]. These are as follows:

- 1- The anterior non-glandular fibromuscular stroma, which contains smooth muscle, helps to squeeze secretions during ejaculation. It merges with the fibromuscular tissue of the urogenital diaphragm.
- 2- The transition zone consists of 2 independent pear shaped lobes situated laterally on either side of the prostatic urethra together with periurethral glands. This is the zone where benign prostatic hypertrophy (BPH) occurs.
- 3- The central zone surrounds the transitional zone posteriorly and encloses the ejaculatory ducts. It is the zone most commonly affected by inflammatory processes (e.g. prostatitis). In benign prostatic hyperplasia, the transitional zone and periurethral glands enlarge considerably compressing the central zone to form a thin layer, the so-called surgical pseudocapsule.
- 4- The peripheral zone is the most posterolateral glandular component of the prostate. The ratio of peripheral zone to central gland tissue gradually decreases from the apex to the base of the gland. The peripheral zone can be compressed and distorted by BPH and it is the site of the majority of prostate cancers.

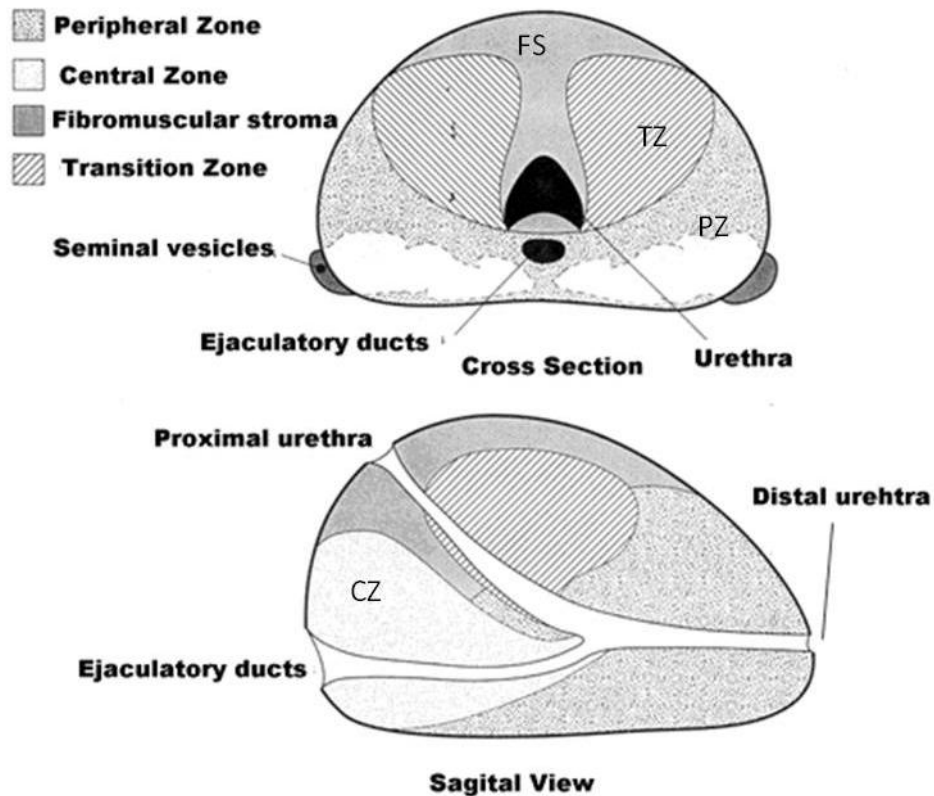


Figure 8. Axial and sagittal views of the prostate showing normal zonal anatomy (obtained from www.aboutcancer.com/prostate anatomy).

The prostate capsule is a fibromuscular layer, most prominent along the base and posterior portions of the lateral borders. It consists of an outer layer, termed the lateral pelvic fascia and an inner layer, the so called prostatic fascia which is inseparable from the prostatic stroma [34]. At the prostatic apex and bladder neck regions, the capsule is lacking and the prostatic connective tissue is inseparable from the surrounding extraprostatic connective tissue [35].

The prostatic capsule is separated from the pelvic muscles by loose connective and adipose tissue containing the periprostatic venous plexus,

arteries, nerves and lymphatics. At the posterolateral aspects of the prostate these structures form the neurovascular bundles containing cavernous nerve fibers that are important for erectile function. At the apex of the prostate, benign prostatic glands are mixed with skeletal muscle bundles of the urogenital diaphragm. This makes assessment of apical tumour extension more difficult.

1.5.1. Prostate arterial supply and venous drainage

The inferior vesical artery supplies the prostate via its urethral and capsular branches. The urethral arteries enter the prostate at the posterolateral vesico-prostatic junction and supply the bladder neck and periurethral zone of the prostate. The capsular branches run in the lateral pelvic fascia posterolateral to the gland along the pelvic sidewall, supplying the outer part of the prostate. The inferior vesical artery also provides branches to the seminal vesicles and the bladder base.

Prostatic veins drain into Santorini's plexus. The deep dorsal vein leaves the penis under Buck's fascia between the corpora cavernosa and penetrates the urogenital diaphragm, dividing into the superficial branch and the right and left lateral venous plexuses [36]. The superficial branch overlies the bladder neck and prostate penetrating through the middle of the puboprostatic ligaments. The lateral venous plexuses are concealed by the prostate and endopelvic fascia travelling posterolaterally and communicate with the pudendal, obturator and vesical plexuses. Also some branches from the lateral plexuses penetrate the pelvic sidewall to communicate with the

internal pudendal vein. After interconnection with other veins and plexuses, the lateral plexuses form the inferior vesical vein which drains into the internal iliac vein.

1.5.2. Prostatic innervation:

The innervation of the prostate comes from the pelvic plexus, which is formed by parasympathetic, visceral fibers arising from the sacral centre (S2 to S4) and sympathetic fibers from the thoracolumbar centre (T12 to L2). The prostatic nerves travel outside the prostate capsule and Denonvillier's fascia and enter the prostate by perforating the prostatic capsule. The neurovascular bundles are located in the lateral pelvic fascia between the prostatic and levator fascia. They continue laterally to the prostate and pierce the urogenital diaphragm to enter the corpora cavernosa. Although nerves within the bundles are very small, they can be identified intraoperatively by using the capsular vessels as a landmark.

1.6. Prostate histology:

The prostate gland consists of stromal elements (smooth muscle cells, fibroblasts and endothelial cells), epithelial elements (secretory cells, basal cells and neuroendocrine cells) and urethral cells which line the urethra [Figure 9]. Secretory cells are located along the glandular lumen and stain for PSA. The basal cells, which consist of low cuboidal epithelium and columnar mucus secreting cells, separate the secretory cells from the basement membrane and neuroendocrine cells which are irregularly distributed.

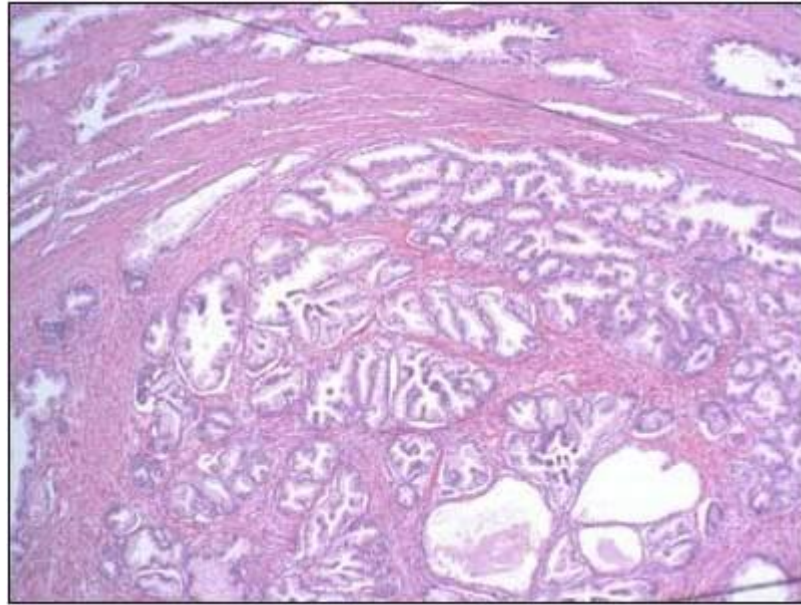


Figure 9. Haematoxylin and eosin section of normal prostate tissue at low magnification (X200), showing glandular units (stained blue/purple) surrounded by stroma elements rich in smooth muscle (stained pink).

1.7. Physiology of prostate:

The main role of the prostate is to produce fluid, which accounts for up to 30% of the semen volume. It aids sperm motility and provides nourishment. Prostatic fluid is a thin, milky alkaline liquid containing citric acid, calcium, zinc, acid phosphatase and fibrinolysin as well as PSA.

1.8. Pathology of Prostate Cancer

Adenocarcinomas account for 95% of prostate cancers and in most of cases they arise from the peripheral zone. In the remaining cases, tumours are located in the transitional zone either in a periurethral or anterior location. Adenocarcinoma of the prostate is multifocal in more than 85% of cases [37].

In the majority of these multifocal tumours, the additional foci of tumour are small and clinically insignificant.

Other histologic variants of prostatic carcinoma include Signet ring cell carcinoma, adenosquamous carcinoma, squamous cell carcinoma, basaloid and adenoid cystic carcinoma, transitional cell carcinoma, small cell carcinoma, sarcomatoid carcinoma, lymphoepithelioma-like carcinoma and undifferentiated carcinoma. Approximately 4% of prostate cancer cases have transitional cell morphology and are thought to have arisen from the urothelial lining of the prostatic urethra. Small cell carcinoma is another type of prostate cancer formed from the hormone producing (neuroendocrine) cells of the prostate. Neuroendocrine differentiation of tumour is more prominent during hormone manipulation. However, a recent study did not support that assumption but suggested that androgen-independent neuroendocrine cells existed before therapy [38].

1.8.1. Prostatic Intraepithelial Neoplasia (PIN)

PIN was first described by Bostwick and Brawer in 1987 [39]. It was identified as a precursor lesion to prostatic carcinoma. It refers to the pre-cancerous end of a morphologic spectrum involving cellular proliferation within prostatic ducts, ductules and acini [39]. The importance of high grade PIN (HGPIN) is its potential to invade and breach the basal membrane, thereby transforming into invasive cancer. HGPIN identifies patients who are at risk of either having a co-existing cancer or subsequently developing one [40].

The incidence of HGPIN ranges between 0.7-20% in prostatic needle biopsies with an average of 8.7% [40].

When HGPIN is present in the biopsy specimen, the pathologist should carefully search the tissue for evidence of invasive carcinoma, as studies of autopsy and radical prostatectomy specimens have shown coexisting prostate cancer in 63-94% of HGPIN cases [41]. The likelihood of identifying coexisting prostate cancer in patients with HGPIN on the first biopsy has increased over the years mainly due to more rigorous biopsy techniques and the use of transrectal ultrasound guidance for directing biopsies [40].

HGPIN has been established to be a precursor of prostate cancer with 33-50% of patients having prostate cancer detected on repeated biopsy [42]. However, the most recent study showed a trend toward decreasing incidence of subsequent cancer, mainly due to better detection of cancer on the initial biopsy [40].

No consensus has been reached about the optimal follow-up time for patients with HGPIN. Some studies have strongly advised repeated prostate biopsy for all patients with HGPIN to identify those with prostate cancer [43], regardless of their PSA findings [44], especially in the first 3 years after diagnosing HGPIN, supporting the concept that HGPIN is a precursor of prostate cancer. A study from John Hopkins Hospital [45] also showed that repeated biopsy identified cancer in 32.2% of men with HGPIN. The greater the number of cores affected by HGPIN, the higher the risk of cancer being detected on repeated biopsies (75% risk of cancer in cases with >3 biopsy

cores involved with HGPIN). By contrast, Epstein *et al* did not recommend routine repeat biopsies within the first year following a diagnosis of HGPIN, since they found that the rate of subsequent prostate cancer detection is similar to that reported following a benign diagnosis on needle biopsy [46].

Other experts have taken different approaches in more recent studies. As the risk of cancer is related to the proportion of the biopsy cores replaced by HGPIN, only multifocal HGPIN warrants re-biopsy, whereas unifocal HGPIN can be managed expectantly [41] with PSA or PSA velocity measurements [47].

1.8.2. Atypical and suspicious small acinar proliferations (ASAP)

ASAP was first described by Bostwick *et al* [48] as the presence of suspicious glands with insufficient cytological or architectural atypia for a definite diagnosis of cancer. Therefore, it is not a specific diagnosis, but an indication of diagnostic uncertainty. Histological appearances are similar to prostate adenocarcinoma but have smaller foci with fewer acini involved, less nuclear enlargement and hyperchromasia, absence of mitosis and lack of infiltration [49] of normal surrounding tissues.

The incidence of ASAP, in a study involving over 1000 prostatic biopsies, was found to be around 4.8% [50] ranging between 1.5-9% for different series [51]. The presence of ASAP on prostate biopsy is a strong predictor of cancer and is much more important than HGPIN. The subsequent prostate cancer detection rate after a diagnosis of ASAP is around 50-55% [51, 52], which is significantly higher than following HGPIN or benign biopsy. Therefore, early (after 3-4 months) repeat biopsies are strongly indicated

after a diagnosis of ASAP [53] and should not be limited to the site of ASAP findings, but extended to the whole gland [52].

Urologists should be aware of ASAP and recognize its significance relative to HGPIN, and arrange appropriately timed follow up and re-biopsy.

1.8.3. Grading system:

The most commonly used system for classifying histologic characteristics of prostate cancer is the Gleason score described by Gleason *et al* in 1974 [54]. It is based on the glandular pattern of the tumour. Both the predominant and the second most prevalent architectural pattern are assigned a grade from 1 to 5 (1 being the most differentiated and 5 being the least differentiated). Therefore, Gleason score 7a (3+4) has better prognosis than Gleason score 7b (4+3). It was concluded that a two tier Gleason system has greater discriminating power in predicting prognosis in patients with prostatic adenocarcinoma. In cases in which only a single pattern is present, the primary grade is doubled to derive the Gleason score [Figure 10].

Over the last decade, there has been a decline in the reported incidence of low-grade prostate cancers as a result of Gleason score reclassification (grade shift). This reclassification resulted in apparent improvement in clinical outcomes, since transferring the more aggressive tumours from the good prognostic group to the bad prognostic group, the prognostics of both groups improve. This finding reflects a statistical artifact known as the Will Rogers phenomenon.

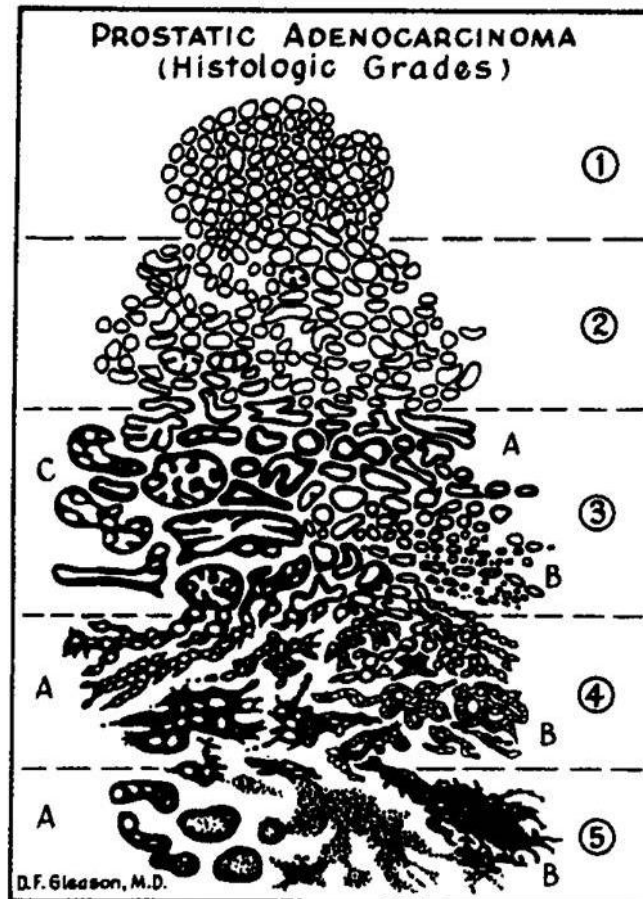


Figure 10. Gleason grading system for prostate cancer. Grades 1 to 5 are defined as detailed below:

Grade 1 tumours consist of small, uniform glands with minimal nuclear changes.

Grade 2 tumours have medium sized acini, still separated by stromal tissue.

Grade 3 tumours show marked variation in glandular size and organization, and infiltrating stroma.

Grade 4 tumours show marked cytologic atypia and extensive infiltration.

Grade 5 tumours are characterized by sheets of undifferentiated cancer cells.

1.8.4. Staging of prostate cancer:

Prostate cancer can spread locally as well as metastatically. Organ confined disease is staged as either pt1 which represents a clinically unapparent tumour diagnosed on histologic findings from transurethral resection or needle biopsy, or as pt2 disease, with tumour involving the prostate gland but not extending to its capsule.

Extraprostatic extension is the term recommended by Epstein *et al* [55] when the tumour extends beyond the normal confines of the prostate gland. This represents stage pt3 disease. Stage pt3a is considered to be present when cancer only extends out of the prostatic capsule into the periprostatic soft tissue and fat or when there is invasion of the neurovascular bundles. Assessment of extraprostatic extension at the apex is more difficult. Some pathologists believe that it cannot be assessed at this site. Others describe apical extraprostatic extension if tumour is seen beyond the level of normal prostatic acini.

Stage pt3b disease is defined as tumour infiltrating the seminal vesicles. It occurs either through tumour penetration of the capsule at the base of the gland into the peri-seminal space and eventually into the seminal vesicles, or less commonly through direct spread via the ejaculatory ducts or as discontinuous metastases. In a study involving 763 patients with prostate cancer, it was found that seminal vesicle involvement is rare (1.2% of patients) in the absence of tumour at the prostatic base [56]. Further

involvement of adjacent organs such as bladder and rectum is considered as stage pt4 disease.

The most frequent sites of metastatic prostate cancer are lymph nodes and bone. The primary lymphatic vessels from the prostate gland drain into the regional lymph nodes of the pelvis. These include the internal iliac (hypogastric), sacral, peri-vesical, obturator, and external iliac lymph node groups. The last 2 sites are considered as the first line of lymphatic spread and are commonly dissected during radical prostatectomy. Occasionally metastases go beyond regional lymph nodes and involve distant lymph nodes including deep and superficial inguinal, common iliac, retroperitoneal (aortocaval nodes), supraclavicular, cervical and scalene nodes.

Bony metastases can occur early without significant lymphadenopathy. Two theories have been proposed for spread: either direct spread through the lymphatics and venous spaces into the lower lumbar spine [57]; or the seed-and-soil theory which believes that tissue factors must be present to allow preferential tumour cell growth in certain tissues, such as the bone [58, 59]. Bony metastases from prostate cancer are commonly osteoblastic (unlike other types of cancers), but osteoclastic lesions can also be found. The underlying mechanisms for prostate cancer-induced osteoblastic activity are poorly understood despite recent studies on the cellular and molecular interactions between prostate cancer and bone cells. A study done by Nadiminty *et al* suggested that over-expression of PSA may be involved in bone remodeling and induction of osteoblastic differentiation [60].

Following in frequency after lymph nodes and bone, the next most common regions of metastatic spread are lungs, bladder, liver, adrenal glands and testes.

There have been several modifications to the staging system for prostate cancer. The currently used staging system is the 2002 modified TNM system (T = tumour, N = node, M = metastasis) [61]. The various stages of disease are as follows:

- T - Primary tumour
- TX - Primary tumour cannot be assessed
- T0 - No evidence of primary tumor
- T1 - Clinically unapparent tumour not palpable or visible by imaging
- T1a - Tumour incidental histologic finding in less than or equal to 5% of tissue resected
- T1b - Tumour incidental histologic finding in greater than 5% of tissue resected
- T1c - Tumour identified by needle biopsy (because of elevated PSA level); tumours found in 1 or both lobes by needle biopsy but not palpable or reliably visible by imaging
- T2 - Tumour confined within prostate
- T2a - Tumour involving less than half a lobe
- T2b - Tumour involving less than or equal to 1 lobe
- T2c - Tumour involving both lobes
- T3 - Tumour extending through the prostatic capsule; no invasion into the prostatic apex or into, but not beyond, the prostatic capsule

- T3a - Extraprostatic extension (unilateral or bilateral)
- T3b - Tumour invading seminal vesicle(s)
- T4 - Tumour fixed or invading adjacent structures other than seminal vesicles (e.g., bladder neck, external sphincter, rectum, levator muscles, pelvic wall)
- NX - Regional lymph nodes (cannot be assessed)
- N0 - No regional lymph node metastasis
- N1 - Metastasis in a single lymph node, 2 cm or less in greatest dimension
- N2 - Metastasis in a single lymph node, more than 2cm but not more than 5 cm in greatest dimension, or multiple lymph nodes, none more than 5 cm in greatest dimension
- N3 - Metastasis in a lymph node more than 5 cm in greatest dimension
- Mx - Presence of distant metastasis cannot be assessed
- M0 - No distant metastasis
- M1 - Distant metastasis
- M1a - Non regional lymph nodes
- M1b - Bone
- M1c – other sites

1.9. Radical prostatectomy

1.9.1. Preoperative clinical staging and prediction

Staging aims to distinguish between localised, locally advanced and metastatic disease in order to decide the optimal treatment pathway and to predict prognosis. The primary assessment of the extent of prostate

carcinoma is made by digital rectal examination (DRE) and serum prostate specific antigen (PSA) measurement. However, prostate cancer detection rate by DRE alone is very poor (2.5%) particularly in patients with low PSA values, as reported by Schroder *et al* from the Rotterdam section of the European Randomized Study of Screening for Prostate Cancer [62]. In addition, there has been no documented correlation between DRE and pathological stage [63]. DRE often underestimates the extent of tumour especially for T3 disease. With a positive DRE, the positive predictive value for cancer detection is significantly dependent on PSA value [64] [Table 2]. However, PSA has a low cancer specificity and no ability in isolation to predict the pathological staging due to the overlap in PSA levels between different tumour stages [65].

PSA ng/mL	Positive Predictive Value for Cancer
0-1	2.8-5%
1-2.5	10.5-14%
2.5-4	22-30%
4-10	41%
>10	69%

Table 2. PPV of PSA for cancer detection in patients with positive findings on DRE. The higher the PSA, the more likely that its elevation is due to cancer. (European Association of Urology Guidelines, 2011)

Partin *et al* [66] combined independent variables including DRE staging, PSA and Gleason score on prostatic biopsy to produce a statistical prediction of the final pathological stage. This has been widely used by urologists to guide patient management and to predict the outcome of radical prostatectomy. For example, a patient with non palpable disease and a PSA value between 4.1 and 6, with Gleason 6 on prostate biopsy, has an 80% chance of having organ confined disease compared to 46% if the Gleason score was 8-10. Various electronic and online applications have been put in place to facilitate the use of Partin's table in clinical practice.

The good predictive accuracy of Partin's table has been confirmed by other authors who have reported area under the curve (AUC) values of 0.784, 0.728, 0.791 and 0.799 for organ-confined tumour, extracapsular extension (ECE), seminal vesicle involvement (SVI) and lymph node involvement respectively [67]. Another predicting nomogram was produced by Kattan *et al* [68]. This was developed from data on a group of 983 men with clinically localised prostate cancer with the intention of predicting 5 year disease recurrence rate for patients with clinically localised PCa undergoing radical prostatectomy. It uses preoperative clinical factors including preoperative PSA, biopsy derived Gleason score and clinical stage [Figure 11].

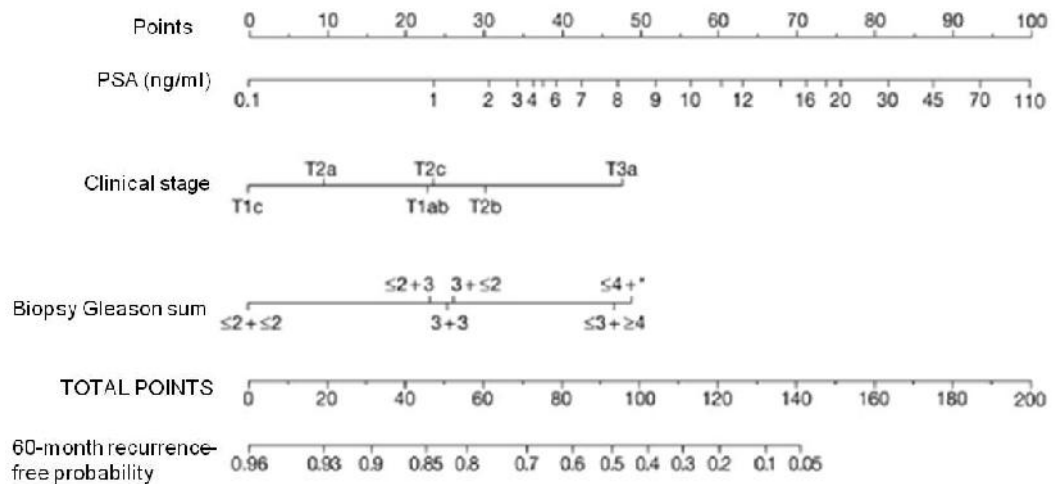


Figure 11. Kattan’s nomogram for predicting prostate cancer recurrence after radical prostatectomy. Adapted from Kattan MW *et al.* A preoperative nomogram for disease recurrence following radical prostatectomy for prostate cancer. *J Natl Cancer Inst* 1998;90:768.

D’Amico *et al* established a prostate cancer recurrence risk stratification scheme for patients undergoing radical prostatectomy and defined risk as low, intermediate or high [69] [Table 3].

Low risk	PSA ≤ 10 ng/mL, and Gleason score ≤ 6, and clinical stage T1c or T2a
Intermediate risk	PSA 10 - 20 ng/mL, or Gleason score = 7, or T2b
High risk	PSA > 20 ng/mL, or Gleason score ≥ 8, or T2c

Table 3. Prostate cancer risk stratification (from D’Amico *et al* [70])

Low-risk patients are most likely to remain disease-free following local therapy, whereas high-risk patients have an increased risk of subsequent biochemical failure and clinical progression. D’Amico’s risk stratification has

been widely used to counsel patients and help decide between active surveillance and active treatment. Low risk cancers generally have slow, often clinically insignificant progression with these patients more likely to die with the disease rather from it.

1.9.2. Anatomic open radical retropubic prostatectomy (nerve sparing procedure)

- The procedure is done through a midline, extraperitoneal, lower abdominal incision.
- Pelvic lymph node dissection is performed if indicated. The advantage of pelvic lymphadenectomy (PLND) during radical prostatectomy is to achieve more accurate staging, as it may influence decision-making with respect to adjuvant therapy. But this is at a cost of increase surgical morbidity and the risk of lymphoedema. The EAU guidelines 2011 reported that in D'Amico's low risk patient group, pelvic lymph node dissection is not necessary as the risk of positive lymph nodes does not exceed 7%. However, it should be performed in intermediate and high risk localised PCa. If PLND is undertaken, an extended approach should be performed to include the obturator and external iliac nodes as limited PLND (obturator nodes only) may miss at least half of the nodes involved.
- The endopelvic fascia is incised where it reflects over the pelvic sidewall and the incision is extended toward the puboprostatic ligament and the levator ani muscular fibers are released from the lateral surface of the prostate down to the apex

- The puboprostatic ligaments are divided to expose the junction between the prostatic apex and the anterior surface of the dorsal vein complex.
- The dorsal vein complex is divided. The precise point of division is important to ensure a negative margin at the apex, good urinary continence whilst avoiding blunt trauma to the neurovascular bundles.
- The prostatourethral junction is then well visualized. The urethra is transected as close to the apex as possible.
- The neurovascular bundle travels between the two layers of lateral pelvic fascia, the levator fascia and the prostatic fascia. To preserve the neurovascular bundle, the superficial layer of lateral pelvic fascia is released from the bladder neck, where it is thickest, and extended toward the apex of the prostate. The neurovascular bundle is then identified and released laterally and posteriorly from the prostatic apex to the midpoint of the prostate.

It has been reported [71] that the prediction of extraprostatic tumour extension (EPE) in the region of the neurovascular bundle (NVB) is greater than 10%, if 2 or more of the following are present:

- PSA >10ng/ml
 - Gleason score >6
 - Average % of biopsy core involved >20%
 - % of cores with tumour >33%
 - Positive DRE
- } Side specific

Therefore, excision of the neurovascular bundle is considered if any of the following occurs:

- Pre-operative factors:
 - Prediction of extra-prostatic extension based on the above features, Partin's table, and/or suspicion of ECE on prostate MR imaging.
 - Patient's desire to maintain sexual function.
 - Palpable apical lesion, high probability of capsular penetration (Partin's table).
- Intra-operatively:
 - Induration in lateral fascia
 - Fixation of neurovascular bundle to prostate
 - Inadequate tissue over lesion after prostate removal (delayed excision)
- Once the neurovascular bundle is freed, the prostate is mobilized to its midpoint, and the attachment between the Denonvilliers fascia and the rectum is divided up to the tip of seminal vesicles.
- Once the prostate is freed completely, the bladder neck is incised anteriorly at the prostatovesicular junction. The arterial branches from the inferior vesical artery to the prostate are ligated and divided. The seminal vesicles are freed from the posterior bladder wall which is then divided at the bladder neck.
- The prostate and the seminal vesicle specimen is removed and inspected for area of possible positive margins

- The bladder neck is reconstructed, sutured to the urethra, and a Foley catheter is placed.

1.9.3. Rationale for radical prostatectomy

In organ confined disease:

Radical prostatectomy is one of the recommended treatments for patients with stage T1 and T2 prostate cancer and a life expectancy of more than ten years. The prognosis is very good when the tumour is confined to the prostate.

In 2005, the Scandinavian Prostate Cancer Group (SPCG) [72] reported the results of a randomized control trial comparing radical prostatectomy with watchful waiting, in the management of early prostate cancer. They found that patients who were treated with radical prostatectomy had lower rates of prostate-cancer death, distant metastasis and local regression. These differences were mainly noticeable at ten years follow up with an absolute risk reduction of 5.3%, 10.2% and 25.1% for prostate-cancer death, metastasis and local regression respectively. The benefit of radical prostatectomy in reducing death from prostate cancer was greater in men aged less than 65 years. An update paper from the same group in 2011 reporting 15 years follow-up results [73], showed a cumulative incidence of death from prostate cancer at 15 years of 14.6% and 20.7% for surgery versus watchful waiting. The survival benefit was also noticed among men with low-risk disease and was confined to men younger than 65 years of age. The number needed to treat (NNT) to avert one death was 15 overall and 7

for men younger than 65 years. Among men who underwent radical retropubic prostatectomy (RRP), those with extracapsular invasion had a risk of death from prostate cancer that was 7 times greater than those without. The paper concludes that radical prostatectomy was associated with a reduction in the rate of death from prostate cancer and that men with extracapsular tumor growth may benefit from adjuvant local or systemic treatment.

The outcome of radical prostatectomy has been studied extensively in Europe and the USA. Most authors looked at follow up cancer specific and overall survival rates for at least 10 years. Table 4 summarizes some of the important studies.

Study	No of Pts	PSA Free Survival %	Metastatic Free Survival %	Cancer specific survival %	Overall Survival %
Gerber 1997 [74]	245		32	57	
Hull 2002 [75]	1000	75	84	98	
Ward 2005 [76]	841	43	73	90	76

Table 4. List of foremost studies looking at outcome following radical prostatectomy

Radical prostatectomy treatment modality was also compared to radical radiotherapy for localised prostate cancer. Kupelian *et al* [77] reviewed 787

patients who were treated with surgery alone or radiotherapy alone, and found a 5 year PSA relapse-free survival rate of 37% and 26% respectively, for high risk patients (PSA>10.0 or Gleason score >7) signifying a definite advantage of surgery, if negative margins were achieved. However, for low risk cases, there was no difference in outcome between radiotherapy and prostatectomy over 5 to 7 years follow up [77, 78].

Unexpectedly, The Prostate Cancer Intervention versus Observation Trial (PIVOT) study have been published in the *New England Journal of Medicine* in July 2012 [79]. The trial enrolled 731 men with localised prostate cancer between November 1994 and January 2002. Men were randomly assigned to either be treated with a radical prostatectomy (RP) or observation. All patients were followed until January 2010. Among men with localised prostate cancer detected during the early era of PSA testing, radical prostatectomy did not significantly reduce all-cause or prostate-cancer mortality, as compared with observation, through at least 12 years of follow-up.

In locally advanced prostate cancer:

Radical prostatectomy for T3 disease often results in incomplete tumour excision, leading to higher morbidity and higher risk of recurrence compared to patients with organ confined disease. Therefore, surgical treatment of clinical stage T3 prostate cancer has been traditionally discouraged.

In recent years, interest in surgery for locally advanced prostate cancer has grown. Clinical over-staging of PCa is relatively frequent and occurs in 23.5%

of cases. These patients would be disadvantaged if their cancers were considered as locally advanced disease and managed with other treatment modalities. Hsu *et al* [80] showed, in a study involved 235 patients with clinically T3 disease, a similarly good biochemical and clinical outcome after surgery for patients with T3 disease and negative margins compared with T2 disease. However, patients with positive margins or positive lymph nodes may require adjuvant or salvage radiotherapy or hormone therapy [81].

According to the guidelines of the European Association of Urology (EAU), radical prostatectomy is an accepted option in selected patients with limited T3a disease, Gleason score of ≤ 8 , PSA $< 20\text{ng/mL}$ and a life expectancy of more than 10 years [64]. If radical prostatectomy is performed, a non-nerve sparing approach and an extended pelvic lymphadenopathy should be performed.

1.9.4. Complications of radical prostatectomy:

Complications of radical prostatectomy according to EAU guidelines [64] are listed in the table below:

Complication	Incidence (%)
Peri-operative death	0.0-2.1
Major bleeding	1.0-11.5
Rectal injury	0.0-8.3
Pulmonary embolism	0.8-7.7
Lymphocele	1.0-3.0
Urine leak, fistula	0.3-15.4
Slight stress incontinence	4.0-50.0
Severe stress incontinence	0.0-15.4
Impotence	29.0-100.0
Bladder neck obstruction	0.5-14.6
Ureteral obstruction	0.0-0.7
Urethral stricture	2.0-9.0
Deep venous thrombosis	0.0-8.3

Table 5. Complications of radical prostatectomy (European Association of Urology guidelines, 2007)

The most common complications are bladder neck stenosis due to anastomotic stricture, urinary incontinence and impotence. Factors that may contribute to the development of an anastomotic stricture include previous transurethral resection of prostate, intraoperative blood loss and urinary extravasation at the anastomotic site. Stricture can be treated effectively with simple dilatation or cold knife incision.

Urinary incontinence remains the most troubling side effects of radical prostatectomy. It is usually secondary to intrinsic sphincter deficiency seen in older men, or damage to the smooth musculature of the urethra by deep suturing the anastomosis or injuring the neurovascular bundles. Preservation of the neurovascular bundles and selecting younger patients can play a role in decreasing the incidence of incontinence. Improvement in incontinence can occur up to 2 years post-surgery, but most commonly within the first year post operatively. Erectile dysfunction after radical prostatectomy is common. Predictive factors for recovery of potency are patient age, preoperative erectile function and the extent of neurovascular bundle preservation.

1.9.5. Radical prostatectomy with positive surgical margins:

A positive surgical margin is defined as the presence of tumour at the inked surface of the resected specimen. It is classified into extraprostatic and intraprostatic. An extraprostatic positive margin is when cancer is cut through after it has escaped the confines of the prostate i.e. cancer extends through the 'capsule' into fat. Whereas, intraprostatic positive margin is when cancer is cut through inside the glandular area of the prostate, therefore, the capsule and fat are missing from the specimen [82].

There are 3 major causes of margin positivity: 1) poor specimen handling leads to artificial positivity, 2) capsular incision and transection of intraprostatic tumour intraoperatively, 3) inability to excise extraprostatic tumour. The most common site of margin positivity is the apex, followed by

the lateral and posterior regions and then the anterior aspect and bladder neck.

Positive surgical margins are found to be an independent predictor of disease progression after radical prostatectomy. Epstein et al reported 10 years biochemical free survival of 79% in negative margin patients, versus 55% in positive margin following radical prostatectomy [83]. However, two factors in margin positivity affect tumour progression [35]. Firstly, the locations of the positive margins, as apical margins do not correlate independently with tumour progression, in contrast to bladder neck margin positivity. Secondly, the degree of margin positivity, with extensive or multifocal positive margins carrying a higher risk of tumour progression than solitary and focal positive margins.

Management of positive surgical margins is still controversial. Some urologists support the active surveillance strategy, as a good proportion of patients with positive surgical margins have long term survival and a reasonable disease-free progression rate [84]. On the other hand several authors [85, 86] have suggested immediate adjuvant treatment with radiotherapy in patients with positive margins, as this was found to improve PSA-free survival and reduce local progression compared with a watchful waiting strategy. The RADICALS trial is attempting to answer this question.

1.10. Pathology reporting of radical prostatectomy specimens

EAU guidelines in 2011 provide recommendations for Pathologists with respect to processing and reporting radical prostatectomy specimens and advise them to follow a standardized checklist. The specimen should be totally embedded either by conventional (quadrant sectioning) or by whole-mount sectioning (preferred). Then the entire surface of RP specimen should be inked before cutting to allow assessment of surgical margin status. The apex should be separately examined.

The pathologist should report the histological type and Gleason grade including the primary and secondary grade. Reporting the percentage of prostatic tissue involved is also preferred. Pathology staging should evaluate the presence of extraprostatic extension at any specific site, the presence of seminal vesicle invasion, the presence of lymph node metastases, including the number of involved nodes. Surgical margin involvement should be recorded if present and whether there is extra or intra-prostatic invasion.

CHAPTER 2

2. IMAGING OF PROSTATE CANCER

Patients who are clinically suitable for radical treatment are considered for radiological imaging to enhance the sensitivity and specificity of the predictive nomograms, to locate the cancer foci, and to exclude extracapsular extension, seminal vesicle involvement or lymphadenopathy.

2.2. Trans-rectal ultrasound scanning (TRUS)

Before the introduction of TRUS, transabdominal ultrasonography was used to detect and stage prostate cancer, with some overlap between the findings in benign and malignant disease [87].

Prostate imaging with endorectal sonography was first described in 1968 by Watanabe and colleagues [88]. The technique did not gain popularity until the late 1980s, when the development of PSA testing increased the need for TRUS biopsy. Initially, TRUS concentrated on the ultrasonic appearances of prostate abnormalities such as benign prostatic hyperplasia (BPH), carcinoma of the prostate, prostatitis, prostatic abscess, and prostatic calculi. Since the evolution of end-firing probes, TRUS has mainly been used to guide and monitor the entire process of needle prostatic biopsy.

Kuligowska et al reported low TRUS detection rates for malignancy, even when coupled with colour Doppler US, with typical values of 57% sensitivity, 61% specificity, 44% PPV, 73% NPV and 60% accuracy [89]. In this and other studies, more than half of prostate cancers were isoechoic with respect

to surrounding tissues and were missed at gray-scale and colour Doppler US. Moreover, benign hyperplasia may appear as a hypoechoic nodule similar to PCa appearance [90]. These results make TRUS an inadequate tool for PCa screening and diagnosis, therefore targeted biopsy should always be accompanied by complete standardized biopsy sampling.

With regard to staging, the specificity of TRUS alone for staging locally advanced disease (T3) was only 25.3%, with sensitivity, PPV and NPV of 80.2%, 47.1% and 60.7% respectively [91]. With known poor staging accuracy rate and operator dependence, TRUS is not recommended as a staging method but still plays a major role in accurately sampling a wide-area of prostatic tissue.

2.3. Computer Tomography (CT)

CT has been employed in newly diagnosed PCa mainly for radiotherapy planning and assessing lymph node metastasis and has an accuracy rate of about 70%. However, due to its low diagnostic staging accuracy of 24% for extraprostatic extension [92], CT lacks the precision needed to evaluate local spread, and newer, more accurate imaging modalities should be used to decide whether or not to proceed to radical prostatectomy.

2.4. Positron emission tomography (PET)

PET studies have been introduced for identifying and localizing prostate cancer. It was found that other prostatic disorders can accumulate choline similar to prostate cancer lesions. PET/CT has been shown to have a high

false negative rate, with a sensitivity of 66% and negative predictive value of 55%, which precludes its use for prostate cancer screening, detection or staging [93].

2.5. Evolution of Magnetic Resonance Imaging

(MRI):

The first successful nuclear magnetic resonance (NMR) experiment was made in 1946 independently by two scientists in the United States (Felix Bloch and Edward Purcell). It was not until the early 1970s that magnetic field gradients were introduced enabling the development of MR imaging. In 1977 the first human body images were obtained by Damadian, using a prototype superconducting magnet.

MRI has particular advantages over CT in that it uses non-ionising radiation, and has high soft tissue resolution and discrimination in any imaging plane. It also provides both morphological and functional information.

MRI of the prostate appears to be the best imaging modality for identifying locally advanced disease [94]. This is due to its excellent soft tissue contrast which allows depiction of the prostate gland zonal anatomy [Figures 12, 13], seminal vesicles [Figure 14] and prostate margins and its relationship to surrounding structures in the pelvis.

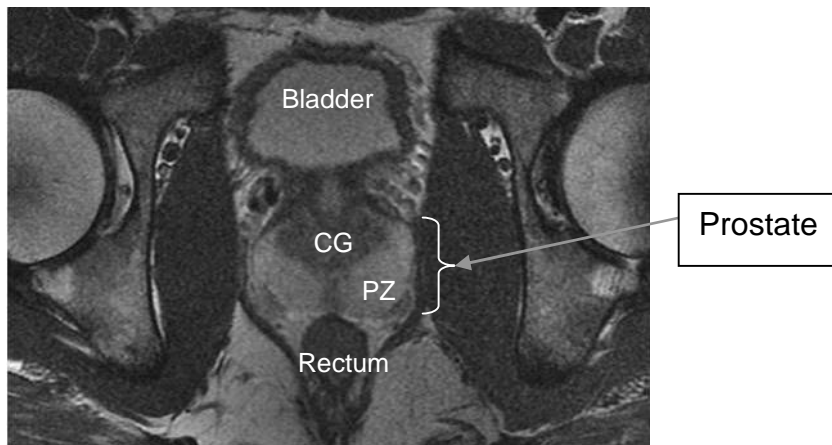


Figure 12. Normal prostate anatomy in a young man, detailing prominent peripheral zones (PZ) and small central gland (CG).

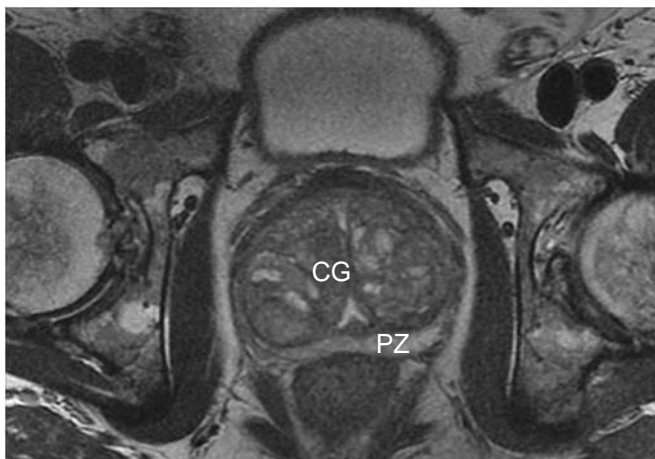


Figure 13. Benign prostatic hypertrophy involving the central gland and compressing the peripheral zones in a man over 60.

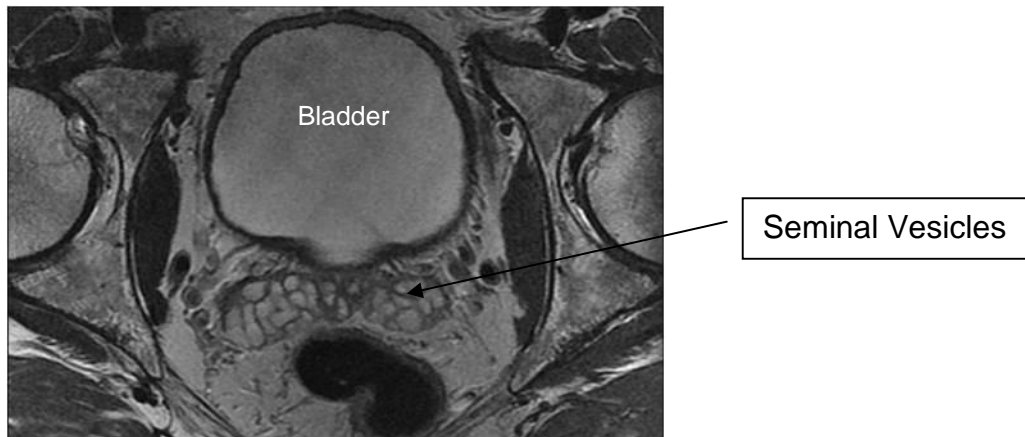


Figure 14. Normal looking seminal vesicles.

MR imaging of the prostate most commonly employs T2 and T1 weighted imaging with most systems operating at 1.5 Tesla. This has produced variable results for staging accuracy, in particular for detecting ECE and SVI. Rouvière et al., in a meta-analysis of 10 studies all performed at 1.5 Tesla [Table 6], reported staging accuracy rates ranging from 60-80%, with a mean sensitivity and specificity of 53% and 83% respectively [95].

In another meta-analysis study, the authors summarized the receiver operating characteristic curve from 23 reports which described the performance of MR imaging, using a field strength of 1.5 Tesla or less, to stage prostate cancer. They found a maximum pooled sensitivity and specificity of 74% [96]. As a result, MRI has not been widely accepted by urologists, especially for patients with low risk of extracapsular disease [97].

	N	Se (%)	Spe (%)	PPV (%)	NPV (%)	Accuracy (%)
Outwater et al	30	68	72	32	-	71
Harris et al	50	57/20 ^a	61/100 ^a	36/100 ^a	79/65 ^a	64/68 ^a
Jager et al	34	36	89	36	88	79
Chefchaomi et al	47	52	100	100	72	79
Presti et al	56	91	49	51	90	-
Yu at al	77	82/47/59 ^b	72/74/67 ^b	70/59/59 ^b	84/64/67 ^b	77/62/64 ^b
Bates at al	20	38	100	-	-	-
Yu et al	53	54/17 ^c	95/94 ^c	76/44 ^c	88/79 ^c	85/76 ^c
Ikonen et al	44	22	99	-	-	95
Corund et al	336	38	94	-	-	77

N number of patients; Se sensitivity; Spe specificity; PPV positive predictive value; NPV negative predictive value.

^a *Results obtained in the 25 first cases/25 last cases*

^b *Results obtained by independent readers with an experience of 3 years/1 year/6 months*

^c *Results obtained by independent readers with an experience of 5 years/2 years*

Table 6. Detection of extracapsular tumour extension on T2 weighted imaging at 1.5T (Rouvier et al)

3 Tesla (T) whole body MR scanning has come into clinical practice since 2002. The rationale for using 3T MR systems is that the higher static magnetic field strength increases the signal intensity achieved without altering the noise. In comparison with 1.5T the signal-to-noise ratio (SNR) [98, 99] is increased by approximately a factor of two at 3T. The increased SNR can be used for higher resolution imaging or reduction in scan time. By employing parallel imaging techniques, the temporal resolution of the MR measurements can also be significantly improved. Better spatial resolution results in the use of a smaller voxel size and hence an improvement in the pathoanatomic details compared to 1.5 T [100].

Additionally the superior temporal resolution for any given region of interest provides better delineation of changes in tissue signal intensity observed during contrast administration. As a consequence of these improvements, the use of MRI for prostate staging is being revisited at 3T with promising early results. In 2006, Kim *et al* examined the detection and depiction of prostate cancer using dynamic contrast-enhanced MR imaging (DCE-MRI) at 3T [101]. The sensitivity, specificity, and accuracy for prostate cancer detection were 55%, 88% and 70% for T2-weighted imaging and 73%, 77%, and 75% for DCE-MRI, respectively. Futterer *et al* assessed the staging accuracy of prostate MRI at 3T compared with histopathology. The author reported 94% accuracy, 88% sensitivity, and 96% specificity for local cancer staging [102]. Researchers have used different techniques to identify malignant lesions and stage the disease and have compared the results with either TRUS biopsies or radical prostatectomy specimen pathological findings. Different methods were used including endorectal coil imaging, diffusion weighted imaging, spectroscopy and DCE-MRI at 3T to improve detection and staging accuracy rates for cancer.

2.6. Basic MR Principles

2.6.1. MRI components:

An MR system consists of the following components:

- 1) A large magnet to generate a strong magnetic field. Magnetic field strength is measured in units of gauss (G) or Tesla (T). One Tesla is equal to 10,000

gauss (the earth's magnetic field is about 0.5 gauss). A 3T MR scanner (GE Healthcare Ltd.) is used in our centre.

2) A radiofrequency (RF) coil is used to transmit a radio signal into the body part being imaged to excite the protons.

3) A receiver coil is used to detect the returning radio signals. An example of a receiver coil is a surface coil composed of a loop of wire, either circular or rectangular, that is placed over the region of interest. Another example is an endorectal coil which is placed in the rectum close to the posterior aspect of the prostate. This provides better signal-to-noise ratio and hence better image resolution.

The effective field of view (FOV) is proportional to the diameter of the surface coil, while the signal-to-noise ratio (SNR) is inversely proportional to the coil size. Therefore, a small surface coil provides the best SNR, but has a limited FOV. This led to the development of phased-array coils, which contain a number of small coils that are used simultaneously to receive the MR signal and reconstruct a composite image. Phased-array coils provide a large FOV, but with the SNR of a small surface coil. This provides a higher spatial resolution and allows thinner slices to be acquired.

A further advance in coil usage includes the development of an integrated endorectal-pelvic phased-array coil. This gives a combined image from both coils for improved SNR and thus better visualization of anatomy [Figure15].

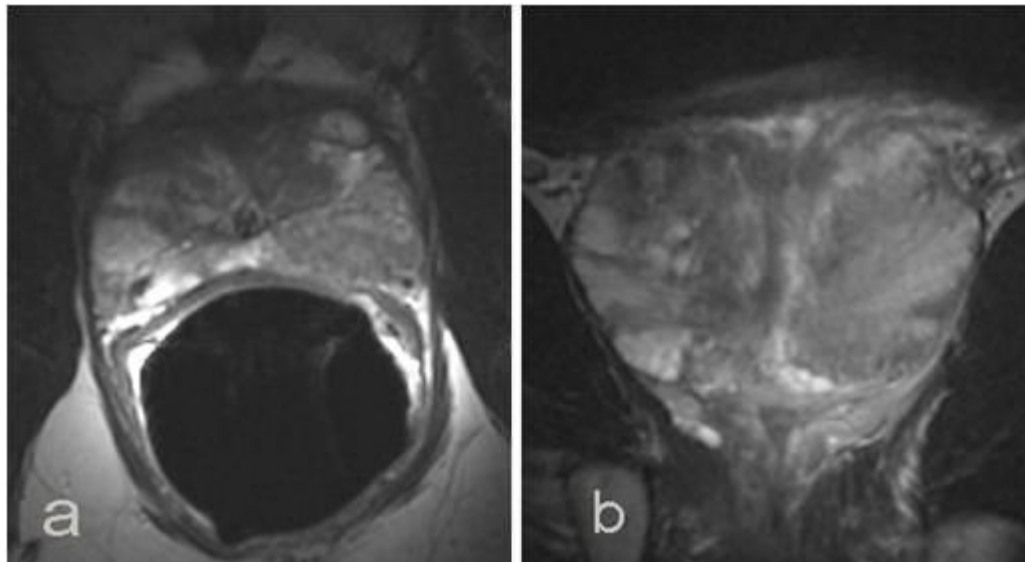


Figure 15. Prostate MR Image using integrated endorectal-pelvic phased-array coil. The endorectal coil is seen in the rectum and filled with air to stabilize it. Axial image (a) and coronal image (b) showing great anatomical details.

- 4) Shim coils to make the magnetic field as homogeneous as possible.
- 5) Gradient coils to produce deliberate variations in the main magnetic field (B_0). There are usually three sets of gradient coils, one for each direction, namely x, y and z. The variation in the magnetic field is used to provide spatial localisation of the signals.
- 6) A computer to reconstruct the radio signals into the final image.

2.6.2. Basic physics:

Protons have a positive electrical charge and are constantly moving like a spinning top. This movement induces a local magnetic field. When a nucleus is placed in the magnetic field of an MRI scanner, proton nuclei align with the main magnetic field (B_0) in two ways: parallel and anti-parallel. The parallel

position is slightly favored, as the nucleus is at a lower (preferred) energy in this position. This results in a net magnetisation pointing in the longitudinal direction of the main magnetic field and this forms the basis of the MR signal. Exposure of individual nuclei to radiofrequency (RF) energy (B1 field) causes nuclei in the lower energy state to jump into the higher energy state, which causes the net magnetisation to spiral away from the B0 field (anti-parallel). This causes a decrease in the longitudinal magnetisation (potentially to zero) and also establishes a transversal magnetisation due to the spinning movements of the protons, [Figure 16] which is termed precession. After a certain length of time, the net magnetisation vector rotates through 90 degrees and lies in the transverse or x-y plane. This rotating angle is called the flip angle.

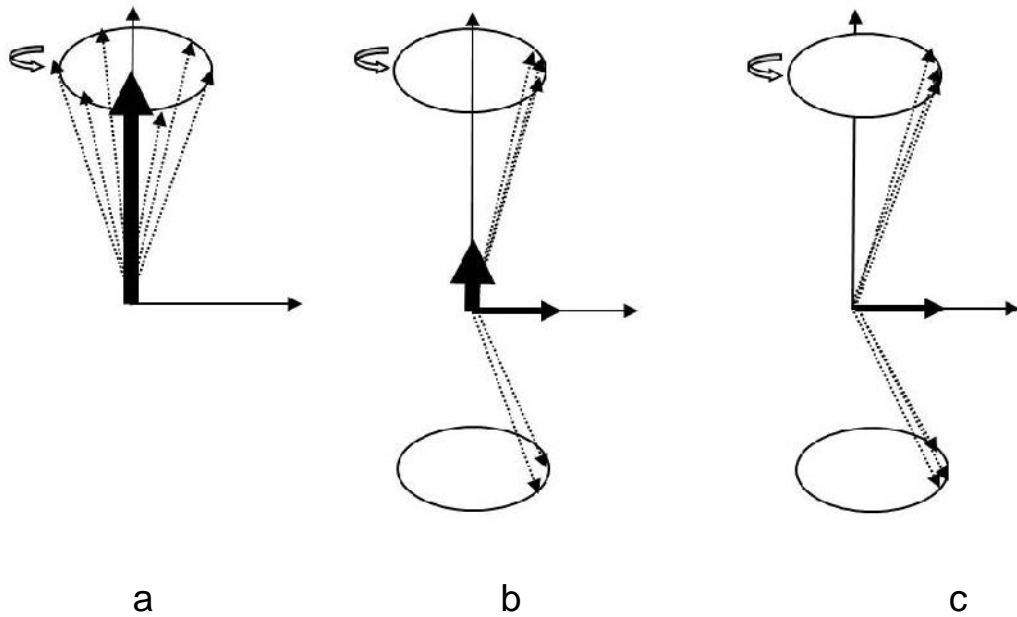


Figure 16. : Longitudinal magnetic vector (a) at B_0 , a new transverse magnetic vector is formed and decrease in longitudinal vector when applying RF pulse (b), longitudinal vector may disappear depending on RF pulse (c). Modified from original Source: MRI from A to Z: A Definitive Guide for Medical Professionals by Gary Liney [103].

The proton spins return to equilibrium when the RF pulse is stopped. Therefore, the transverse magnetisation disappears and the longitudinal magnetisation grows back to its original size. Different “pulse sequences” can be achieved by changing the strength, duration and nature of the RF pulse given.

2.6.3. *T1, T2, TR and TE*

T1 relaxation:

This is characterized by the return of the longitudinal magnetisation in the direction of the main magnetic field to its ground state, so called the longitudinal relaxation. It is associated with loss of energy to the surroundings the so-called lattice, hence the name spin-lattice relaxation. The T1 relaxation time is the time for the longitudinal magnetization to recover to 69% of its original length. . Five times T1 indicates full recovery.

T2 relaxation:

This is characterized by the loss of the transverse magnetisation. This is not associated with loss of energy to the surrounding lattice, therefore, it is called spin-spin relaxation. The T2 relaxation time is the time for 69% loss of signal due to dephasing. Five times T2 would be full loss of transverse magnetisation.

Different tissues have varying T1 and T2 relaxation times. For example, water has a long T1 and a long T2, whereas fat has shorter T1 and T2.

Time to repetition (TR):

This is the time taken to repeat the RF pulse [Figure 17]. Using a short TR helps to differentiate between tissues by their differences in T1 relaxation time, since tissue with a long T1 time will be hit by the next RF pulse before the longitudinal vector grows back to its original size, leading to a short transverse vector in the subsequent excitations. The resulting picture

showing the differences in signal intensity of tissues due to the differences in T1 relaxation time is called a T1-weighted image.

Time to echo (TE):

This is the time between the initial 90 degree RF pulse and the spin echo (the signal received after the 180° pulse) [Figure 17]. Sending a 180° pulse at a certain time (half of TE) makes the protons turn around and precess in the opposite direction which enhances the signal returned from tissue. Using a long TE time helps to differentiate between tissues by maximising the differences in T2 relaxation times. Tissues with long T2 relaxation times, such as fluid, give a higher signal on T2 weighted image.

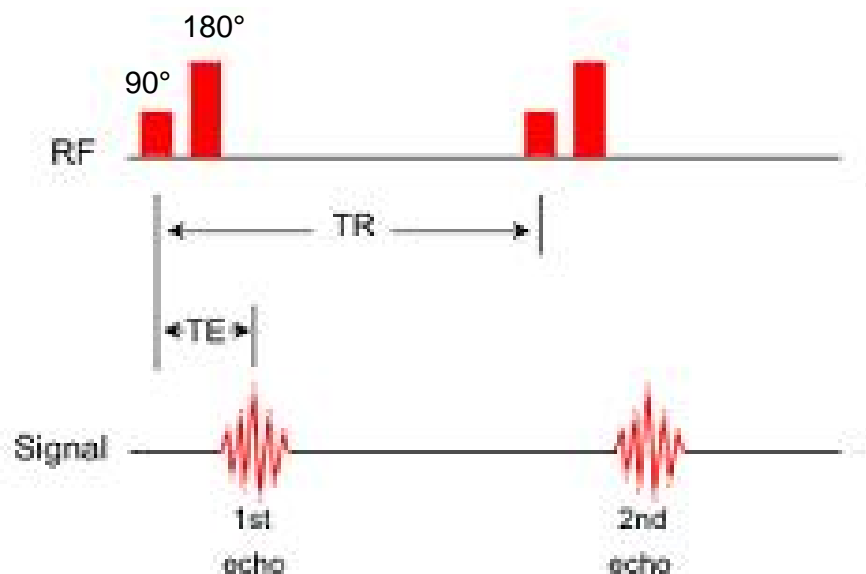


Figure 17. Spin echo pulse sequence showing the time to repetition (TR) between two radio frequency pulses giving two signals, and time to echo (TE) between the initial 90 degree RF pulse and the signal received after 180 degree RF pulse.

A T2 weighted image has a long TR and a long TE. A T1 weighted image has a shorter TR and a short TE.

A proton density image has a long TR and a short TE. It is neither T1 nor T2 weighted, but is mainly affected by the difference in proton density present. The more protons, the higher the signal obtained. Using the spin echo pulse sequence, the timing can be adjusted to give T1-weighted, proton density, or T2-weighted images.

In the prostate gland, the peripheral zones are formed mainly by glandular tissue which contains a high concentration of fluid and therefore has a long T2 and T1 resulting in high signal intensity on T2 weighted image (looks bright). In prostate cancer, there is displacement of fluid within the acini by tumour, which leads to a shorter T2 (looks dark on T2 weighted imaging) [figure 18].

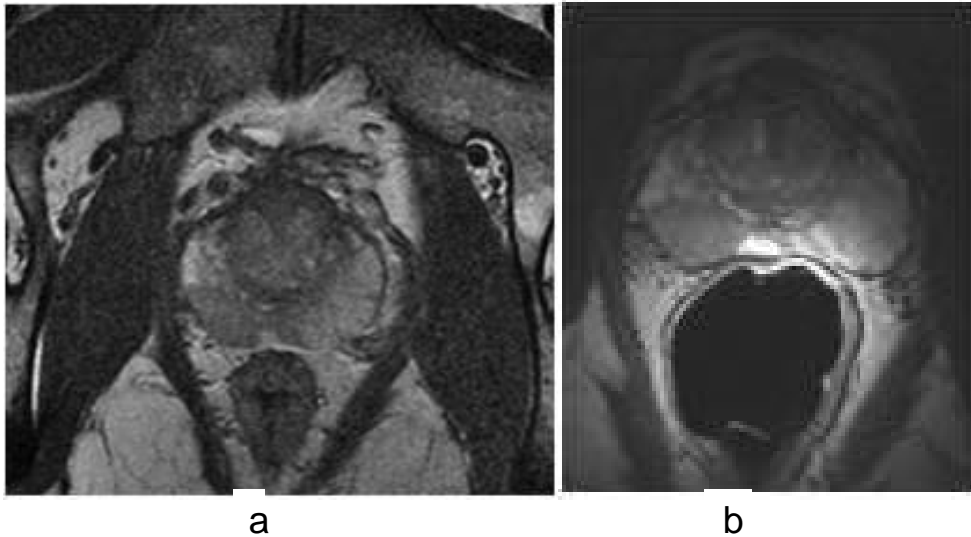


Figure 18. T2 weighted image of prostate using the pelvic phased array coil (a) and the endorectal coil (b). This shows a normal left peripheral zone (bright) and a malignant lesion in the right peripheral zone (dark). Brightness flare occurs in the peripheral zones of the gland due to the proximity of the coil to the gland and signal decrease in the anterior part of the gland.

Blood products present in the prostatic tissue secondary to haemorrhage following biopsy have short T1 and T2, therefore look dark on T2 weighted images and bright on T1 weighted images [Figure 19].

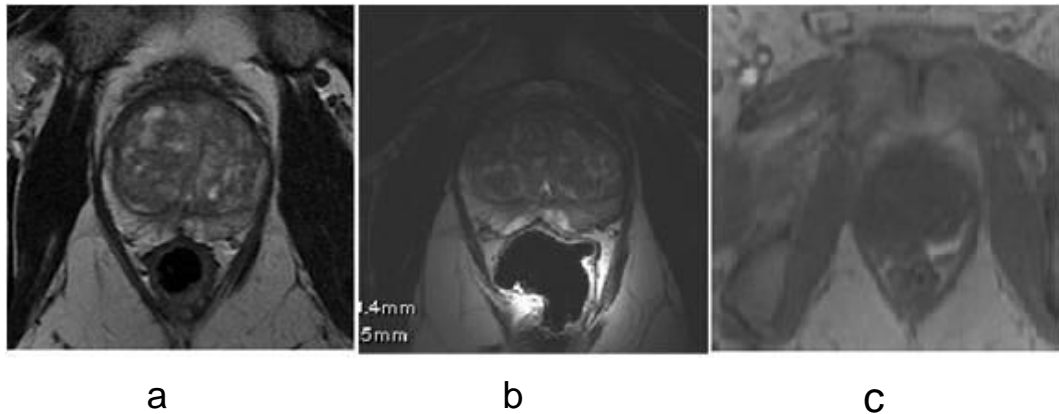


Figure 19. T2 weighted images using the pelvic phased array coil, showing an area of low signal intensity in the left peripheral zone (a). Same lesion is seen on endorectal imaging (b). T1 weighted image showing the corresponding location with an area of haemorrhage seen as a “bright” area in the left peripheral zone (c).

The scan time is mainly affected by TR, matrix size and number of excitations (NEX). Increasing any one of these parameters increases the minimum scan time.

The matrix is an array of numbers in rows and columns (frequency and phase encoding steps). A matrix with m rows and n columns is called an m x n matrix (m and n are called its dimensions). The MR matrix is used to determine the scan resolution. Increase in matrix size produces better

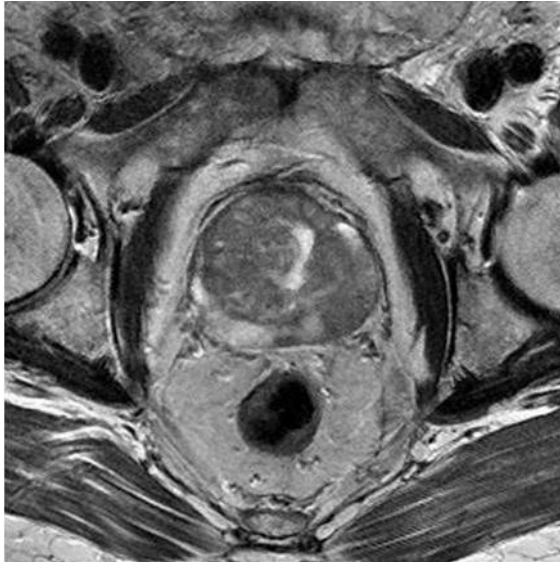
scan resolution, but increases the scan time. For relatively high resolution prostate imaging we used a matrix of 384 x 256.

The number of excitations (NEX) refers to the repetition of the signal measurements several times. By summing the signal generated, the SNR is improved resulting in better image quality, but the imaging time increases.

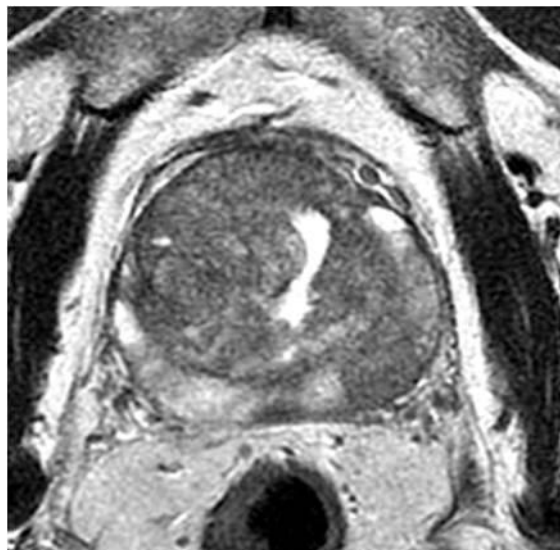
Spatial resolution determines how "sharp" the image looks. Low resolution will give either fuzzy edges, or a pixelated appearance to the image. Spatial resolution is determined by matrix size and field of view (FOV). Increasing the matrix size or decreasing the FOV increases spatial resolution, but at the expense of either decreased signal-to-noise or increased scan time. To obtain images of high resolution with high signal-to-noise requires longer scan times.

Field of view (FOV) is the image area that contains the region of interest to be examined. It is defined in units of mm². Dividing the FOV size by the matrix size gives the voxel size; hence, increasing the FOV in either direction increases the size of the voxels and decreases the resolution. The smaller the FOV the higher is the resolution and the smaller the voxel size. Choice of FOV size depends on the clinical question that needs to be answered. In prostate imaging a large FOV covering the pelvis with a reasonable image resolution is obtained to assess the pelvic lymph node status and bony pelvis [Figure 20a], whereas a smaller FOV with much

higher image resolution is obtained to image the prostate and assess tumour location and capsular involvement [Figure 20b]



a) Low resolution, high FOV image
Image parameters:
FSE-XL;
TR=4000 ms; TE=97 ms;
BW 31.7;
thk=5mm, 1mm gap;
matrix=512x384, 2NEX;
FOV 24x24;
acq time=5:49



b) High resolution, small FOV image
Image parameters:
FSE-XL;
TR=3000 ms; TE=97 ms;
BW 41.7;
thk=3mm, 0mm gap;
matrix=384x256,
4NEX;
FOV 20x20;
acq time=6:50.

Figure 20. Low resolution pelvic image (a) is useful for detecting pelvic lymph node disease and bony disease, whereas high resolution image (b) is mainly to look at the prostate anatomy and pathology.

Choosing the best slice thickness is very important to answer the clinical question. Thin slices covering only the studied organ give precise details to

identify abnormalities for that organ. Thicker slices with wider field of view are useful in overall assessment of the surrounding structures.

Signal-to-noise (SNR) ratio is measured by calculating the difference in signal intensity between the area of interest and the background. Many of the scan parameters affect signal-to-noise. The signal within an image can be improved by increasing TR, FOV, slice thickness and NEX or by decreasing TE and matrix size.

2.6.4. *Contrast agents and dynamic contrast enhanced MRI (DCE-MRI)*

Dynamic contrast enhanced imaging techniques use fast MRI sequences to repeatedly image a volume of interest during the intravenous administration of contrast agents. MR contrast agents such as gadolinium di-ethylene-triamine-penta-acetic acid (Gd-DTPA) were first introduced into clinical MR practice by Heywang *et al* in 1986 [104]. This was the first paramagnetic agent approved for clinical use, and was used initially for breast and brain MR imaging.

Gadolinium is a low molecular weight paramagnetic agent which is toxic in its free state; hence it is bound to DTPA to prevent toxicity. It has an effect on signal intensity by shortening T1 and T2 relaxation time, based on the assumption that there is a linear correlation between the tissue concentration of Gd-DTPA and the longitudinal relaxation rate, R1 [105]. Therefore, it causes an increase in the signal intensity of tissue on T1-weighted images

(which is the predominant imaging technique used after contrast medium injection). This is termed enhancement. Tissues that take up contrast look bright on T1 weighted imaging [Figure 21].

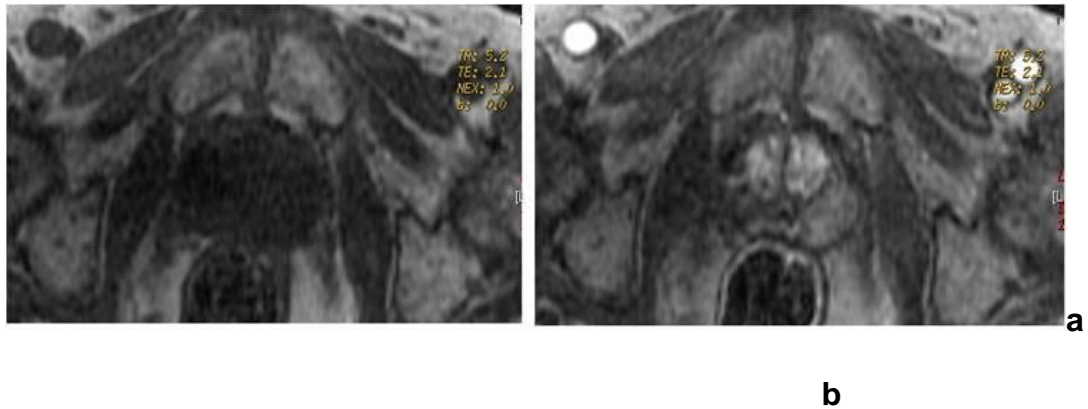


Figure 21. T1 weighted images of the prostate. Pre (a) and post (b) contrast administration. The area suspicious of malignancy on the left PZ, takes up contrast and looks bright on T1 weighted image post-contrast. Also note the enhancement of the vessels.

Following the intravenous injection of Gd-DTPA, it is rapidly distributed throughout the blood plasma extravasates into the interstitial space (wash-in phase) and then diffuses back into the vasculature (wash-out phase). Since the GD-DTPA is not distributed equally throughout the body, but is taken up by vascularised tissue, signals from different tissues will be affected differently. This causes an enhancement of vascular malignant tumours and these can be identified from the surrounding non-enhanced tissues [Figure 22].

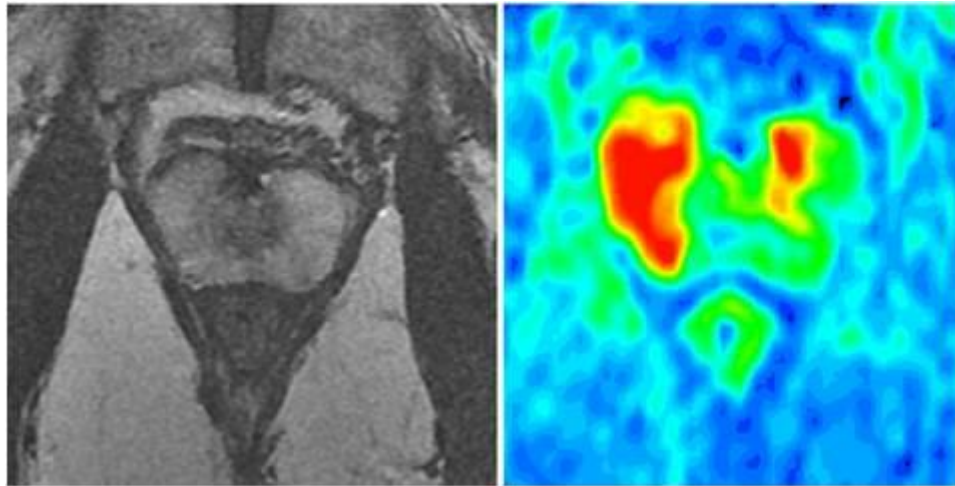
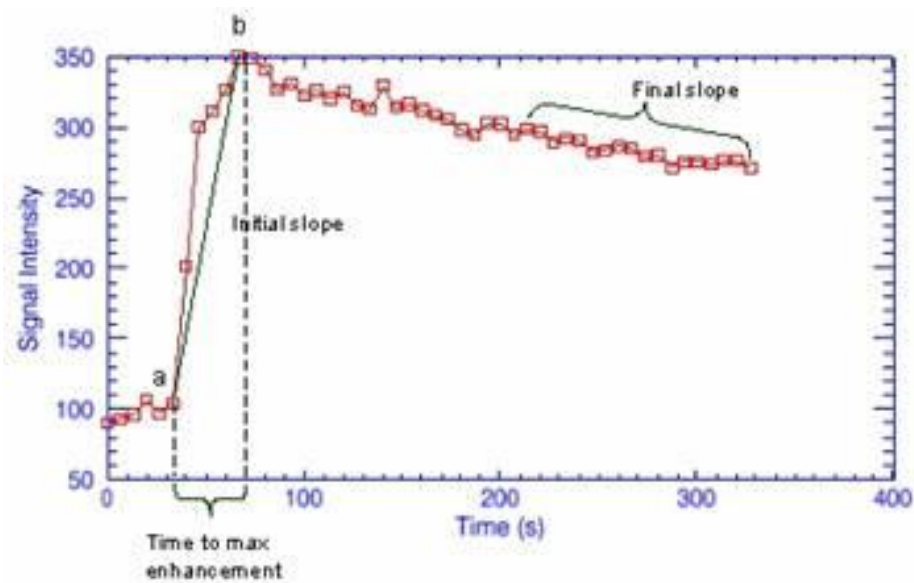


Figure 22. Showing the enhancement of malignant tissue in the prostate gland, which is not otherwise seen on T2 weighted imaging. On the left is a T2 weighted image showing a slightly darker right peripheral zone compared to the left but not diagnostic of cancer. On the right is the contrast enhanced image showing the increased uptake (demonstrated by the red areas) in both peripheral zones. Histology confirmed cancer in the areas highlighted in red.

The time course of the enhancement effects reflects the status of tissue microcirculation and can be monitored by dynamic contrast-enhanced MRI (DCE-MRI). DCE-MRI was introduced by Kaiser *et al* in 1989 [106]. It was initially studied in breast MRI. The authors acquired images of the region-of-interest pre contrast and subsequently every 60 seconds during and after contrast injection giving a time course of images. They measured the signal intensity changes that occurred in the early post contrast period.

By dynamically acquiring MR data, it allows generation of tissue contrast concentration time curves which can be used in pharmacokinetic studies. In

other words, it allows measurement of the signal intensity (SI) of regions of interest (ROI) before arrival of contrast agent (base line); and observes the increase in SI during the wash-in phase and the decrease of SI during the wash-out phase. As well as construction of SI time curves [Figure 23] this technique allows the measurement of various dynamics parameters of contrast enhancement, such as maximum enhancement Index (MaxEI), time to maximum enhancement (Tmax), initial and final



slopes.

Figure 23. Signal intensity – time curve for a typical malignant lesion: The enhancement curve consists of an early upslope to reach peak intensity and a wash-out phase. The figure shows the time point at which contrast reaches the prostate (a) and the maximum enhancement (b) achieved. Time to maximum enhancement (a-b), initial and final slopes can be obtained as shown.

Maximum enhancement index (MaxEI) is defined as the peak SI achieved during the dynamic examination. Time to maximum (Tmax) is defined as the

time taken for the SI to reach its maximum (MaxEI). Enhancement index at 30s (EI at 30s) is defined as the percentage rise in signal at 30s, compared to the initial pre-contrast signal. Initial slope is defined as the SI change in the first 30s following contrast administration. This reflects the wash-in phase. Final slope is defined as the SI change for the final 2 minutes of the SI time curve. This reflects the wash-out phase. The area under curve (AUC) is defined as the integral of the percentage enhancement over the first 4 minutes of contrast uptake.

These parameters were found to be strongly related to tumour blood flow, the capillary permeability, and surface area. They have been used successfully to differentiate between cancer and normal tissue in the breast, bone, and brain. Kuhl *et al* [107] subdivided the signal intensity time curve into three types depending on the curve shape: type I, a steady enhancement; type II, signal intensity reaches a plateau after the initial rise; or type III, washout of signal intensity occurs during the duration of the examination. The authors found that the shape of the signal intensity time curve is an important factor in differentiating between enhancing benign and malignant lesions, as the type III time course is a strong indicator of malignancy [Figure 24].

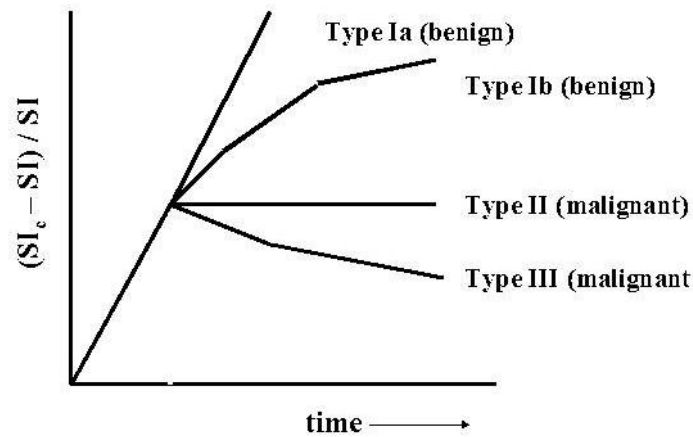


Figure 24. Shapes of signal intensity curves as demonstrated by Kuhl *et al.* Type I shows continuous enhancement throughout the dynamic study, either as a straight line Ia or curved line Ib. Type II is a plateau curve following an upstroke. Type III is a rapid washout time course.

Using this method, Kuhl reported a sensitivity of 91%, a specificity of 83% and an accuracy of 86% in distinguishing benign from malignant breast lesions [107].

Pharmacokinetic modelling is a mathematical process that uses all the signal intensity data to give numeric values relating to the permeability and the contrast exchange rate between the plasma and the extra-vascular extra-cellular space (K^{trans}), the blood volume (V_b) and extra-cellular extra-vascular volume (V_e) of a region of interest.

Studies have demonstrated altered pharmacokinetic parameters in regions of increased enhancement in the prostate when compared with normal

peripheral zone at 1.5T [108, 109]. These parameters can be used to differentiate benign from malignant lesions objectively and may provide additional information useful in diagnosis, staging and localisation. Schlemmer et al [110] demonstrated an association between the pharmacokinetic parameters obtained from DCE-MRI and tumour angiogenesis, in particular, microvascular density in prostate cancer.

Pharmacokinetic modelling also allows researchers to display K^{trans} maps [Figure 25] for better identification of tumour site and extent based on abnormal vascular morphology.

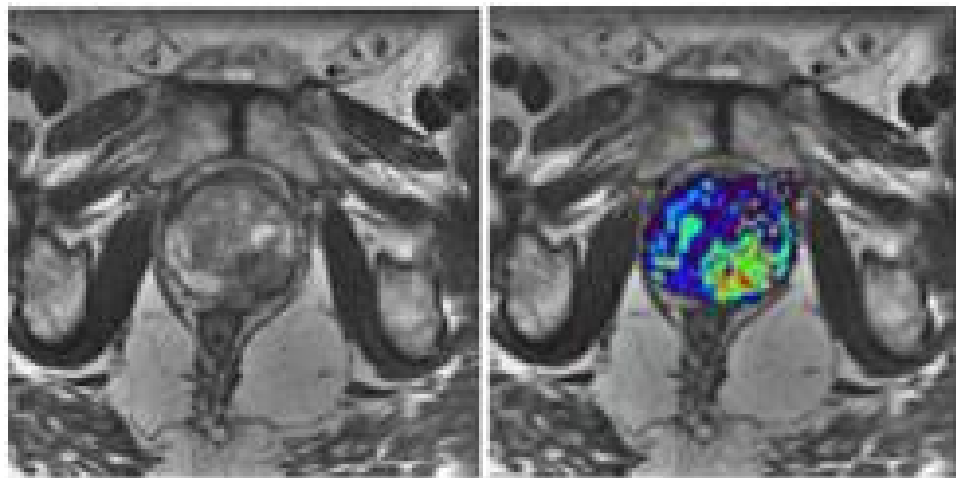


Figure 25. PK map (right) showing an area of increase permeability which correlates with low signal intensity on the corresponding T2 weighted image (left).

There has been a significant rise in the clinical use of DCE-MRI in prostate cancer. Although T2 weighted imaging can show the areas of malignancy in

the peripheral zones of the gland, other pathologies such as haemorrhage and scarring can mimic the appearance of tumour on T2 weighted imaging, leading to low sensitivity [111], while other tumours may be isointense with normal tissue leading to a low specificity [103]. This led to the inclusion of DCE MRI as part of the MR investigations for prostate cancer. It has become a promising diagnostic tool in the management of prostate cancer through its ability to spatially map the increased microvascular density and permeability that is associated with malignant tumour growth. DCE has been shown to significantly improve prostatic tissue characterisation and in turn the diagnostic and staging accuracy. At 1.5T, DCE-MRI improves accuracy, sensitivity and specificity for prostate cancer detection by 26%, 31% and 22% respectively relative to T2-weighted imaging as reported by Kim *et al* [112]. The same group assessed the use of DCE MRI at 3.0T, with higher temporal and spatial resolution, and again found it to be superior to T2-weighted imaging since 15 out of 64 cancers were detected only by DCE MRI.

The diagnostic accuracy of DCE-MRI in prostate cancer is further discussed in Chapter 3.

2.6.5. Diffusion weighted imaging:

Diffusion weighted imaging (DWI) is an MRI technique that is dependent on the random movement of water molecules (Brownian motion) in the studied organ. This reflects the diffusion of water in the interstitial space, providing information on the biophysical properties of the tissue such as extracellular

fluid, cell density and tissue organisation. The diffusion properties of the tissue examined can be quantified by calculating the diffusion coefficient of water, known as the apparent diffusion coefficient (ADC). It is called apparent because its value is influenced by the water diffusion as well as other factors including perfusion and T2 relaxation time of tissue. It can be calculated by acquiring a minimum of two images with different gradient duration and amplitude (*b* value). The *b* value is a parameter that reflects the degree of diffusion weighting. The ADC can be mapped on to an anatomical image, using diffusion as the contrast. This allows visual assessment of the location of the tumour as it appears as an area of decreased signal [Figure 26].

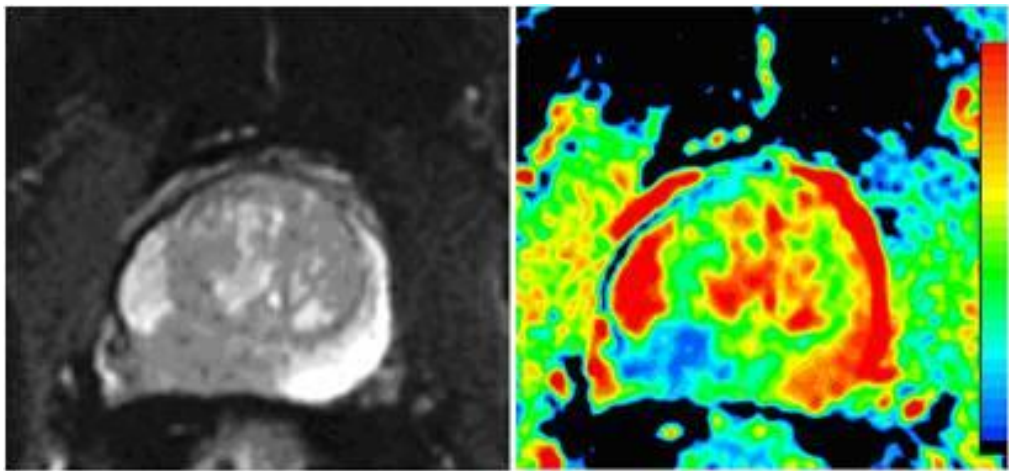


Figure 26. Diffusion weighted image of prostate gland (a) showing an area of low signal intensity in the right peripheral zone representing a malignant lesion. Corresponding ADC map reflecting low ADC in right peripheral zone using *b*-values of 0 and 500 s/mm² (b).

The acquired map depends on the spatially distributed diffusion coefficient of the region of interest which is independent from T2 weighted value. Diffusion-weighted imaging has the distinct advantage of being acquired very rapidly, and creating an enhancement map without the use of contrast.

In 1950, Hahn *et al* discovered that the MR signal was influenced by diffusion. In 1965 when Stejskal and Tanner [113] introduced the pulsed gradient spin echo the development of diffusion weighted imaging (DWI) began. It is the only technique that is able to assess molecular diffusion in vivo and it has been shown to have diagnostic potential.

The first successful clinical application of DWI was in imaging the brain of patients who had suffered from acute stroke. Areas which were injured during a stroke showed up "darker" on an ADC map compared to healthy tissue [114]. MR diffusion weighted imaging was then examined in breast cancers and reduction in ADC values was noted in malignant breast lesions [115, 116].

The role of DWI in prostate cancer has been evaluated and the technique found to be feasible. The extensive ductal structure of the normal prostate compared with the highly restricted intracellular and interstitial spaces encountered in prostate cancer, produces substantial differences in water diffusivity and thus the potential for high image contrast. The clinical role of DWI in prostate cancer evaluation has been studied on 1.5 and 3.0T field strength scanners. Reports have shown its efficacy, as a sole technique, in

differentiating cancer lesions from normal peripheral zone (PZ) [117-120] with sensitivity and specificity for tumour identification ranging from 84 to 94% and 72 to 91% respectively. Miao et al [121] showed that DWI has a better performance in prostate cancer detection compared with T2 weighted imaging alone (area under the ROC curves of 0.89 for DWI versus 0.82 for T2w imaging). These findings were supported with results from other studies [122, 123] which have also showed the superiority of combined DWI and T2 weighted imaging compared to T2 weighted imaging alone (AUC of 0.89-0.93 versus 0.81-0.87 respectively). Mazaheri et al [124] also showed the improved differentiation between tumour and PZ using combined data from DWI and spectroscopy compared to spectroscopy alone (AUC of 0.85 versus 0.74 respectively).

With advances in MR gradient coils, single shot echo planar imaging (EPI) has emerged as the technique of choice for diffusion measurements in the prostate providing better resolution ADC images [125]. A study by Issa et al [126] using EPI DW imaging also showed statistical differences in ADC values between normal PZ, BPH and cancerous prostatic regions.

In Chapter 4, I describe my experience in MR diffusion imaging on a 3.0T system using whole mount radical prostatectomy specimen as a reference.

Chapter Three

3. THE CLINICAL ACCURACY OF MULTI-SEQUENCE MRI AT 3 TESLA IN LOCALISING AND STAGING PROSTATE CANCER

3.1. Objective

The aim of this study is to assess the accuracy of 3 Tesla MRI for cancer staging and lesion localisation in patients with newly diagnosed prostate cancer. High resolution T2 weighted images, endorectal imaging, and dynamic contrast-enhanced MRI (DCE-MRI) were used and compared with pathological findings from whole mounted radical prostatectomy (RP) specimens.

3.2. Methods

3.2.1. Patients selection

Approval from the Local Ethics Committee was granted to analyze data from patients who were scanned at the University of Hull, Centre for Magnetic Resonance Investigations (CMRI).

All patients had histological confirmation of prostate cancer diagnosis based on trans-rectal ultrasound guided biopsy (TRUS). This was performed by a consultant radiologist or an experienced sonographer from Hull and East Yorkshire NHS Hospitals.

Patients were then reviewed in the outpatient urology clinic to discuss the diagnosis of prostate cancer, explain further staging methods and the treatment options. All patients who are considered for radical prostatectomy were referred for MR prostate examination for radiological staging. Patients who had a contraindication to MRI were excluded.

The MRI examination was performed approximately six weeks following the TRUS prostate biopsy to allow the prostatic haemorrhage and inflammation to resolve in order to reduce MR artifacts.

3.2.2. Patients preparation

On arrival at the CMRI, patients were interviewed to check suitability for scanning and were asked to complete and sign a safety questionnaire, having read and understood all the questions. They were also asked to indicate if they were happy for their scans to be used for research purposes.

A data sheet was completed by the doctor overseeing the MR examination detailing relevant history, investigations and the indication for performing prostate MRI. The MR examination was then explained in detail to the patient.

A 20 gauge Venflon® was placed in a vein on the dorsum of the hand or in the ante-cubital fossa. Patients were positioned supine on the examination table and entered the bore of the magnet feet first. Earplugs were provided to protect against the scanner noise, as the scanner acoustic levels may

exceed 99 dB and can cause hearing impairment. Earplugs have a noise reduction rating of at least 28 dB. A safety squeeze ball was given to patients to trigger an alarm in case of emergency or feeling unwell.

For contrast injection, we used a disposable MRI kit (Spectris Solaris, Medrad) consists of a 65 ml syringe for contrast media, a 115 ml syringe for saline. A 2438 mm long low pressure connector tube was attached to both syringes at one end and to the Venflon at the other. This was used to achieve rapid delivery of the MR contrast agent followed by 15 ml of saline flush. 80 ml of saline for continuous slow flushing was used to keep the cannula patent.

A 3.0T 8-channel pelvic phased-array coil (GE Healthcare) was used for pelvic imaging. The coil consists of 2 pieces, a posterior section lying under the patient, and an anterior section positioned over the region of interest. The two sections of the coil are aligned in the z-direction and their relative positions maintained using Velcro straps [Figure 27]. The coil is housed in a soft, flexible foam material for patient comfort and safety. While the patient is being advanced into the scanner bore, a laser light is aligned with the centre of the coil for accurate positioning of the region of interest within the bore.

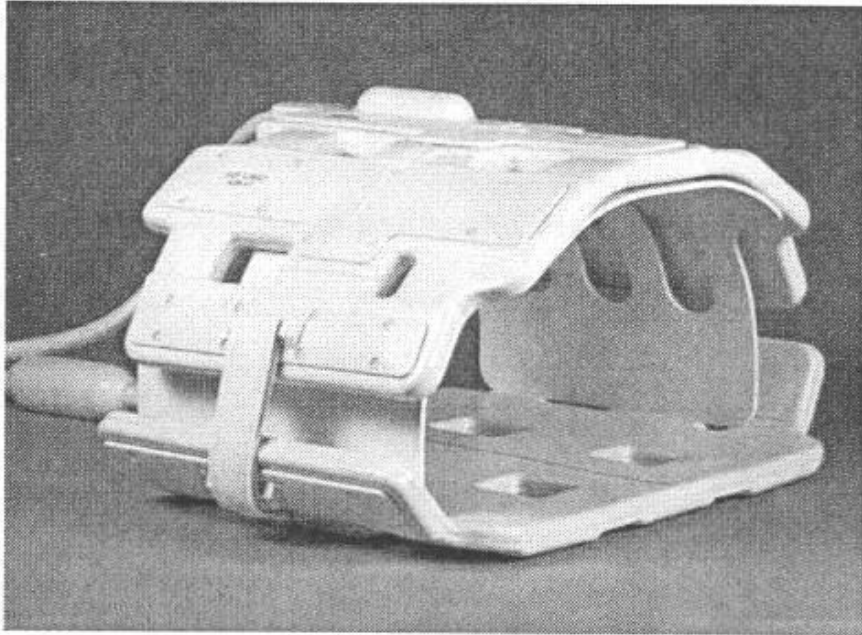


Figure 27. A 3 Tesla 8 channel torso phased-array coil. The figure shows the anterior and posterior elements connected with Velcro straps. The plastic inner bridge can be positioned over the patient to support the anterior elements if the weight of the device is uncomfortable.

Two bags of Manganese Chloride (2.5L each) were applied on patient's pelvis to reduce the dielectric effect. MRI scanning was performed after intravenous injection of 20 mg of hyoscine-N-butylbromide (Buscopan, Boehringer Ingelheim Ltd) to suppress bowel peristalsis. No bowel preparation was required.

3.2.3.MR examination

73 consecutive patients (mean age 62 years, range 51-71), with biopsy proven prostate cancer, underwent imaging at 3.0T MR system (Signa HDx, GE Healthcare, Milwaukee, USA) using multi-sequence MRI including T2 weighted, DCE-MRI, and an 8-channel phased array and an endorectal coil for signal reception (as detailed below), before undergoing radical prostatectomy (RP).

The following sequences were obtained:

- Three plane localizer
- Low resolution axial T2 weighted fast spin-echo (FSE) images to assess pelvic lymph nodes and bones, covering the area from the perineum up to the aortic bifurcation.
- High resolution axial and coronal T2 weighted FSE to assess the prostate and surrounding structures (TR/TE: 3100/97.3 ms, slice thickness: 3.0 mm, inter-slice gap 0.0 mm, matrix 384 x 256, field of view 20 x 20 cm, number of slices 26, TA 6:50 mins). The axial T2w images were obtained in a plane perpendicular to the long axis of the gland.
- T1 weighted DCE-MRI was acquired axially using 3D Fast Spoiled Gradient Recalled (FSPGR) sequence (28° flip angle, field of view 30 x 30cm, matrix 256 x 128, 24 locations per slab, TR/TE 5.1/2.1 ms, parallel imaging factor of 2, temporal resolution 8.36 s per volume, providing 35 slice locations in approximately 4:45 mins). This was obtained immediately before, during and after bolus administration of

0.1 mmol/kg body weight Gadolinium-DTPA based contrast agent (Omniscan, Nycomed-Amersham, Norway) at a rate of 3 ml/s using a power injector (Spectris Solaris, Medrad, Indianola, Pennsylvania) followed by 15 ml saline flush.

- Endo-rectal imaging was then performed in 33 patients. For the first 14 cases a rigid ERC (Global Research Centre GRC, München, Germany) was used in isolation to obtain the images. For the remaining 19 cases (following a hardware upgrade) an integrated endorectal-pelvic phased array inflatable coil was obtained and used [figure 28].



Figure 28. Endorectal coil with inflatable balloon to ensure retention which can be integrated with pelvic phased array coil.

The insertion of endorectal coil was facilitated using lubrication. Following insertion, the covering balloon was insufflated with 60 ml of air and the coil was pulled back and secured in position. The endorectal coil has the tendency to migrate cephalad during the

inflation of the balloon, resulting in suboptimal visualization of prostate apex. Therefore, gentle traction on the coil was applied as the balloon was filled. The endorectal coil was then connected to the PPA coil. The following sequence parameters were obtained (TR/TE: variable/166.8 ms, slice thickness 2.5 mm, no inter-slice gap, matrix 256 x 224, field of view 14 x 14 cm, number of slices 22 obtained over 3:35 mins).

All MR images were analyzed using an Advantage Windows Workstation (GE Medical System), operating at 4.2-03 software level and using the Functool software package.

3.2.4. MR image evaluation

MR images were reviewed by two independent readers (LWT and BZ). Reader 1 has more than 15 years experience in MRI and reader 2 has 2 years experience in prostate MRI. Each series was assessed independently for tumour localisation and staging using a standard form developed for this project [Figure 29]. A final report using the combined sequences was also documented.

Name: _____

Date of scan _____

Tumour localisation

Number of abnormal areas: _____

Locations

	Right	Left
Apex anterior		
Apex posterior		
Middle anterior		
Middle posterior		
Base anterior		
Base posterior		

Tumour Staging

Extra capsular extension:

- 1) Definitely not present
- 2) Probably not present
- 3) Possibly present
- 4) Probably present
- 5) Definitely present

Seminal vesicle involvement

- 1) Definitely not present
- 2) Probably not present
- 3) Possibly present
- 4) Probably present
- 5) Definitely present

Figure 29. The proforma used by each reader to evaluate each series independently. The area of tumour was drawn on the prostate illustration.

Tumour localisation

T2 weighted images and DCE-MRI were used to localize tumour presence in the prostate gland. Hypointense areas in the high signal intensity peripheral zone on T2 weighted images were considered as suspicious of prostate cancer. Also homogeneous, irregularly shaped hypointense areas within the central gland, which were identifiable separately from co-existing BPH features and cysts, were considered as suspicious for malignancy. At DCE-MRI, areas demonstrating early, rapid and intense contrast uptake with subsequent plateau or wash-out phase (as described previously) were considered suspicious for the presence of malignancy.

The prostate was divided into 12 areas (left and right, apex, middle and base, anterior and posterior). Each area was assessed for the presence or the absence of suspected malignancy.

Tumour staging

Capsular involvement was evaluated on the basis of five specific features described in the literature as highly indicative of extra capsular extension (ECE) [127]. These features were as follows: asymmetry of the neurovascular bundles, obliteration of the recto-prostatic angle, irregular bulging of the prostatic contour, low signal intensity within the periprostatic fat and overt extracapsular tumour.

Seminal vesicle involvement (SVI) was suspected when focal low signal intensity was present in one or both seminal vesicles on high resolution T2w

images and contrast uptake evident on DCE images. Pelvic lymph nodes were also assessed to exclude lymphatic metastases. Final staging was recorded according to the TNM classification [61]. The likelihood of ECE and SVI was rated with a 5-point scale [Figure 29].

3.2.5. Histologic evaluation

Radical retropubic prostatectomy was performed by an experienced urological surgeon. A nerve sparing procedure was performed in all patients except those with suspected locally advanced disease (T3) on MR imaging or digital rectal examination, or patients with intermediate and high risk factors according to D'Amico risk stratification. Lymph node dissection was also performed in selected patients as per guidelines.

Prostatectomy specimens were examined after routine preparation. The prostate was weighed and measured in three dimensions; fixed in 10% formaldehyde for 24 hours, painted in colour coded inks to identify left and right side, whole mounted and then sectioned at 5 mm intervals in a plane perpendicular to the long axis of the gland. The orientation of sectioning was performed to match the MR slice orientation. The sections were then embedded in large paraffin blocks. 3 µm thick slices were cut from the superior surface of each section and stained with hematoxylin and eosin (H&E) for subsequent microscopic examination.

All tumour foci were outlined on the whole mount H&E slides by an experienced pathologist [Figure 30]. Apical and basal sections were cut and

examined separately for the presence of cancer. The seminal vesicles were also examined for any spread of cancer [Figure 31].

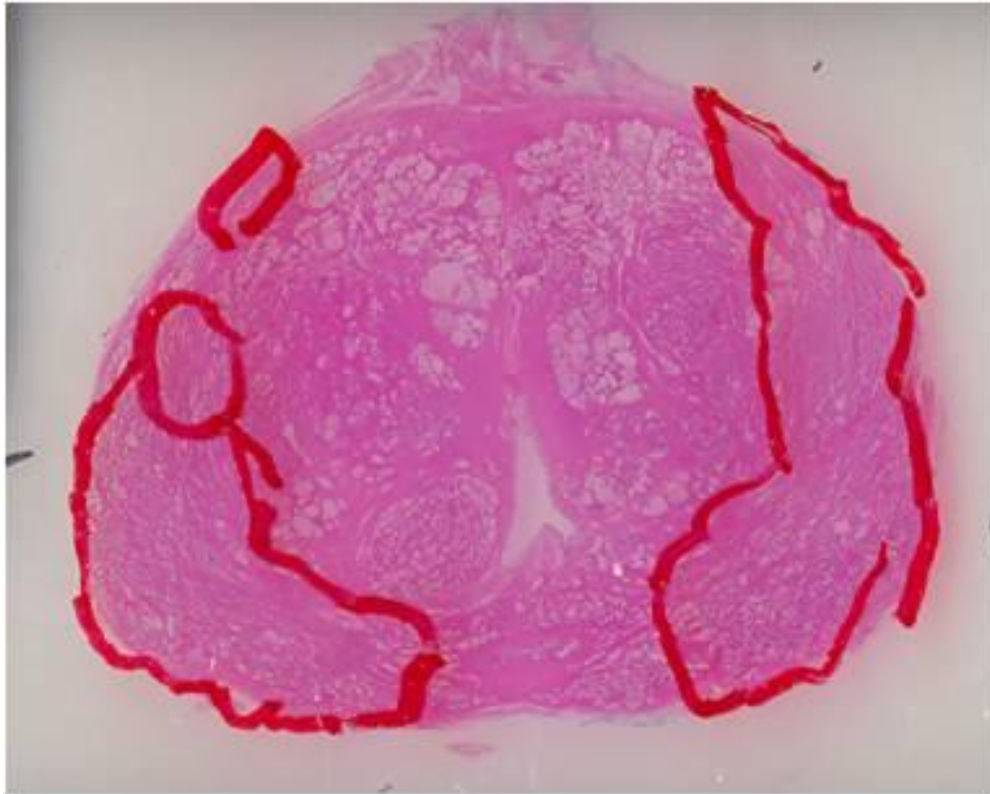


Figure 30. H&E slide of whole mount prostate specimen with cancer foci outlined in red.



Figure 31. Sections obtained from prostatic apex (first 3 on left), base (middle 3) and seminal vesicles (last 2 on right). Evidence of cancer was noted in the apical sections (black dotted areas).

Extra prostatic extension (T3a) was considered to be present on histopathologic assessment if cancer cells were found beyond the capsule, in the adjacent adipose tissue or in the perineural spaces of the neurovascular bundles [82]. Stage T3b was diagnosed if cancer involved the seminal vesicles. A positive surgical margin was defined as cancer cells touching the inked surface of the prostate [82]. Tumours were staged as Tx if there was focally no extracapsular tissue demonstrable at the site of margin positivity where the prostate was incised through the capsule due to surgical error.

Details of the extracapsular extension for tumours were recorded. These included the location and the degree of ECE [Figure 32].

Pathology details

Extra capsular extension

Tumour 1:

- Degree of ECE: T2 Microscopic T3 Macroscopic T3
- Location:

	Right	Left
Apex		
Middle anterior		
Middle posterior		
Base anterior		
Base posterior		

- Size in mm:

Tumour 2:

- Degree of ECE: T2 Microscopic T3 Macroscopic T3
- Location:

	Right	Left
Apex		
Middle anterior		
Middle posterior		
Base anterior		
Base posterior		

- Size in mm:

Tumour 3:

- Degree of ECE: T2 Microscopic T3 Macroscopic T3
- Location:

	Right	Left
Apex		
Middle anterior		
Middle posterior		
Base anterior		
Base posterior		

- Size in mm:

Seminal Vesicle Involvement

Negative Positive

Surgical margins

Negative Positive

Location

	Right	Left
Apex		
Middle anterior		
Middle posterior		
Base anterior		
Base posterior		

Figure 32. The proforma that was used to document pathology details including localisation, staging and surgical margins.

3.2.6. Statistical analysis

Statistical analysis was performed using SPSS for windows (version 13.0). Sensitivity, specificity, positive predictive value, negative predictive value and accuracy for localizing prostate cancer were calculated using cross-tabulation with the prostatectomy histopathologic results as the reference standard.

Kappa statistics were used to evaluate the inter-observer agreement between the two readers. The following terms were used to describe the strength of agreement: $\kappa = 0 - 0.20$, poor agreement; $\kappa = 0.21 - 0.40$, fair agreement; $\kappa = 0.41 - 0.60$, moderate agreement; $\kappa = 0.61 - 0.80$, substantial agreement; and $\kappa = 0.81 - 1.00$, near perfect agreement [128]. The probability of extracapsular and seminal vesicle invasion was graded on a scale of 1-5, which allowed for receiver operating characteristic (ROC) analysis and obtaining descriptive statistics from 2 cutoff points.

3.3. Results

3.3.1. Patients demographic data

All recruited patients were eligible for the study (73 patients). 31 patients presented with lower urinary tract symptoms, whereas 4 patients presented with urinary tract infection, one patient with acute urinary retention, one patient with haematuria, and 36 patients were asymptomatic (cancer was identified through the well-man clinic or screening).

Digital rectal examination identified 60 patients with clinical stage of T1c and 13 patients with T2 disease. Mean PSA was 7.6ng/ml (range 1-16). Gleason score varied from 6 to 9 [Table 7].

Gleason score	Number of patients (percentage)
3+3=6	20 (27.4%)
3+4=7	42 (57.5%)
4+3=7	4 (5.4%)
4+4=8	2 (2.7%)
4+5=9	5 (6.8%)

Table 7. Pre-operative TRUS prostate biopsy results. The majority of cases that were suitable for RP were Gleason Grade 6 or 7.

3.3.2. Localisation data

The 12 prostatic areas were combined into apex, base, mid anterior (representing the central gland), and mid posterior (representing the peripheral zone) to facilitate statistical calculations.

Histopathologic analysis

Pathological examination of RP specimens detected cancer foci in 177 areas out of a total of 292 areas (73 patients multiply by 4 areas). The number of cases with cancer involvement in individual areas is detailed in Table 8.

	Number	Percentage (the number of positive cases / total number of patients x 100)
Apex	35	47.9%
Base	22	30.1%
Central gland	49	67.1%
Peripheral zone	71	97.3%

Table 8. Mapping tumour presence on pathology slides showed that the peripheral zone is most commonly affected by cancer compared to central gland, base and apex.

66 patients (90.4%) had 2 or more tumour foci in the prostate gland. While the majority affected the peripheral zones, only two cases had a central gland tumour only. In 47 cases (64.4%) tumour was present in both peripheral zones and central gland. In 12 cases (16.4%) all prostate areas had tumour involvement.

MRI data

The number of cases with suspicion of malignancy according to region is detailed in Table 9 for T2 weighted imaging and in Table 10 for DCE-MRI for both readers 1 and 2.

	Number*	Percentage (%)*
Apex	37/29	50.7/39.7
Base	39/21	53.4/28.8
Central gland	28/23	38.4/31.5
Peripheral zones	69/66	94.5/90.4

(* Results from reader 1 / results from reader 2)

Table 9. The number of cases, for each anatomical region, with T2 weighted features suspicious of cancer presence.

It is clear from Table 9 that, by using T2 weighted imaging, reader 1 assigned 173 areas as suspicious for cancer compared to 139 areas assigned by reader 2. The main areas of discrepancy were the prostatic base and apex.

By using DCE-MRI, reader 1 assigned 164 areas as suspicious for cancer compared to 144 areas assigned by reader 2. The discrepancy in the number of suspicious foci identified in the prostatic base and apex areas is much less compared to T2 assessment alone [Table 10].

	Number*	Percentage (%)*
Apex	33/24	45.2/32.9
Base	31/21	42.5/28.8
Central gland	36/30	49.3/41.1
Peripheral zones	70/69	95.5/94.5

(* Results from reader 1 / results from reader 2)

Table 10. Represents the number of cases for each anatomical region that showed high signal intensity following administration of contrast for readers 1 and 2.

Interobserver agreement:

For T2 weighted imaging, there was an overall moderate agreement between the two readers (K = 0.58). By selecting each region individually [Tables 11-14] there was a moderate agreement in reporting an area as suspicious of malignancy at the apex (K = 0.56), peripheral zones (K = 0.42), and central gland (K = 0.55). However, looking at the base of the gland, there were 21 cases reported as suspicious for malignancy by reader 1 but not identified by reader 2 with only a fair interobserver agreement (K = 0.36).

Apex (T2 weighted)		Reader 2		Total
		normal	Suspicious of cancer	
Reader 1	normal	32	4	36
	Suspicious of cancer	12	25	37
Total		44	29	73

Table 11. The number of normal and suspicious cases at the apex for both readers identified on T2 weighted imaging.

Base (T2 weighted)		Reader 2		Total
		normal	Suspicious of cancer	
Reader 1	normal	31	3	34
	Suspicious of cancer	21	18	39
Total		52	21	73

Table 12. The number of normal and suspicious cases at the base for both readers identified on T2 weighted imaging.

Central gland (left & right sides) T2w image		Reader 2		Total
		normal	Suspicious of cancer	
Reader 1	normal	99	6	105
	Suspicious of cancer	18	23	41
Total		117	29	146

Table 13. The number of normal and suspicious cases at the anterior middle region (central gland) for both readers identified on T2 weighted imaging.

peripheral zones (left & right sides) T2w image		Reader 2		Total
		normal	Suspicious of cancer	
Reader 1	normal	22	5	27
	Suspicious of cancer	24	95	119
Total		46	100	146

Table 14. The number of normal and suspicious cases at the posterior middle region (peripheral zone) for both readers identified on T2 weighted imaging.

It is noted from all the above tables that both readers agreed in identifying the majority of normal looking areas. However, for all anatomical regions of the prostate, reader 1 identified more regions suspicious of cancer. These were considered by reader 2 to be normal.

For DCE-MRI, there was an overall substantial agreement between the two readers ($K = 0.68$). The best agreement was reached in the peripheral zone region (middle posterior) with $K = 0.65$ and central gland ($K = 0.68$). However, moderate agreement was noted in the apex ($K = 0.57$), base ($K = 0.59$).

Tables 15-18 illustrate the results for all anatomical regions for both readers.

Apex (DCE)		Reader 2		Total
		normal	Sus of ca	
Reader 1	normal	37	3	40
	Sus of ca	12	21	33
Total		49	24	73

Table 15. The number of normal and suspicious cases at the apex for both readers identified on DCE-MRI.

Base (DCE)		Reader 2		Total
		normal	Sus of ca	
Reader 1	normal	40	2	42
	Sus of ca	12	19	31
Total		52	21	73

Table 16. The number of normal and suspicious cases at the base for both readers identified on DCE-MRI.

Central gland (left & right sides) DCE image		Reader 2		Total
		normal	Sus of ca	
Reader 1	normal	89	4	93
	Sus of ca	16	37	53
Total		105	41	146

Table 17. The number of normal and suspicious cases at the central gland for both readers identified on DCE-MRI.

Peripheral zones (left & right sides) DCE image		Reader 2		Total
		normal	Sus of ca	
Reader 1	normal	23	8	31
	Sus of ca	9	106	115
Total		32	114	146

Table 18. The number of normal and suspicious cases at the peripheral zones for both readers identified on DCE-MRI.

The main pitfall in the DCE-MRI agreement between the two readers was the number of cases reported by reader 1 as suspicious for malignancy but overlooked by reader 2. Those were 12/73 (16.4%) cases for apical region,

12/73 (16.4%) for basal region, 16/146 (10.9%) for central gland, and 9/146 (6.1%) for peripheral zones.

Localisation accuracy (MRI versus pathology)

The MRI data was correlated with pathology data on a region by region basis. Figure 33 is an example of the correlation between the MR using T2 weighted imaging and DCE and histopathology.

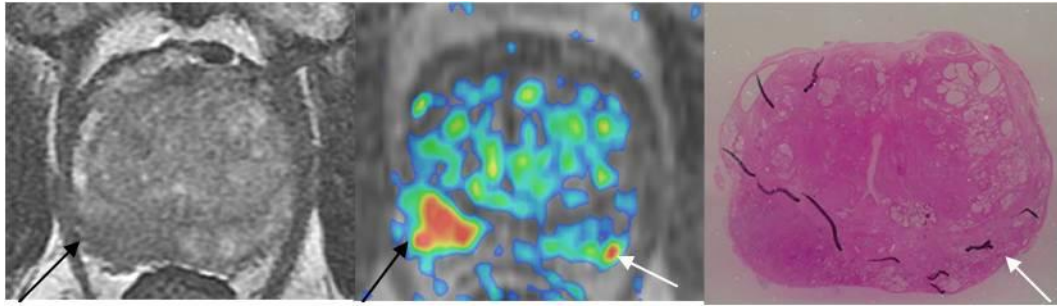


Figure 33. T2 weighted image (left) demonstrating low signal intensity in the left peripheral zone (black arrow). This correlates with high contrast uptake on DCE image (middle). The correlation with H&E stained histopathology slide (right) is also noted. There is an additional small area of uptake in the right peripheral zone seen on DCE image (white arrow) which correlated with scattered islands of malignant cells seen histologically.

The sensitivity, specificity, positive predictive value, negative predictive value and accuracy of tumour localisation were determined after combining the regions into apex, base, central gland, and peripheral zones. The results are shown in Table 19 for T2 weighted imaging and in Table 20 for DCE-MRI independently.

T2 weighted FSE imaging	Sen (%)	Spec (%)	PPV (%)	NPV (%)	Acc (%)
Apex	74/48	71/68	70/58	75/59	72/58
Base	95/50	65/80	54/52	97/78	74/71
Central gland	53/38	91/83	92/82	48/40	65/53
Peripheral zone	91/73	57/53	90/87	59/32	84/69

Table 19. Sensitivity, specificity, positive predictive value, negative predictive value, and accuracy of tumour localisation on T2 weighted imaging. Results from reader 1 / reader 2 are provided for each parameter.

Tumour localisation using T2 weighted imaging demonstrated over-estimation of cancer presence in the peripheral zones signified by the high sensitivity and low specificity. This may be as a result of low signal intensity changes secondary to haemorrhage following prostate biopsy, leading to high false positive rate. On the other hand, studying the central gland, there is under-estimation of cancer with low sensitivity. This is most likely due to the difficulty in identifying cancer separate from benign disease leading to a high false negative rate.

Similar results for sensitivity were noted using DCE-MRI [Table 20] with high sensitivity for tumour presence for peripheral zones and lower sensitivity for central gland. However, the specificity for peripheral zone is much improved using DCE-MRI.

DCE-MRI	Sen (%)	Spec (%)	PPV (%)	NPV (%)	Acc (%)
Apex	74/57	81/89	78/83	77/69	78/73
Base	90/72	78/90	64/76	95/88	82/84
Central gland	69/59	91/95	94/96	59/53	76/71
Peripheral zone	90/88	71/64	93/91	64/56	87/83

Table 20. Sensitivity, specificity, positive predictive value, negative predictive value and accuracy for tumour localisation by DCE-MRI.

Results from reader 1 / reader 2 provided for each parameter.

On further analysis, the overall sensitivity and specificity for the whole prostate gland (including all zones) based on T2 weighted imaging is 75% and 76% respectively for reader 1 and 55% and 78% for reader 2. Whereas, when DCE-MRI was applied, there was a noticeable improvement in the above parameters especially for reader 2 who achieved a sensitivity of 70% and specificity of 88% with an accuracy rate of 78% [Table 21].

Whole gland	Sen (%)	Spec	PPV	NPV	Accuracy
T2W	75/55	76/78	81/78	69/56	75/65
DCE-MRI	79/70	83/88	87/89	74/68	80/78

Table 21. Sensitivity, specificity, positive predictive value, negative predictive value and accuracy for tumour localisation in the whole gland. Results from reader 1 / reader 2 detailed. An improvement in all parameters was noted for DCE-MRI compared to T2 weighted imaging.

By utilizing DCE-MRI data, the less experienced reader achieved comparable results to those obtained from the T2 weighted imaging reported by the experienced reader (area under ROC curve of 79 versus 76 respectively) [Figure 34]. This indicates the importance of using DCE sequence if the MRI is reported by a general radiologist or a trainee as well as on a general basis.

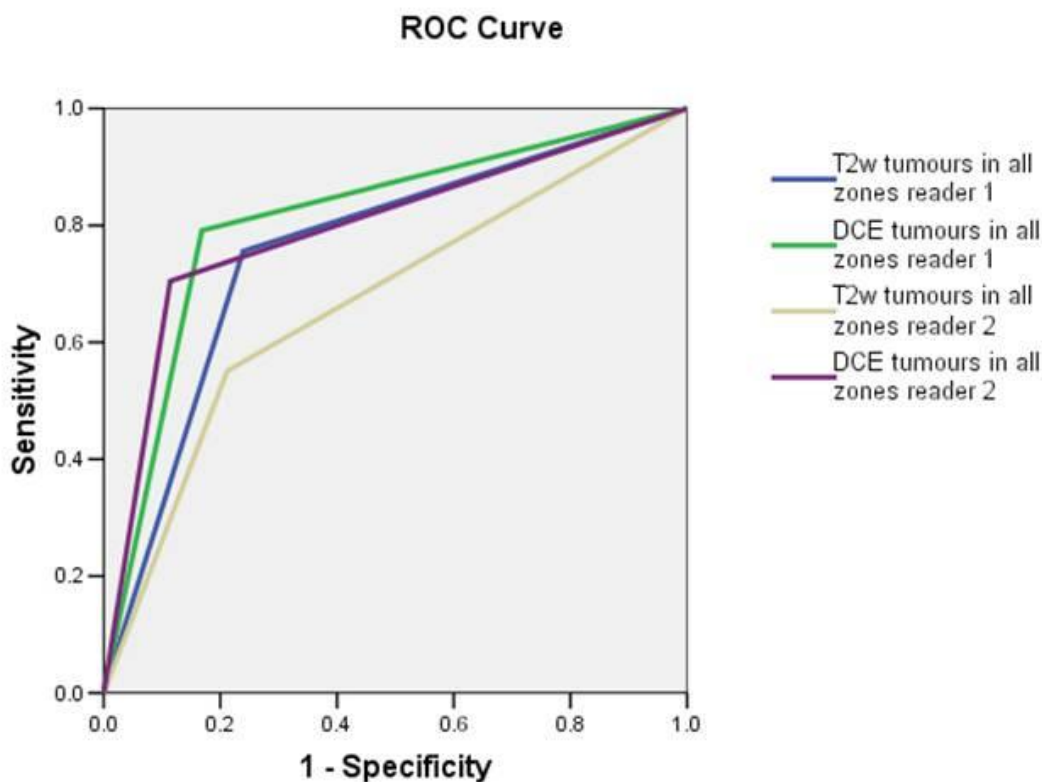


Figure 34. The ROC curve for tumour localisation using T2 weighted imaging and DCE-MRI for reader 1 and 2. AUC for T2 w imaging is 76 and 67 for reader 1 and 2 respectively. AUC for DCE-MRI is 81 and 79 for reader 1 and 2 respectively.

3.3.3. Staging data

Histological staging data:

The majority of cases (56 cases, 76.7%) were staged as organ confined disease (pt2). 15 cases (20.5%) had local invasion of cancer and were staged as pt3 (11 as pt3a and 4 as pt3b). Two cases were not staged (Tx) due to intra-prostatic positive margins at the site of cancer, therefore, accurate staging could not be done. These two cases were excluded from the staging analysis [Figure 35].

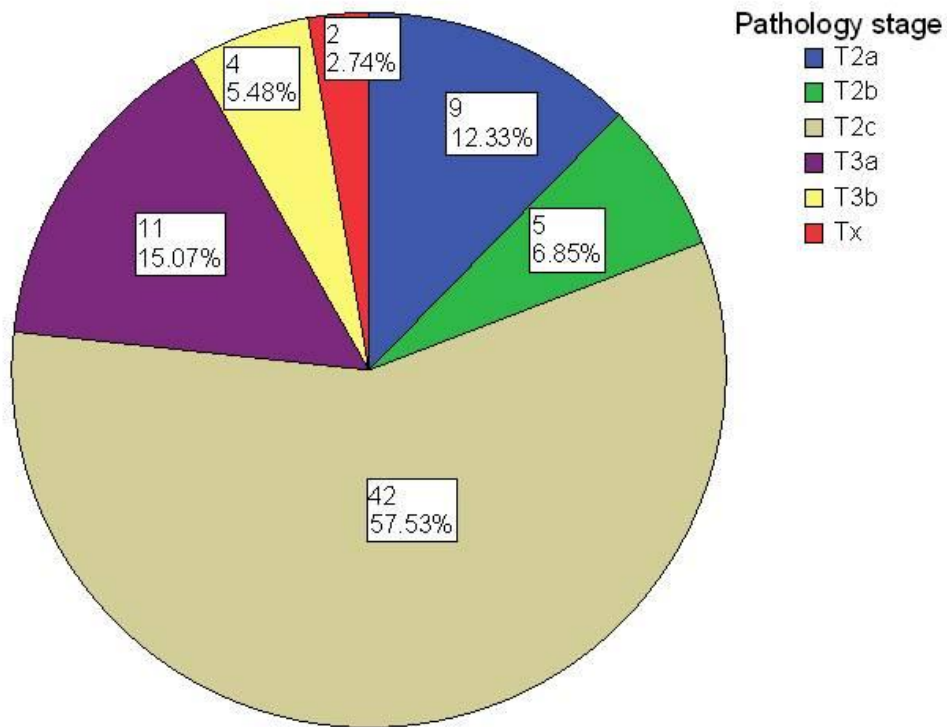


Figure 35. Demonstrate the number and percentage of cases according to pathological stage.

MRI detection of ECE:

Areas suspicious for ECE on MRI were compared with H&E slides as discussed above [Figure 36].

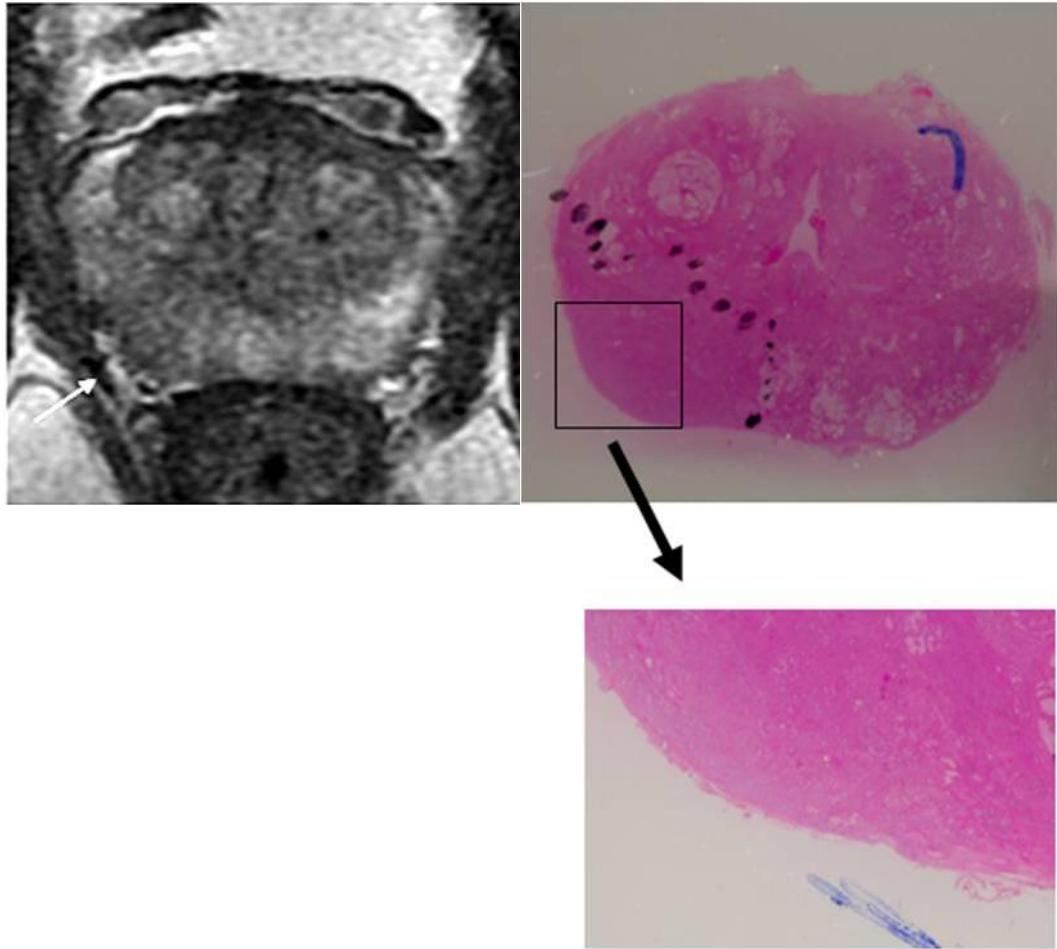


Figure 36. T2 weighted image (left) demonstrates a tumour involving the left peripheral zone with an area suggestive of extracapsular extension (white arrow). This corresponds with tumour extracapsular extension on H&E histology slide (x10 and x20 magnification).

For readers 1 and 2, ROC curves for the detection of local extracapsular extension on T2 weighted imaging using PPA coil alone [Figure 37], showed that an AUC of 0.87 for reader 1 (95% confidence interval: 0.76 to 0.98) and an AUC of 0.83 for reader 2 (95% confidence interval: 0.69 to 0.96). The weighted k statistic was 0.43 which indicated moderate agreement between readers.

ROC Curve for detection of ECE using PPA coil

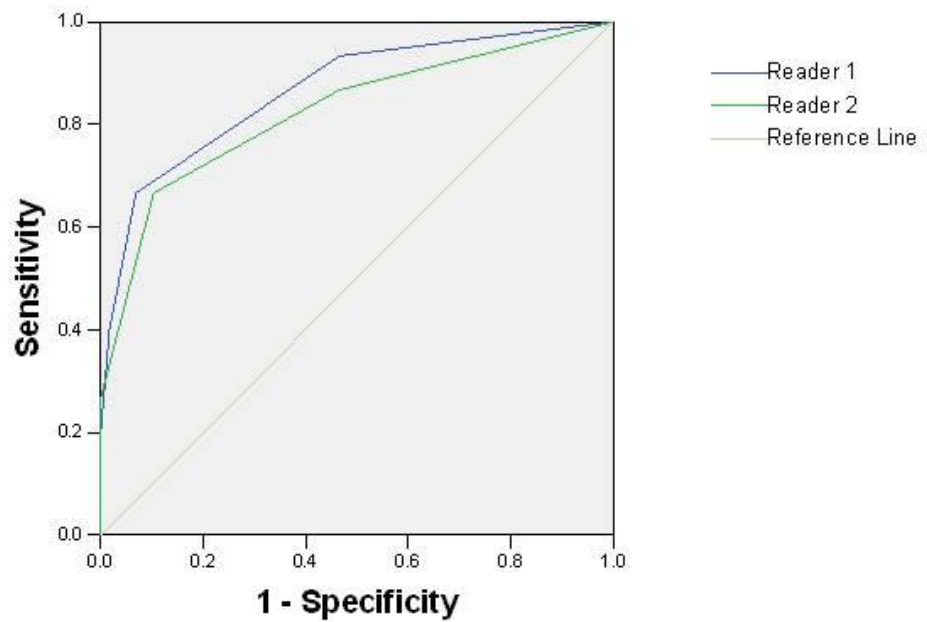


Figure 37. ROC curves for T2 weighted detection of ECE using PPA coil for readers 1 and 2.

Using endorectal coil imaging, the ROC analysis [Figure 38] showed a better detection of ECE for reader 1 with an AUC of 0.93 (95% confidence interval: 0.84 to 1.0) and for reader 2 with AUC of 0.87 (95% confidence interval: 0.73 to 1.0). The weighted k statistic was 0.43 which indicated moderate agreement between readers.

ROC Curve for the detection of ECE using endorectal imaging

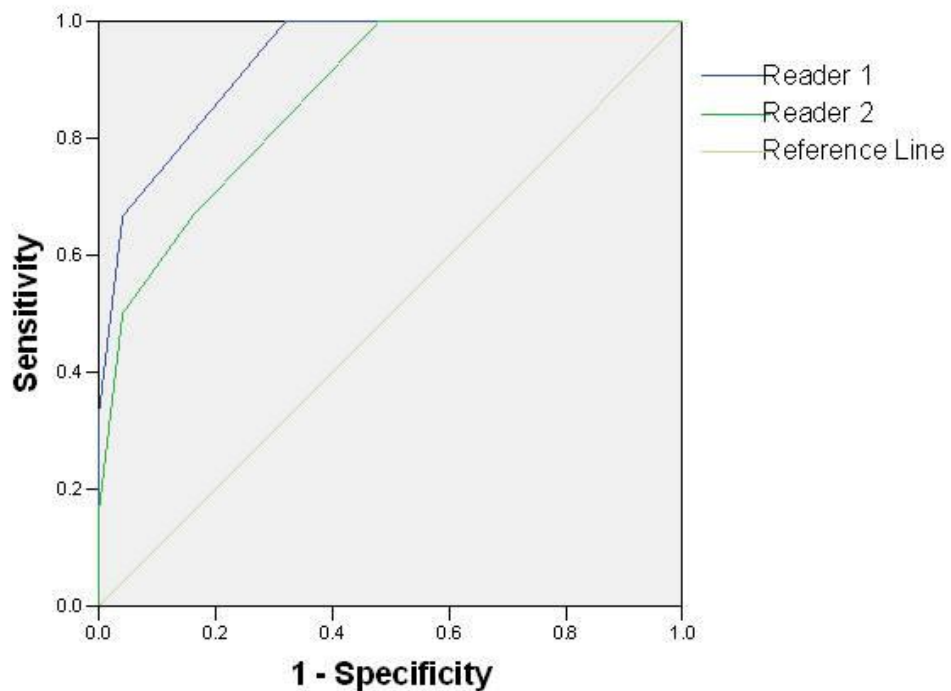


Figure 38. ROC curves for T2 weighted detection of ECE using an endorectal coil for readers 1 and 2.

The five point scoring system was dichotomized in order to assess the sensitivity and specificity of T2 weighted imaging using PPA and endorectal coil in demonstrating extracapsular extension. Two cutoff points were explored. Cutoff point 1 assumed that values of 1 and 2 indicate the absence of ECE and that values of 3-5 indicate the presence of ECE. Cutoff point 2 assumed that values of 1, 2 and 3 indicate the absence of ECE and that values of 4 and 5 indicate the presence of ECE. Tables below demonstrate the staging descriptive analysis for both readers at two cutoff points using a PPA coil [Table 22] and an endorectal coil [Table 23].

	Sen (%)	Spe (%)	PPV (%)	NPV (%)	Accuracy (%)
Cutoff	67 (43 – 90) /	93 (87 –99) /	71 (48 – 95) /	92 (84 – 98) /	88 (80 – 95) /
1	67 (43 -90)	87 (82 – 97)	63 (39 – 86)	91 (84 – 98)	85 (77 – 93)
Cutoff	40 (15 – 64) /	92 (95–100) /	86 (60–100) /	86 (78 – 94) /	86 (78 – 94) /
2	31 (8 – 53)	98 (95 – 100)	83 (54 – 100)	84 (75 – 93)	84 (76 – 92)

Table 22. Staging descriptive analysis for detection of ECE from T2 weighted imaging for reader 1 / reader 2, using a pelvic phased array coil. Sensitivity, specificity, positive predictive value, negative predictive value, and accuracy for two cutoff points. 95% confidence intervals shown in parenthesis.

From the table above, it is clear that both readers have high specificity for detecting extracapsular cancer extension with reasonable sensitivity of 67%. As expected, reader 1 has a better staging accuracy than reader 2 due to being more experienced in evaluating prostate MR imaging.

	Sen (%)	Spe (%)	PPV (%)	NPV (%)	Accuracy (%)
Cutoff	67 (22 – 95) /	96 (80–100) /	80 (28 – 99) /	92 (72 – 99) /	90 (74 – 98) /
1	67 (22 – 95)	92 (74 – 99)	67 (22 – 95)	92 (72 – 99)	87 (70 – 96)
Cutoff	33 (4 – 77) /	100(86–100)/	100(16-100) /	86 (68 – 96) /	87 (70 – 96) /
2	50 (12 – 88)	96 (78 – 100)	75 (19 – 99)	89 (71 – 98)	87 (70 – 96)

Table 23. Staging descriptive analysis for detection of ECE from T2 weighted imaging for reader 1 over reader 2 using an endorectal coil. Sensitivity, specificity, positive predictive value, negative predictive value, and accuracy shown for two cutoff points. 95% confidence intervals in parenthesis.

Although no change in sensitivity between PPA and ERC data was noted, there was an improvement in specificity and positive predictive value for both readers. The results of reader 2 using endorectal coil are similar to those achieved by reader 1 using pelvic-phased array coil. This might indicate the necessity of using an ERC for trainees during the learning curve.

With regard to seminal vesicle involvement, a total of four cases of SVI were observed on histopathology examination, but in only two of these cases did combined T2 weighted and DCE MR imaging show changes suspicious of cancer involvement [Figure 39].

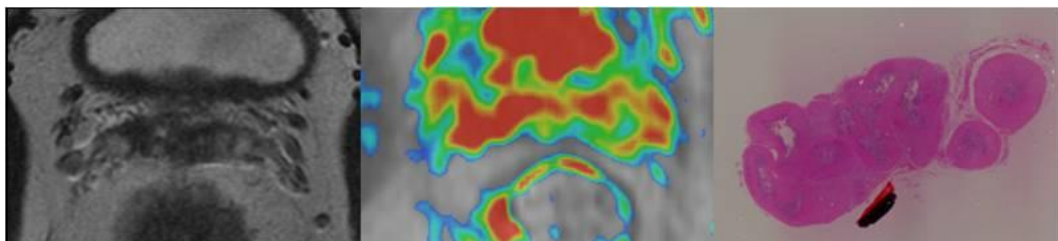


Figure 39. An example of seminal vesicle involvement. Low intensity areas seen in both seminal vesicles (left) with high contrast uptake on DCE-MRI (middle). These findings correlated with tumour involvement pathologically.

In addition, a further two cases which were positive on MRI were negative for cancer on histological examination. One of these cases, the tumour abuts the seminal vesicle but does not invade the muscular layer. This low sensitivity and PPV is biased by the small number of cases with suspected SVI on MRI who subsequently underwent RP. Due to the low number of SVI, a full statistical analysis was not done.

3.4. Discussion

Tumour staging:

At the present, the major role of MR imaging in prostate cancer is the evaluation of local staging, especially the detection of extracapsular extension.

In this study, the use of pelvic-phased array and endorectal coil in detecting extracapsular extension displayed 67% sensitivity, 96% specificity, 80% PPV, 92% NPV, and 90% accuracy for the experienced reader. These staging results are similar to the previously documented results in large centres using 3 Tesla MRI [102, 129]. This showed superior results for 3.0T compared to 1.5T MRI. Although we did not perform a comparative field strength study on the same group of patients, the accuracy of staging at 3.0T was higher than the historical reported data for 1.5T (60-80%) [96, 130].

Most radiologists report MR images leaning toward high specificity, but maintaining reasonable sensitivity, to prevent overstaging which may lead to a potentially curative surgical treatment being withheld on the basis of false positive MR imaging result. In our centre, we also showed a reasonably good sensitivity of 67% for cancer staging for the use of PPA and ER coils. In 15 cases with confirmed ECE on pathology, 10 cases were detected on MRI. This was constant for both readers. For the remaining 5 cases, pathological analysis of the specimen showed minimal microscopic invasion of cancer into the prostate capsule only. Detection of microscopic invasion on imaging remains impossible. In clinical practice, missing minimal microscopic capsular invasion on MRI may not alter the patient's management as there is

growing evidence that radical prostatectomy as a primary treatment for early T3 disease can achieve good cancer control and survival [131]. However, detection of ECE on MR imaging, as demonstrated by a PPV of 80% using an ERC, may affect the surgical technique, as a nerve sparing procedure would not be performed on the suspicious side with the intention of achieving better cancer control.

In a limited population of 27 patients considered for radical prostatectomy, Augustin et al [129] compared the accuracy of 3T MRI with the Partin tables for predicting pathologic stage. In the detection of extracapsular extension, MRI had an accuracy of 85.2%, a sensitivity of 66.7%, and a specificity of 100%. Correlation with extracapsular extension was considerably higher for MRI findings (Spearman $r = 0.780$) than for the Partin tables (Spearman $r = 0.363$). Overall, 3T MRI was significantly more accurate than the Partin tables in predicting the final pathologic stage, and therefore should have more impact on treatment decisions, especially with regard to nerve-sparing procedure.

Staging according to D'Amico risk classifications:

There has been further debate amongst urologists and radiologists about whether preoperative MRI should be employed only for intermediate and high risk groups according to D'Amico risk stratification. Kim et al [132] analysed the role of a combined DWI and DCE-MRI protocol (at 1.5T) in predicting the local stage, and found high values of sensitivity 92.3%, specificity 93.1%,

PPV 85.7%, and NPV 96.7%, when only cases with clinically high-risk disease features were analysed.

Roethke et al [133], performed a subgroup analysis in 385 patients, comparing the MRI staging data in low risk and intermediate/high risk groups. The authors found no significant difference in specificity between groups, but poor (and much lower) sensitivity of only 20% was reported in the low risk group.

In a subgroup analysis of our data, we found high accuracy rates for both low risk and intermediate/high risk groups [Table 24]. However, low sensitivity was also noted for detection of extracapsular extension in the low risk group (33%), similar to previous documented studies. These results could be affected by the small number of patients with histologically confirmed extracapsular extension in low risk group (one case in our cohort).

	Low risk (PSA < 10 and Gleason = 6)	Intermediate/high risk (PSA ≥ 10 and Gleason ≥ 7)
Patients (n)	20	53
Sensitivity (%)	33	81
Specificity (%)	100	88
PPV (%)	100	64
NPV (%)	89	95
Accuracy (%)	90	87

Table 24. Sensitivity, specificity, positive and negative predictive values for prediction of ECE according to the D’Amico risk classification.

Despite the documented low sensitivity in detecting ECE in low risk group, MRI still carries great value for evaluation and counseling for two main reasons:

- 1) About 25-30% of cases with a diagnosis of Gleason 6 PCa on biopsy will be upgraded to Gleason 7 or above on histopathology examination of the radical prostatectomy specimen. These patients are therefore at a higher risk of extracapsular extension and/or positive resection margins.
- 2) If MRI shows no evidence of tumour in patients with low-risk PCa, it could represent an additional criterion to choose active surveillance. In contrast, patients with visible tumour on MRI, particularly in the case of large volume disease, may be candidates for repeat biopsies to confirm tumour aggressiveness, and thus suggest a radical treatment.

Tumour localisation:

The second important role of prostate MRI is the localisation of tumour within the prostate gland. This has potential clinical benefits, including improved accuracy of MR-guided biopsy, improved focusing of irradiation for intensity-modulated therapeutic radiotherapy, and improved guidance of other modern focal ablation techniques such as cryotherapy and high intensity focused ultrasound. We used a whole mounted prostatectomy specimen as the 'gold standard' reference test for clinical validation of MR imaging in localizing tumour foci. However, there are emerging biopsy techniques such as transperineal template biopsies which can obtain histology samples from the

whole gland including the transitional zones at intervals of 5mm diameters. These techniques are now acceptable as a standard reference test for imaging evaluation without subject patients to major surgery.

In this study, the detection of prostate cancer within the prostate by T2 weighted alone is limited, with overall sensitivity, specificity, and accuracy of 75%, 76%, and 75% respectively for reader 1, and 55%, 78%, and 65% respectively for reader 2. The lower sensitivity and higher specificity results for reader 2, suggest over-estimation of cancer presence on T2 weighted imaging. This limitation means that prostate cancer cannot be reliably distinguished from other T2 hypointense lesions such as prostatitis, haemorrhage and atrophy, all of which present with low signal intensity changes.

DCE-MRI provides higher prostate cancer localisation accuracy than that achievable by T2 weighted imaging alone, especially for the less experienced reader, with accuracy rates of 80% versus 75% for reader 1, and 78% versus 65% for reader 2 respectively. Moreover, by using DCE imaging, reader 1 detected 15 pathologically confirmed tumour areas (1 apex, 9 central gland, and 5 peripheral zone) that were not detected by T2 weighted imaging. Similarly, reader 2 detected 34 tumour areas (7 apex, 6 base, and 21 peripheral zone) based on DCE imaging that were missed on T2 weighted imaging.

The best localisation results using DCE imaging were achieved in assessing the peripheral zones with marked improvement in specificity from 57% to 71% for reader 1, and from 53% to 64% for reader 2. This high specificity was achieved whilst maintaining a sensitivity of 90% and 88% for readers 1 and 2 respectively.

The prostate apex is the main problematic area to assess with MR imaging. This is mainly because of the lack of a well-defined capsule to separate it from the periprostatic tissues, and the presence of the neurovascular bundles. This gives a relatively poor accuracy rate for both T2 weighted and DCE MR imaging.

Our research outcome is comparable with results from previous published studies. Delongchamps et al, in a study involved 57 patients, reported a sensitivity of 79% and specificity of 92% using combined data for T2 and DCE in the peripheral zones only. With regard to the transitional zone (TZ) tumours, the author reported a sensitivity of 47% and a specificity of 77% for tumour detection using DCE-MRI. In our study, the experienced reader maintained a good sensitivity of 71% with a high specificity of 90%.

Reader's experience:

Reader experience is one of the most important factors in accurate staging of prostate cancer. A study at the Memorial Sloan-Kettering Cancer Centre compared the detection of PCa extracapsular extension by genitourinary and general body radiologists [68]. The authors demonstrated a significant

increase in the detection accuracy of extracapsular extension when endorectal MR images were interpreted by genitourinary radiologists compared to general body radiologists with AUC values of 0.83 versus 0.64 respectively.

Another recent study compared the accuracy of MRI staging according to the level of experience [134]. The paper showed that the experienced reader reached a staging efficiency of 86.96%, whereas the less experienced reader only reached a staging efficiency of 56.52%. The authors indicated that the performance of a less experienced reader does not meet the expectations of the technique, and they emphasized that MR imaging with a combined phased-array and endorectal coil can achieve a good correlation with histopathology in terms of local prostate cancer staging, but only if performed by an experienced radiologist.

In this study the less experienced reader improved his localisation accuracy by using dynamic contrast-enhanced MR imaging (accuracy of 65 versus 78 for T2W and DCE MRI respectively). The parametric maps generated on the MR workstation helped draw the attention of the less experienced reader to areas of prostate cancer. With regard to staging, the use of endorectal coil mainly improved the staging specificity for the less experienced reader from 87% to 92%.

Therefore we believe that there is a considerable learning curve in the interpretation of prostate MR images. A radiology trainee should be using the

best available MR technology in terms of DCE-MRI and endorectal coil imaging to achieve a maximum accuracy in staging and localising prostate cancer.

One of the limitations in my study was the potential for verification bias. In our department, MR imaging is performed in all patients who are considered for RP. Therefore the result of MRI, especially the findings of overt ECE or SVI, may have contributed to the decision to cancel RP. This bias could have inflated the accuracy, sensitivity and specificity rates due to better selection of organ confined disease at surgery. Correction for this verification bias remains impossible.

Another point to note is that the histology sections were cut at 5mm intervals. This means that tumours less than 5 mm diameter may get missed on histological evaluation. Therefore, there were not included in the MR evaluation as these tumours were considered to be clinically insignificant. This was agreed by the European consensus meeting in December 2009, as the panel recommended excluding clinically insignificant cancer as defined of a lesion smaller than 0.5 cm³ in assessing the detection rate for each MRI sequence [135].

3.5. Conclusion:

In conclusion, using 3 Tesla MRI, an experienced reader was able to localize prostate cancer foci with good sensitivity and specificity overall, especially for peripheral zones where most cancers occur. Using DCE-MRI further enhances the sensitivity and specificity especially for non experienced clinicians.

Endorectal 3.0T MR imaging achieves a high spatial resolution, revealing excellent anatomical details to allow adequate staging and to facilitate clinical decision making. Moreover, the experience of the reporting clinician is hugely important to maintain a high accuracy rate with balance between sensitivity and specificity.

Chapter Four

4. CORRELATION OF APPARENT DIFFUSION COEFFICIENT WITH CELL DENSITY IN PROSTATE CANCER

4.1. Objective

Notwithstanding the increasing use of DWI in prostate cancer imaging at both 1.5 and 3.0 Tesla, there has been no work examining the relationship between ADC and histopathological variables such as cell density (CD). Studies on breast, brain and metastatic prostate cancers suggest that a rise in ADC values, caused by the loss of cellular density during effective treatment, may provide an early quantitative assessment of positive tumour response [115, 136, 137].

CD may be indicative of tumour aggressiveness, as several clinical studies have indicated increased metastatic activity from highly cellular tumours [138, 139]. The increased cellularity of malignant lesions restricts water motion due to a reduction in the extracellular space, thereby, resulting in lower ADC values. Initial results have demonstrated a significant negative correlation between the ADC values of tumour regions and cell density in breast tumours, human gliomas, metastatic brain tumours and human melanoma xenograft [116, 140-142]. Guo et al [116], showed that tumour cellularity has

a significant influence on the ADC values obtained in both benign and malignant breast lesions, malignant regions with high cell density having a lower ADC value than benign regions with a low cell density ($r=-0.542$).

To my knowledge, this is the first study assessing the diagnostic potential of ADC parameters in prostate cancer via correlation with cell density determined by hematoxylin and eosin stained whole mount radical prostatectomy specimens.

4.2. Methods

Approval from the Local Ethics Committee was granted and written consent obtained from all patients for their MR images to be used for research purposes. Thirty two patients with biopsy proven prostate cancer were recruited from December 2005 to December 2007. They were referred from the Urology Department for MR staging prior to radical prostatectomy. The mean age was 62 years, mean PSA was 7.6 ng/ml (range 2.5 - 16 ng/ml). Gleason scores were as follow: 5 were Gleason 6 (3+3) ; 23 were Gleason 7 (20 cases Gleason 3+4 and 3 cases Gleason 4+3); 1 was Gleason 8 (4+4) ; and 3 were Gleason 9 (2 cases Gleason 4+5 and one case Gleason 5+4).

The median interval between trans-rectal ultrasound-guided prostate biopsy and MR examination was six weeks to allow the inflammation and haemorrhage following biopsy to resolve; this was adequate to obtain good quality diffusion images. None of the patients received any treatment prior to MRI.

MRI was performed on a 3.0 Tesla scanner (Signa HDx, GE Healthcare, Milwaukee, USA) using an eight-channel pelvic phased array receiver coil. Preparation of patients was as described in chapter 3. After conventional T2 weighted imaging, DW images were obtained axially using a single shot dual spin-echo echo-planar imaging (EPI) sequence with b -values of 0 and 500 s/mm^2 . Other acquisition parameters included: TE = 65.7 ms (fractional echo); TR = 4000 ms; matrix size = 224 x 224; field of view = 26 x 26 cm; slice thickness = 5 mm; slice gap = 1 mm; average = 16; receiver bandwidth = 250 kHz; total acquisition time = 2:08 minutes.

Patients then proceeded to radical retropubic prostatectomy as the sole radical treatment. Prostatectomy specimens were prepared and examined as described in chapter 3. Experienced pathologists outlined regions of tumour on the H&E slides. Five randomly positioned areas from within the most representative sections of the outlined tumour and separately from normal peripheral zone were examined using x200 magnification, digitally photographed and then analysed using 'in-house' developed MATLAB software. This software utilises adaptive histogram thresholding to segment the darker stained cell nucleus [Figure 40].

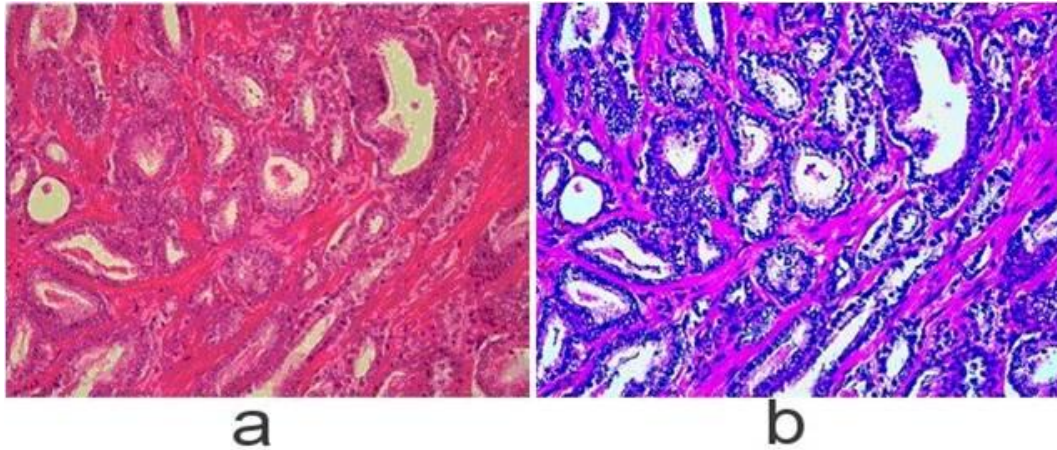


Figure 40. Images of H&E stained prostatic carcinoma at x200 magnification, before (a) and after processing (b) using MATLAB software. Cell nuclei are highlighted in blue and connective stroma in pink.

This threshold was constant for all patients to reduce subjectivity bias. An automated estimation of CD was obtained by measuring the number of nuclei over a square unit of tissue. MR images were then analysed using an Advantage Windows Workstation (GE Medical System), operating at 4.2-03 software level and using the Functool software package. Regions of interest (ROIs) were manually drawn around tumour and normal PZ on the DW images using the whole mounted specimens as reference [Figure 41].

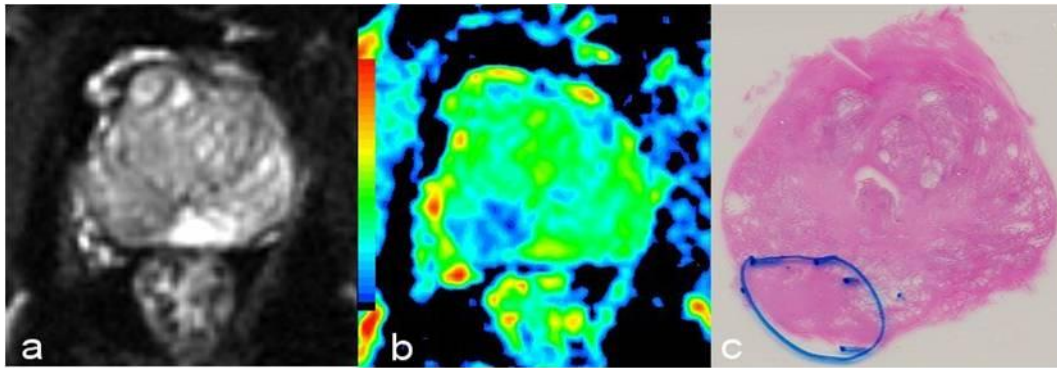


Figure 41. a) Diffusion weighted image of the prostate showing area of low signal intensity in the right PZ. b) ADC map demonstrating the low diffusivity in the right PZ indicated by the blue pixels. c) The corresponding H&E pathology slide showing the presence of tumour area on the right PZ as marked.

Each pathologic slice was visually matched to a corresponding MR image based on the location of the ejaculatory ducts, diameter of the prostate, any identifiable benign hyperplastic nodules, and approximate distance from the base or apex. To be considered a match, the tumour must be in the same anterior or posterior half of the prostate and at the same level from the superior to inferior aspect of the gland. In difficult cases, pathology slices were cross-referenced with T2 weighted images to identify the most accurate location of the malignant lesion. The ROIs were then transferred on to the DW images matching the same level and position of the chosen T2 weighted slice. A researcher with at least 7 years experience in prostate MRI, and myself with two years experience in prostate MRI drew all ROIs by consensus. The ADC maps were automatically constructed on a pixel-by-pixel basis and ADC values for each ROI were generated utilizing the MR

manufacturer software (Functool). ADC values were then correlated with the CD of the corresponding ROI on H&E stained slides.

Statistical analysis was performed using SPSS for windows (version 13.0). The Kolmogorov-Smirnov test was used to demonstrate deviation from the normal distribution. A paired t test was used to determine the statistical differences between normal PZ tissue and tumour ADC values and between the mean values for CD obtained from the five histological areas of both normal PZ and tumour examined. The Pearson's test was utilized to identify any correlation between ADC and CD values. Receiver operating characteristic (ROC) analysis was employed to assess the different ADC cutoff values for prostatic cancer in the PZ.

4.3. Results

Thirty two patients were included in the trial analysis. One case showed extensive infiltration of the gland by cancer which did not spare any normal PZ area for ADC calculation. In this case only the data from tumour ADC and CD were employed.

The mean, standard deviation, and range of ADC and CD values for tumour and normal PZ regions are presented in Table 25.

	Mean	SD	Minimum	Maximum
Tumour ADC ($\times 10^{-3} \text{ mm}^2/\text{s}$)	1.45	0.27	0.78	2.08
PZ ADC ($\times 10^{-3} \text{ mm}^2/\text{s}$)	1.90	0.33	1.37	2.77
Tumour CD (%)	18.89	4.93	10.70	28.42
PZ CD (%)	9.22	3.23	2.12	14.28

Table 25. The mean values for tumour and PZ ADC and CD are shown.

Tumour regions have lower ADC and higher cell density.

The calculated ADC values for cancer and normal PZ were consistent with those previously reported in the literature. ADC values were significantly lower ($p < 0.001$) in regions pathologically determined to be tumour ($1.45 \pm 0.27 \times 10^{-3} \text{ mm}^2/\text{s}$) compared to regions assigned as normal peripheral zone tissue ($1.90 \pm 0.33 \times 10^{-3} \text{ mm}^2/\text{s}$), with a mean difference of $0.45 \times 10^{-3} \text{ mm}^2/\text{s}$ (CI: 0.36-0.53). Similarly, the average cell density over the 5 fields was significantly higher ($p < 0.001$) in tumour compared to normal peripheral zone tissue ($18.89 \pm 4.93\%$ vs. $9.22 \pm 3.23\%$), with a mean difference of 9.67% (CI: 7.84-11.50). Figure 42 demonstrates the ADC and cell density results for all patients.

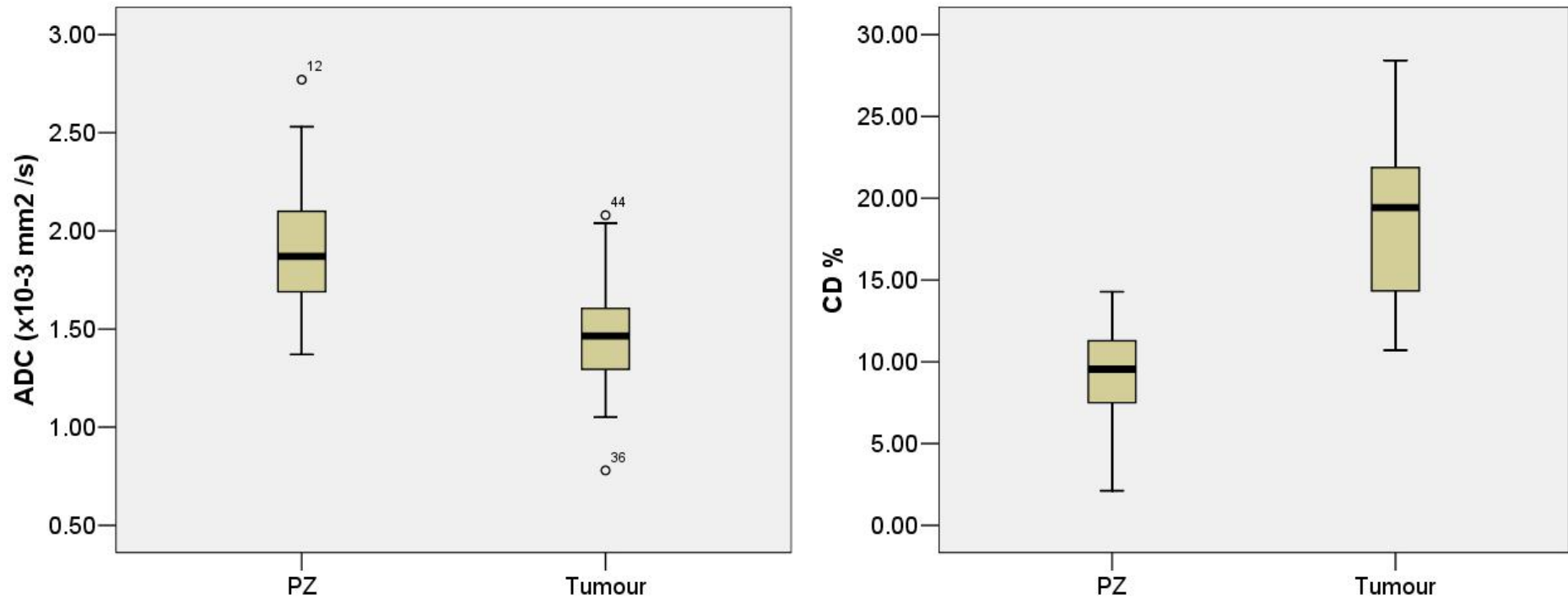
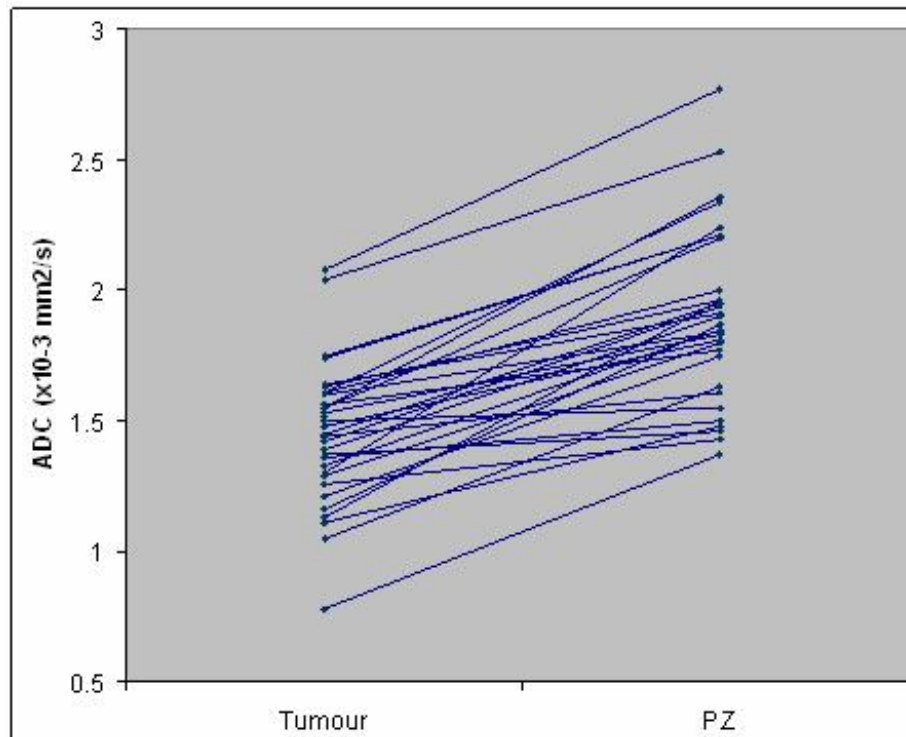
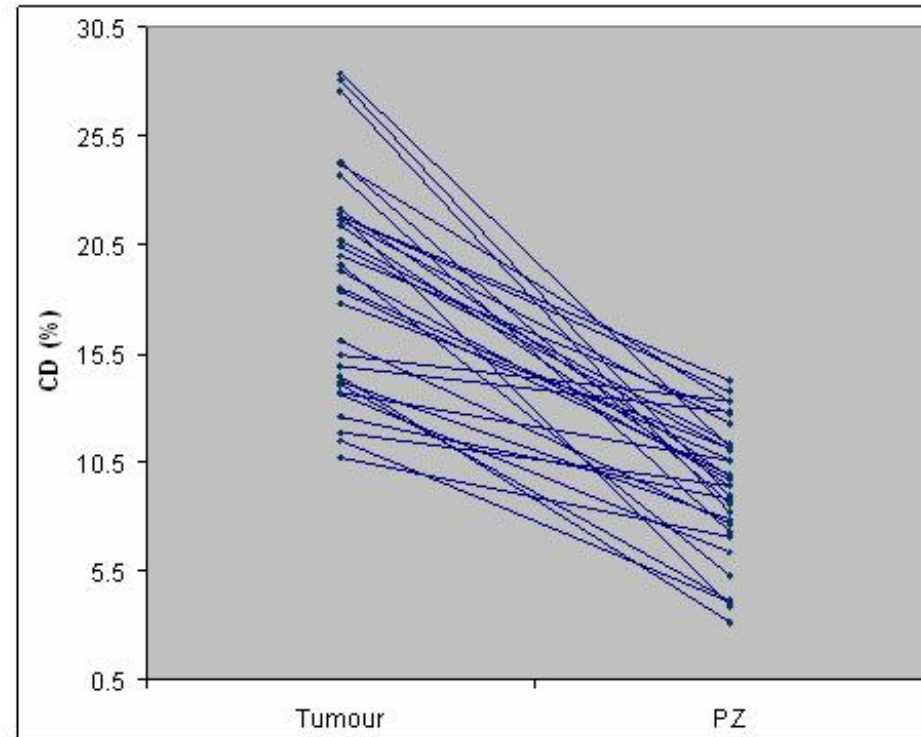


Figure 42 Boxplot showing the differences in mean CD and ADC between the PZ and cancer areas. There is a degree of overlap between the 2 tissues.

Despite the overlap between the two tissue types, all cancer lesions had lower ADC value and higher cell density compared to normal PZ within the same gland [Figure 43].



a



b

Figure 43. The differences in ADC values and cell density between tumour and normal PZ for all cases. Although there is a noticeable overlap in values between individuals, all cancer lesions demonstrated lower ADC values and higher CD values than normal PZ tissue.

If a cutoff value of $1.62 \times 10^{-3} \text{ mm}^2/\text{s}$ based on the ROC curve for ADC values is used, the resulting sensitivity and specificity for malignancy are 81% and 78% respectively. The area under the curve for diagnosing cancer, based solely on the ADC value, was 0.86 giving a predictive value for cancer of 0.71. [Figure 44].

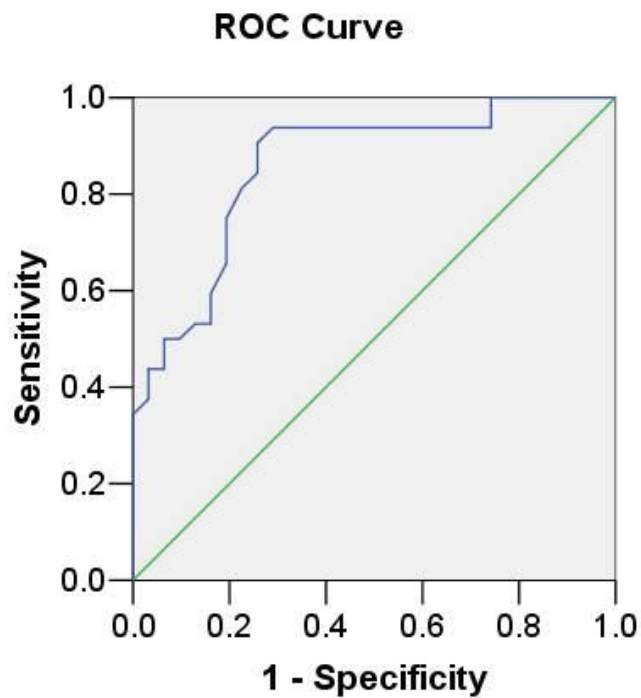


Figure 44. The blue line shows the ROC curve for ADC data. The AUC for tumour detection accuracy is 0.86.

There was a highly significant correlation between the ADC values and CD ($r = -0.50, p < 0.0001$) regardless of tissue type. The scatter plot in Figure 45 shows reduced ADC values from tissue demonstrating increased CD values. Furthermore, high CD values were seen in malignant lesions which had lower ADC values compared to normal PZ.

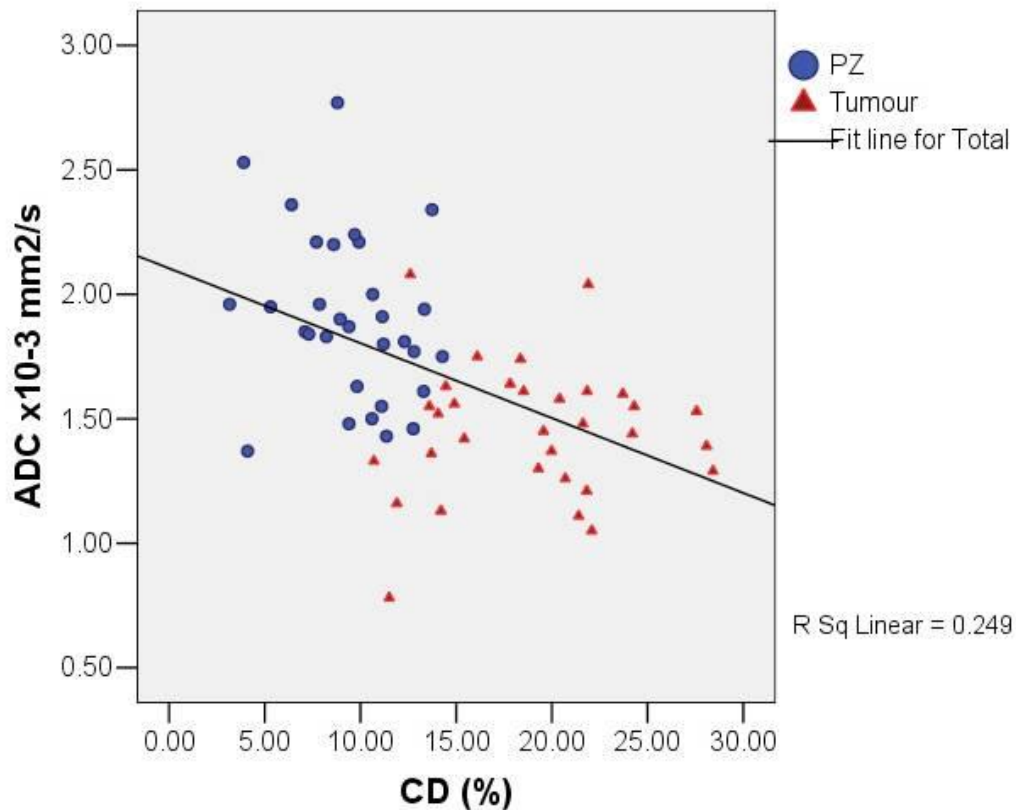


Figure 45. Scatter plot of the estimated CD (expressed as a percentage of surface area occupied by nuclei per high power field) with ADC value. A significant correlation ($p < 0.0001$) is obtained between the ADC value and the percentage CD for both tissue types (normal PZ and tumour).

Although there is a statistically significant correlation between tumour ADC and PSA ($r = -0.40$, $p = 0.024$), of note no significant correlation was noted between CD and PSA ($r = 0.12$, $p = 0.49$). Similarly Gleason score did not correlate with neither ADC nor CD ($r = -0.28$, $p = 0.115$ and $r = -0.03$, $p = 0.84$). By assessing the primary Gleason grade (as the most common pattern of cancer cells in the studied lesions) there was a moderate negative correlation with ADC ($r = -0.335$), but this did not achieve statistical

significance ($p= 0.061$). A poor correlation was noted between Gleason grade and CD ($r= 0.057$, $p= 0.758$). This limited correlation is possibly due to the small range of Gleason scores with the majority of cases (71.8%) recorded as Gleason 7.

4.4. Discussion

The extensive ductal structure of the normal prostate compared with the highly restricted intracellular and interstitial spaces encountered in prostate cancer, produces substantial differences in water diffusivity and thus the potential for high image contrast using DWI.

There have been several studies at 1.5 Tesla reporting statistical differences in ADC between prostate tissue types, especially between malignant lesions and normal peripheral zone [119, 123, 143, 144]. Ren et al [145] demonstrated significant differences in ADC values between normal prostatic tissue in volunteers and prostatic diseases including prostate cysts, BPH and prostate cancer. They suggested the use of this technique in the differential diagnosis of prostatic diseases.

In general, ADC values have been found to be significantly lower in malignant compared with non-malignant prostate tissue, leading to an improvement in tumour detection and identification, compared with T2 weighted imaging alone, with sensitivity and specificity values of 50% and 79.6% respectively for T2w alone, versus 73.2% and 80.8% for combined DWI and T2w imaging [146]. With advances in MR gradient coils, single shot

echo planar imaging (EPI) has emerged as the technique of choice for diffusion measurements in the prostate providing better resolution ADC images [125]. A study by Issa et al [126] using EPI DW imaging also showed statistical differences in ADC values between normal PZ, BPH and cancerous prostatic regions.

However, at 1.5 Tesla, the signal-to-noise ratio (SNR) is intrinsically low, and DW image quality is relatively poor. With the advent of 3.0 Tesla clinical scanners and improved receiver coils combined with parallel imaging, high SNR with low distortion DW images can be obtained within reasonable scan times. Consequently, the production of ADC maps of the prostate for clinical purposes is even more viable. Recent studies showed substantial promise using 3.0 Tesla diffusion imaging to differentiate between benign and malignant prostate tissue [117, 118, 120, 121, 147].

ADC values were found to be significantly lower in tumour regions compare to normal PZ [117, 118]. The criteria for a suspected malignancy on the ADC map was the presence of a hypointense focus relative to adjacent normal prostate tissue with or without comparison to T2 weighted images. This lacks direct correlation with the gold standard of histopathology. Therefore, researchers have used transrectal biopsy findings as a reference. The diffusion images were divided into regions and labeled as malignant or benign according to ADC values and compared with histology from biopsy samples for statistical analysis [121, 144, 146, 148]. There are a few disadvantages using this method: 1) the number of TRUS biopsies varies

from patient to patient; 2) biopsy findings do not provide tumour mapping and accurate localisation in relation to the whole prostate cannot be achieved; and 3) registering the TRUS and ADC images is difficult and the two procedures are often done by different clinicians. Recent reports have achieved a better comparison by using the whole mounted pathology specimen following radical prostatectomy. Mapping of tumour regions could then be drawn and direct comparison with ADC map performed [120, 122].

By using a 3.0 Tesla magnetic field for superior signal and with reference to whole mounted radical prostatectomy specimens, our results confirmed the previously documented evidence that ADC measurement is useful in differentiating normal PZ from malignant prostatic lesion. Most malignant lesions (81%) showed ADC values lower than our arbitrary cutoff value of $1.62 \times 10^{-3} \text{ mm}^2/\text{s}$ [Figure 46].

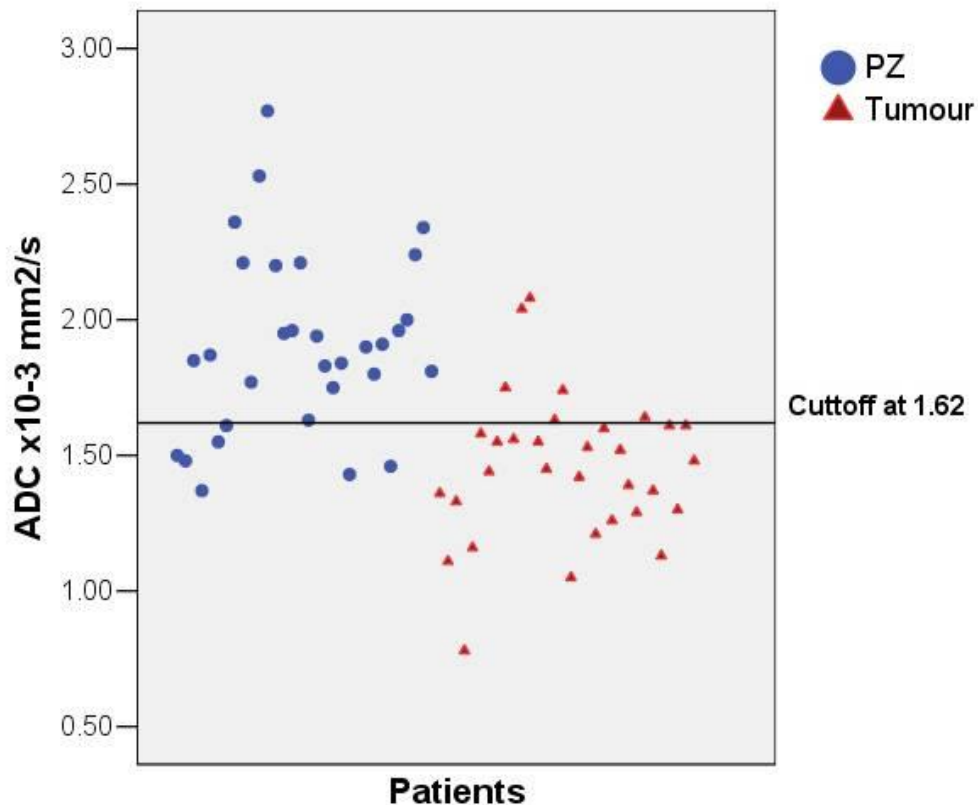


Figure 46. Using a cutoff ADC value of $1.62 \times 10^{-3} \text{ mm}^2/\text{s}$, a good separation is noted between tumour and normal PZ ADC values.

However, there was considerable overlap between ADC values of tumour and normal PZ; this indicates that the use of ADC value alone for tissue discrimination could result in misdiagnosis. It is recommended that interpretation of ADC values be carried out in comparison with ADC values for benign PZ in the same gland.

The increased cell proliferation in prostate cancer regions leads to the noted increased cell density of 18.89% for malignant foci versus 9.22% for normal PZ. As expected, the malignant tissue structure is compact with a loss of interstitial space, resulting in the restricted diffusion, which led to lower ADC

values in pathologically confirmed malignant lesions compared to normal PZ ($1.45 \times 10^{-3} \text{ mm}^2/\text{s}$ vs $1.90 \times 10^{-3} \text{ mm}^2/\text{s}$).

The correlation between ADC and CD is of great importance and can lead to future research. With reference to our results, we looked at CD as a characteristic of cancer that is related to cell proliferation. Measuring ADC values in suspected lesions pre-operatively can predict the CD, which may then reflect the cancer aggressiveness. Highly cellular cancers have a smaller interstitial space, hence a lower ADC. Through identification of the areas of highest cellularity, it might be possible to predict cancer aggressiveness. This will provide an additional diagnostic feature of preoperative prostate MRI.

There are some limitations to our study. First, a relatively small number of patients had no follow up data for PSA recurrence or cancer specific survival. This needs to be addressed in future studies in which a 5 or 10 years follow-up period would be required to identify any prognostic value of measuring ADC preoperatively.

Second, there were some difficulties in registering the exact site of the examined pathological lesion with the site of the ADC measurement, despite the use of identifiable landmarks. This was mainly due to specimen shrinkage and the different angulations, ranging between 10 to 20 degree, in which pathology and MRI axial sections were obtained.

Third, this study focused on the peripheral zone as it is the most common location of cancer, however, minority of cancer are located in the transitional zone and can be difficult to identify. In our cohort, three patients had both transitional zone and peripheral zone cancers. The ROIs in these cases were placed only in the peripheral zone lesions to obtain consistency of data and reduce bias. The central gland has a different cellular structure (compact fibromuscular stroma) compared to peripheral zone. It would be interesting to see the results of ADC and CD in central gland tumour in a larger study.

4.5. Conclusion

Tumour cellularity has a significant impact on ADC values obtained from malignant lesions and normal PZ. Differentiation between malignant lesions and normal PZ with DWI and the prediction of CD may have an important role in prostate cancer management.

Chapter Five

5. DESCRIPTION OF MR DERIVED ENHANCEMENT PARAMETERS IN PATHOLOGICALLY CONFIRMED PROSTATE CANCER AND NORMAL PERIPHERAL ZONE REGIONS

5.1. Objective

Research into angiogenesis has produced mounting evidence that alterations in microcirculation (blood circulation at capillary level) play an important role in the pathogenesis of many neoplastic diseases [149]. Abnormal angiogenesis is often accompanied by a change in physiological variables, such as capillary permeability and increased blood flow. In prostate cancer, studies have shown that microvessel density is an independent predictor factor of pathological stage [150] and has a significant association with the incidence of metastases [151]. A greater density of tumour vessels increases the opportunity for tumour cells to enter the circulation and subsequently develop metastases. Bettencourt et al [152] reported that microvascularity is a prognostic marker allowing prediction of tumour recurrence in patients undergoing radical prostatectomy.

Normally assessment of angiogenesis can be achieved only when pathologic specimens are obtained. However, many investigators have been attempting

to find reproducible, non-invasive, and quantitative methods of assessing neovascularisation in cancer. Dynamic contrast-enhanced MRI (DCE MRI) has been a promising diagnostic tool in the management of prostate cancer through its ability to spatially map the microvascular density, blood flow and permeability that is associated with malignant tumour growth [153-155].

Previous studies have analysed the signal intensity (SI) time curve utilising multi-compartment physiological models. These demonstrate the altered pharmacokinetic parameters in regions of increased enhancement due to malignancy, with results obtained at both 1.5 and 3 Tesla [156-158]. However, these models are complicated to derive, require longer DCE-MRI examination (more than 5 min) to allow the accumulation of contrast agent, and require extensive post processing.

This study aims to identify the differences in enhancement parameters between malignant prostatic lesions and normal peripheral zone (PZ), with reference to whole mount histopathology specimens, using model-free simple mathematical descriptions of SI time curves acquired using DCE-MRI at 3 Tesla.

5.2. Methods

5.2.1. Patients

Approval from the Local Ethics Committee was granted and written consent obtained from all patients for their MR images to be used for research purposes. Fifty two patients with biopsy proven prostate cancer were

recruited from January 2005 to December 2007. They were referred from the Urology Department for MR staging prior to radical prostatectomy. The mean age was 63 years (42-71), mean PSA was 7.6 ng/ml (2.5 - 16 ng/ml), Gleason score ranges from 6 to 9 with the majority of cases (61.5%) being Gleason 7. The minimum interval between trans-rectal ultrasound guided prostate biopsy and MR examination was six weeks to allow the inflammation and haemorrhage following biopsy to resolve. None of the patients received any treatment prior to MRI.

5.2.2. Image Acquisition

MRI was performed on a 3 Tesla scanner (Signa HDx, GE Healthcare, Milwaukee, USA) using an eight-channel, torso phased array, receive only coil. Patient preparation as discussed in chapter 3. After conventional T₂-weighted imaging, DCE-MRI was acquired axially using a 3D Fast Spoiled Gradient Recalled (FSPGR) sequence (18° flip angle, field of view 30 x 30 cm, matrix 256 x 128, TR/TE 5.1/2.1 ms, parallel imaging factor of 2, slice thickness 4-5 mm, temporal resolution 6.67 to 8.36 s per volume providing 700 to 800 images in 4:45 to 5:35 min). This was acquired immediately before, during and after bolus administration of 0.1 mmol/kg body weight Gadolinium-DTPA based contrast agent (Omniscan, GE Healthcare, Amersham) delivered by power injector (Spectris Solaris, Medrad, Indianola, Pennsylvania) at a rate of 3 ml/s, followed by 20 mls of normal saline. All MR images were analysed using a dynamic image viewing and analysis programme (XDIVA) developed using IDL (ITT Visual Information Solution, Boulder, Colorado).

5.2.3. Histological study

Patients proceeded to radical retropubic prostatectomy as the sole radical treatment. Prostatectomy specimens were prepared and examined as described in chapter 3. An experienced consultant pathologist outlined regions of tumour on the H&E slides.

5.2.4. Histology and DCE-MRI correlation

Regions of interest (ROIs) were manually drawn around tumour and normal PZ on the DCE images using the whole mounted specimens as reference [Figure 47].



Figure 47. The cancer regions are outlined on the H&E stained pathology slide of the whole mounted prostatectomy specimen (left). T2 weighted image shows a low signal intensity area in the right peripheral zone (middle). The positive enhancement integral image (right) shows the corresponding area of tumour (outlined in red) and an area of normal peripheral zone (outlined in grey). The high contrast uptake seen in the central gland on the positive enhancement integral image reflects the presence of hypervascular benign prostatic hypertrophy in most cases.

Each pathologic slice was visually matched to a corresponding MR image based on the location of the ejaculatory ducts, the diameter of the prostate, any identifiable benign hyperplastic nodules, and approximate distance from the base or apex. To be considered a match, the tumour must be in the same anterior or posterior half of the prostate and at the same level from the superior to inferior aspect of the gland. When only one cancer area was identified a similar sized area of normal PZ area was outlined. However, when more than one malignant lesion was identified in the prostate, equal numbers of normal PZ regions were assigned to facilitate statistical comparison. There were potentially some difficulties in registering the site of the examined pathological lesion with the site of the DCE measurement despite the use of identifiable landmarks. This was mainly due to specimen shrinkage and small differences in angulations ranging between 10 and 20 degrees, in which pathology and MRI axial sections were obtained.

5.2.5. Data analysis

The DCE MR images were used to automatically construct a “positive enhancement integral” map on a pixel-by-pixel basis. The XDIVA application was then used to outline ROIs in tumour and normal PZ, and to construct the SI-time curve. The point where the contrast reaches the prostate gland and causes the SI to begin to rise was visually marked on the SI-time curve. The application then automatically extracts parameters to measure changes in Enhancement Index (EI) over time for each ROI drawn on DCE images [figure 48], where Enhancement Index is defined as $(SI_t/SI_0) - 1$.

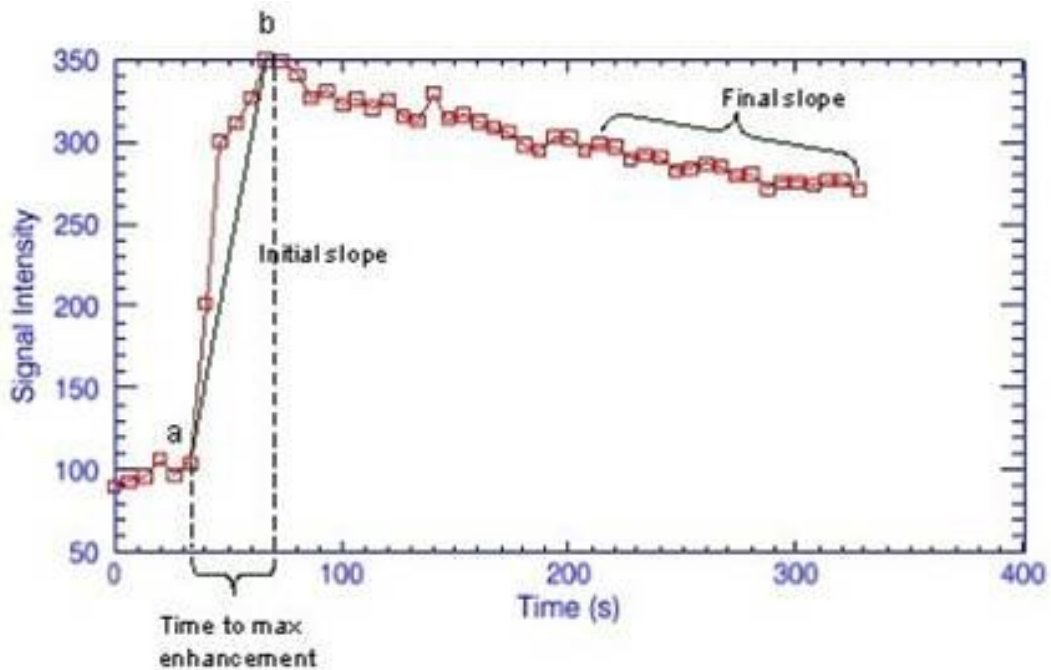


Figure 48. Signal intensity time curve for a typical malignant lesion (type 3 curve). X-axis shows time in seconds, and y-axis shows signal intensity (arbitrary unit). This illustrates the time when the contrast reached the prostate (a), maximum enhancement achieved (b), the time to maximum enhancement (b-a), initial and final slopes.

These enhancement parameters included the following:

Maximum Enhancement Index (MaxEI) was defined as the peak EI during the dynamic examination. Time to maximum (Tmax) was defined as the time taken for the EI to reach this maximum (MaxEI), taking the point where the contrast reaches the prostate as zero (point a in figure 48). Enhancement Index at 30s (EI₃₀) was defined as the fractional rise in signal at 30s compared to the initial pre-contrast signal. Initial slope was defined as the fractional change in signal per minute (1/min) following initial enhancement. This reflects the wash-in phase. Final slope was defined as the fractional change in signal per minute (1/min) for the final 2 minutes of the EI time

curve. This reflects the wash-out phase. The area under curve was defined as the integral of fractional enhancement over the first 4 minutes of contrast uptake following initial enhancement, and was corrected for differences in temporal resolution. The 4 minute period reflects the shortest acquisition time for the DCE-MRI series used in the study. Acquisition time changes were necessary due to scanner software upgrades and protocol development.

The types of SI time curves were described as: type 1, when SI increases with no subsequent decrease or leveling; type 2 when SI increases to a peak then levels off; and type 3 when SI increases rapidly and then decreases after a peak [Figure 49].

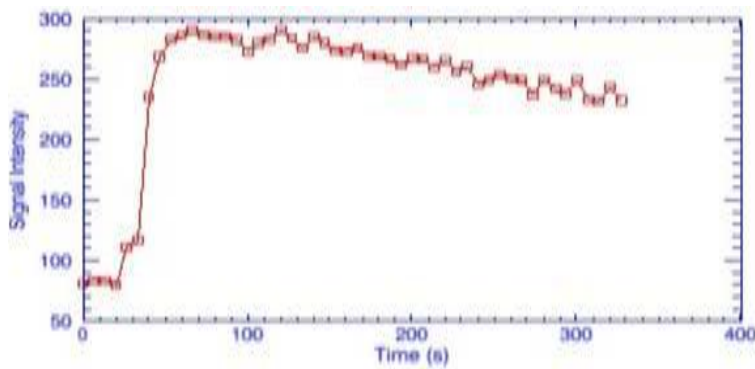
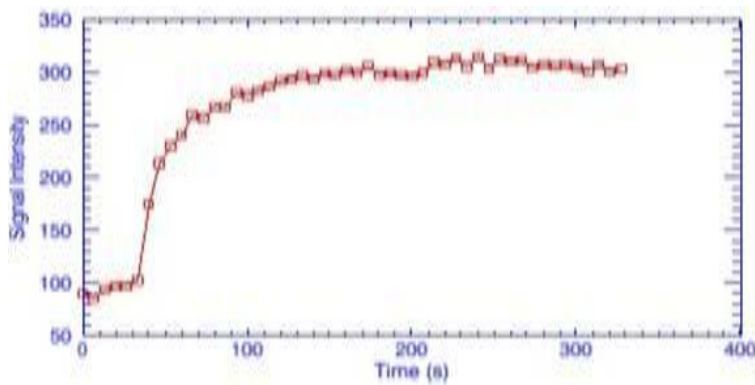
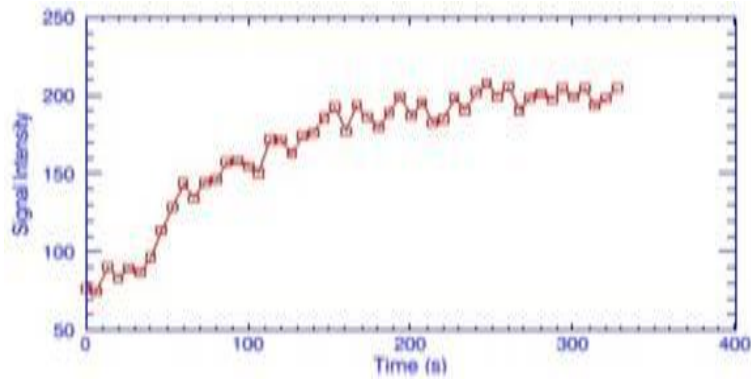


Figure 49. Types of SI time curve: Type 1 curve demonstrates slow SI rise with no subsequent washout (top); type 2 curve demonstrates rapid rise in SI and subsequent plateau with no rapid washout (middle); type 3 curve demonstrates rapid uptake in SI and rapid washout (bottom).

Statistical analysis was performed using SPSS (version 13.0, SPSS Inc., Chicago, IL, USA). The Kolmogorov-Smirnov test was used to demonstrate deviation from the normal distribution. A paired t-test was used to evaluate the statistical differences between PZ and tumour DCE parameters. Chi-square test was employed to test the difference in curve types. Receiver operating characteristic (ROC) analysis was employed to 50 ROIs (randomly selected 25 lesions and 25 normal PZ ROIs) to assess the different DCE parameter cut-off values for prostatic cancer in the PZ. These cut-off values were then used to test the sensitivity, specificity, positive predictive value, negative predictive value for the remaining 90 ROIs. Logistic regression analysis was utilized to identify the sensitivity and specificity of combined DCE parameters in identifying prostate cancer. Confidence intervals (CI) for ratios were calculated using the following formula as described by Gardner and Altman [159]:

$$p - (N_{1-\alpha/2} \times SE) \text{ to } p + (N_{1-\alpha/2} \times SE),$$

Where p is the observed proportion of subjects, $N_{1-\alpha/2}$ is the appropriate value from the standard normal distribution for the $100(1 - \alpha/2)$ percentile, SE is the standard error. For a 95% CI $N_{1-\alpha/2} = 1.96$.

5.3. Results

Seventy malignant lesions were identified in 52 patients and were compared with 70 regions of normal PZ. Table 24 demonstrates the differences in DCE-MRI parameters between malignant lesions and normal PZ.

Parameters	Region		P value
	Cancer lesion	Normal PZ	
MaxEI (a.u.)*	2.71 ± 1.09	1.74 ± 0.70	<0.0001
TMax (min)	2.04 ± 0.91	3.30 ± 0.66	<0.0001
EI at 30s (a.u.)	2.22 ± 1.04	1.04 ± 0.51	<0.0001
Initial slope (1/min)	4.44 ± 2.08	2.08 ± 1.03	<0.0001
Final slope (1/min)	-0.07 ± 0.14	0.08 ± 0.13	<0.0001
nAUC (a.u.)	9.34 ± 3.84	5.44 ± 2.17	<0.0001

*a.u. (arbitrary unit)

Table 26. Mean ± standard deviation values for all DCE parameters for cancer lesions and normal PZ. Statistically significant p value when tested utilizing paired T-test.

Malignant prostatic lesions had a 56% higher MaxEI compared to normal PZ and took nearly half the time to reach that maximum ($p < 0.0001$). Hence, at 30s, cancer lesions had double the EI compared to normal PZ. Similarly, the wash-in rate as represented by the initial slope was much higher in cancer lesions compared to normal PZ ($4.44 \pm 2.08/\text{min}$ versus $2.08 \pm 1.03/\text{min}$). Whilst the wash out rate, characterised by the final slope, was $-0.07/\text{min}$ for the cancer lesions (the negative value representing the reduction in signal

during the washout phase) that for normal PZ was 0.08/min. The area under the SI time curve was 72% higher in malignant lesions compared to normal PZ. This signifies the increased quantity of contrast accumulated as a consequence of changes in extracellular extravascular space, vessel permeability and perfusion.

ROC analysis was performed on a randomly selected set of 25 pairs of cancer and normal PZ ROIs to select cut-off values which were then used to assess the sensitivity, specificity and accuracy for each parameter individually for the remaining 45 pairs. The cut-off values for MaxEI, Tmax, EI30s, initial slope, final slope and nAUC were 1.93, 3.02min, 1.30, 2.59/min, 0.12/min, and 6 respectively. The ROI was labeled "malignant" if the value for the parameter was above the given cut-off values for MaxEI, ET30s, initial slope and nAUC and below the cut-off values for Tmax and final slope. Using these cut-off values, the most effective parameters were the EI30s and the initial slope with sensitivity of 87% and specificity of 76% as shown in Table 27.

	AUC	Chosen cut-off	Sensitivity (%)	Specificity (%)	PPV (%)	NPV (%)	Accuracy (%)
MaxEI	0.80	1.93	82 (71 - 93)	72 (56 - 85)	74 (62 - 86)	80 (68 - 92)	77 (68 - 85)
Tmax	0.89	3.02	84 (73 - 95)	76 (64 - 88)	77 (65 - 88)	83 (71 - 94)	80 (72 - 88)
EI (30s)	0.91	1.29	87 (77 - 97)	76 (74 - 92)	78 (67 - 89)	85 (74 - 96)	81 (73 - 89)
Initial slope	0.91	2.59	87 (77 - 97)	76 (74 - 92)	78 (67 - 89)	85 (74 - 96)	81 (73 - 89)
Final slope	0.76	0.12	73 (60 - 86)	74 (61 - 87)	74 (61 - 87)	73 (60 - 86)	74 (65 - 83)
nAUC	0.85	6.00	87 (77 - 97)	67 (53 - 80)	72 (59 - 85)	83 (71 - 95)	77 (68 - 85)

Table 27. AUC values for all enhancement parameters with the resulted sensitivity, specificity, positive predictive value (PPV), negative predictive value (NPV) and accuracy for tumour identification based on the pre-determined cut-off values. 95% confidence intervals are shown in parenthesis. (MaxEI: maximum enhancement index (arbitrary unit); Tmax: time to maximum enhancement (in minutes); EI: enhancement index (arbitrary unit); Initial and final slopes (arbitrary unit); nAUC :normalised area under SI-time curve (arbitrary unit))

A combination of parameters proved even more powerful as demonstrated by logistic regression analysis. The resulting sensitivity, specificity, positive predictive value, negative predictive value and accuracy for the combined DCE-MRI data are detailed in Table 28. This shows a good sensitivity of 89% and specificity of 90%. The only parameters that contributed significantly to the logistic regression model were MaxEI, Tmax and the area under SI time curve. After excluding the other parameters, there was no significant change in results, with a sensitivity of 89%, and specificity of 91%.

LRA parameters	Sensitivity (%)	Specificity (%)	PPV (%)	NPV (%)	Accuracy (%)
All parameters	89 (81 – 96)	90 (83 – 97)	90 (83 – 97)	89 (81 – 96)	89 (84 – 94)
Only significant parameters	89 (82 – 96)	91 (84 – 98)	91 (85 – 98)	89 (81 – 96)	90 (85 – 95)

Table 28. Logistic regression analysis results including all enhancement parameters (2nd row) and after excluding the non-significant parameters (3rd row). 95% confidence intervals are shown in parenthesis.

By looking only at the types of SI time curve, the following results are obtained: in the cancer group, 24 cases were type 3, 39 cases were type 2, and seven cases were type 1. Whereas in the normal PZ group, none of the cases were type 3, 25 cases were type 2, and 45 cases were type 1 (Chi-square test = 18.05, $p < 0.0001$). Significant overlap in type 2 curve is noted. These are the difficult cases that require a better way to separate lesions from normal PZ. When selecting only cases with type 2 curve (39 tumour and 25 normal PZ), the difference in enhancement parameters remains highly significant (Table 29).

Parameters	Region		P value *
	Cancer lesion	Normal PZ	
MaxEI	2.91 ± 1.34	1.86 ± 0.81	<0.0001
TMax (min)	1.87 ± 0.81	2.88 ± 0.78	<0.0001
EI ₃₀	2.43 ± 1.24	1.36 ± 0.64	<0.0001
Initial slope (/min)	4.86 ± 2.48	2.72 ± 1.27	<0.0001
Final slope (/min)	-0.06 ± 1.55	0.03 ± 0.13	=0.009
nAUC	10.08 ± 4.70	6.17 ± 2.66	<0.0001

(* Paired T test.)

Table 29. By selecting cases with type 2 SI time curves only, the mean ± standard deviation values for all DCE parameters in cancer lesions and normal PZ remains statistically significant. A paired T-test was used to evaluate differences.

Employing the logistic regression model, with only the significant parameters (MaxEI, Tmax, AUC) included for type 2 curve cases, showed high sensitivity, specificity, positive predictive value, negative predictive value and accuracy for tumour identification: 90% (95% CI= 80% to 99%), 84% (95% CI= 70% to 98%), 90% (95% CI= 80% to 99%), 84% (95% CI= 70% to 98%) and 88% (95% CI= 79% to 96%) respectively. This allows identification of malignant lesions even though they demonstrate type 2 curve pattern.

5.4. Discussion

With the introduction of Gadolinium contrast agent, advances in MR sequences with improvements in spatial and temporal resolution, DCE-MRI has become commonly used in the evaluation of prostate cancer. Alonzi et al [153] reviewed the use of dynamic imaging in prostate cancer and demonstrated an improvement in sensitivity, specificity and accuracy in cancer localisation and staging, compared to T₂-weighted imaging alone. Jager et al [160] reported improvement in tumour localisation mainly based on enhanced sensitivity of DCE-MRI compared to T2 weighted imaging (73.5% versus 57.5% respectively).

Several studies [111, 161, 162] have shown that, after giving a gadolinium-based contrast agent, prostate cancer enhances earlier and washes out faster than normal PZ. Liney et al [163], in a study of 12 patients, reported a shorter time to reach maximum enhancement in suspected prostate cancer lesions compared to normal PZ (2.48 min versus 3.74 min). Padhani et al [164] showed a significant difference in signal intensity parameters between normal PZ and tumour, but there was no direct histological correlation. Other studies at 1.5 Tesla [111, 161, 162, 165] have used whole mount prostatectomy specimens as a standard reference to correlate with regions of interest (ROI) co-registered on DCE images obtained preoperatively. Significant differences in various DCE parameters were noted between cancer and normal PZ regions.

To our knowledge, this study is the first to evaluate simple model free enhancement parameters at 3 Tesla using whole mount radical prostatectomy specimens as reference. At 3 Tesla, compared to 1.5 Tesla, there is a doubling of the signal-to-noise ratio which can be used to improve spatial resolution and, by employing parallel imaging techniques, the temporal resolution of the MR measurements can also be significantly improved. The superior temporal resolution for any given region of interest provides better delineation of changes in tissue signal intensity observed during contrast administration.

During the dynamic series of our study, we noted that contrast reaches the prostate gland in 24-28 seconds. This depends on several factors such as cardiac output and the vascularity of the prostate. Measuring the enhancement parameters from the time the contrast reaches the prostate (position *a* in Figure 48), rather from the time of contrast injection, gives consistency to the obtained data and reduces bias.

Alternative approaches exist to analyse data obtained by DCE-MRI. Fully quantitative kinetic parameters can be derived from concentration-time curves that are mathematically fit using one of a number of recognised pharmacokinetic models. These models require knowledge of native tissue T_1 and the arterial input function, both of which can be variable and subject to significant errors. The approach chosen here, whereby the evaluated parameters are model free indices (often called semi-quantitative) that describe tissue enhancement using a number of simple descriptors, reflects

the clinical requirements of radiologists to make a diagnostic decision. These model free parameters are relatively straightforward to calculate; they do however, have some limitations including the fact that they may not accurately reflect the changing contrast medium concentration in tissue.

The maximum enhancement during the early phase of DCE-MRI was earlier and higher in prostate cancer lesions compared to normal PZ. This reflects the increase in vascular perfusion and the accumulation of contrast agent in cancer lesions. However, this measurement is not consistent in cases where the enhancement continues to increase or remains relatively constant throughout the experiment time (4 minutes in this study), as the time to maximum enhancement can only give a correct value if the studied signal reaches its maximum enhancement before the end of the experiment. This should be interpreted with caution. Moreover, our algorithm uses a strictly numeric search and does not take into account any noise spikes which may occur following the change of the curve from maximum upslope to a more flat slope. Improvement to the algorithm need to be addressed in future studies. This includes filtering out the noise spikes and the use of the initial 90% of max enhancement of Noworolski [166].

The initial slope reflects the degree of early enhancement in the tissue. The increase in signal enhancement does not derive from the contrast agent in the blood vessels only, but from the accumulation of contrast in the interstitial space. The initial slope reflects mostly the vascular permeability and the size of interstitial space. We determined the initial slope from the time between

the contrast reaching the prostate (start of the signal intensity rise) and the 30s time point. This was in line with the reports of other studies, which found that DCE scanning window between 30s and 60s after contrast injection allows a good depiction of cancer within PZ [162, 165].

Delayed imaging obtained 3-4 min after injection is useful to appreciate the wash-out phase of the contrast agent and helps to discriminate cancer from normal PZ. In agreement with the results of other studies [162, 167], we found that contrast wash-out was significantly more prominent in cancer than in normal PZ, as determined by the negative final slope (-0.067 versus 0.088 /min). This reflects the increased vascular permeability and /or increase vasculature surface area in cancers as the increased concentration of contrast in the interstitial space leaks back into the vasculature and drains out from the cancer lesions more rapidly than from normal tissue.

The shape of the SI time curve provides additional information. Although there is a degree of overlap between cancer and normal PZ curves, all type 3 curves were related to cancerous lesions, whereas 86.5% of type 1 curves were related to normal PZ. The difficulty arises in evaluating cases with a type 2 curve, since there is a considerable overlap between the two tissue types. However, by evaluating the SI time curve parameters, highly significant differences between tumour and normal PZ regions could be achieved with good sensitivity and specificity. This suggests that a simple visual assessment of DCE-MRI based on the curve shape may not differentiate between malignant and normal enhancing tissues leading to low

diagnostic accuracy. Further assessment using this simple technique may lead to a better result for tumour identification.

This semi-quantitative assessment of DCE parameters may have an important role not only in tumour localisation, but also in assessment of prostate cancer response to anti-androgen therapy. Padhani *et al* [168] have assessed the effects of hormone treatment on vascular permeability, as evaluated by DCE-MRI, and have shown a significant reduction in tumour permeability following androgen deprivation.

There are some limitations to the use of MRI in prostate cancer patients. Post biopsy haemorrhage leads to artefacts which are known to interfere with MR image interpretation and result in overestimation of tumour volume. Previous studies [169, 170] have recommended deferring an MRI examination for at least 3 weeks after biopsy, to obtain more reliable tumour localisation and staging accuracy. We deferred all MR examinations for 6 weeks, which was adequate to obtain good quality images in our cohort of patients.

We failed to identify any significant correlation between the DCE-MRI parameters and PSA or Gleason score. This is in line with previous reports [160, 164]. A correlation between enhancement parameters and Gleason score may have been expected, since the latter has been shown to correlate with microvessel density measurement [171]. However, the lack of correlation seen may be explained by selection bias in our series, as the majority of

patients (88.4%) undergoing radical prostatectomy for potentially organ confined disease had either Gleason 6 or 7.

We did not study the enhancement patterns of prostatitis or central gland benign prostatic hypertrophy (BPH) lesions. Previous reports failed to establish a significant difference in enhancement pattern between BPH and cancer lesions [153, 162, 164]. Also, you would expect that prostatitis can cause increased vascularity and permeability due to the release of inflammatory factors, however, the features of DCE-MRI in prostatitis have not been published in peer reviewed journal. Therefore, the accuracy of DCE-MRI in detecting cancers in central gland or in the presence of prostatitis remains to be determined.

5.5. Conclusion:

DCE-MRI is a simple, quick technique which allows evaluation of malignant lesions based on their abnormal vascular features. The significant differences in DCE-MRI parameters between cancer and normal areas can improve the localisation of tumour foci, which may have many potential uses including directing prostate biopsy or targeting cancer lesions for minimal invasive treatment.

Chapter Six

6. THE POTENTIAL ROLE OF 3 TESLA MRI IN PATIENTS WITH RISING PSA BUT NEGATIVE PROSTATIC BIOPSIES

6.1. Introduction

The management of patients with a persistently increasing serum prostate specific antigen (PSA) level and negative prostatic biopsies can be difficult, debatable and represents a great diagnostic challenge to urologists.

Patients with a negative first set of trans rectal ultrasound-guided (TRUS) biopsies often undergo multiple repeated biopsies, prompted by the presence of atypical suspicious cells in the first biopsy, rising PSA and/or abnormal digital rectal examination [105]. The reported detection rate of malignancy in the second set of biopsies is 10-23% [172, 173] but can be up to 41% when more than two sets of biopsies were performed [174]. The European Prostate Cancer Detection Study [172] reported their findings in a cohort of 1051 men with PSA values between 4.0 and 10.0 ng/mL. After an initial cancer detection rate of 22% with sextant biopsy, their subsequent positive biopsy rates were 10%, 5% and 4% for the second, third and fourth attempts respectively. Researchers have also examined the role of extended, repeated biopsy (saturation biopsy) when approximately 20 biopsies are done under general anaesthetics. Stewart *et al* [175] performed saturation biopsies in 224 men in whom previous negative biopsies had been reported.

Cancer was detected in 34% of patients, of which 68% warranted radical prostatectomy. In a recent study a group from Leicester [176], assessed a standardized 36 core template-assisted transperineal prostate biopsy technique in 40 patients with elevated PSA and previous multiple prostate biopsies. They detected prostate cancer in 68% of patients, with Gleason score ranges from 6 to 9. They concluded that the technique is safe and effective and should be considered in this cohort of patients.

The reported data detailed above shows the lack of sensitivity of TRUS for detecting prostate cancer. Due to the high false negative rate of TRUS biopsy, a more reliable imaging modality to detect prostate cancer and direct prostatic biopsy is needed. Although MRI has been used mainly for localisation and staging of biopsy proven prostate cancer, a few studies have focused on the role of MRI in patients with previously negative TRUS biopsy [177-180]. Researchers have used various sequences, with a wide variation in the reported sensitivity and specificity [181].

In this study, the role of MRI at our centre in the assessment of patients with rising PSA and previous negative TRUS biopsy, using dynamic contrast enhancement and endorectal imaging is evaluated.

6.2. Methods

6.2.1. Patients recruitment

This was a prospective, single arm, consecutive patient study. Ethical and trust approval was obtained prior to recruitment. The protocol was reviewed

by two external referees. Inclusion criteria were patients who were considered for repeat TRUS biopsy, on the basis of abnormal clinical examination, persistent PSA elevation or the presence of suspicious cells on previous biopsies. Exclusion criteria were contraindications to MRI. The patient information leaflet was reviewed by the local Research Consumer Panel and validated. Patients were invited to enter the study and were given the information leaflet at least 7 days prior to MRI scanning to allow sufficient time to make an informed decision about participation. Formal consent was obtained from all patients.

Twelve patients were included in the study with ages ranging from 60 to 72 years and a mean age of 65.7. The mean PSA value was 7.6 ng/mL, ranging from 4.2 to 16 ng/mL. All patients had at least one previous set of TRUS biopsies which were negative for malignancy. Time from the most recent set of TRUS biopsies to study entry ranged from 4 to 100 weeks (median 22 weeks). The indication for repeat TRUS biopsy was persistently elevated PSA value in 7 patients and the presence of suspicious cells on initial biopsy in 5 patients.

6.2.2. MR examination

MR preparation, parameters for T2 weighted and DCE-MRI and the use of endorectal coil imaging have already been described in Chapter 3. All studies were read by 2 clinicians in consensus (one MR radiologist and one research fellow in prostate MRI). In each image, the prostate gland was assessed for tumour involvement. Suspicious areas were localised by assigning them into

posterior/ anterior, lateral/ medial, base/ mid/ apex and left/ right sectors. The MR information was based on the combined data from T2 weighted imaging and DCE-MRI and were formally reported by an experienced MR radiologist. The images were classified as normal or suspicious based on areas of low signal intensity on T2 weighted imaging and/or areas of increased contrast uptake on DCE-MRI. Images were then saved onto CD for subsequent use in directing TRUS biopsy [Figure 50].

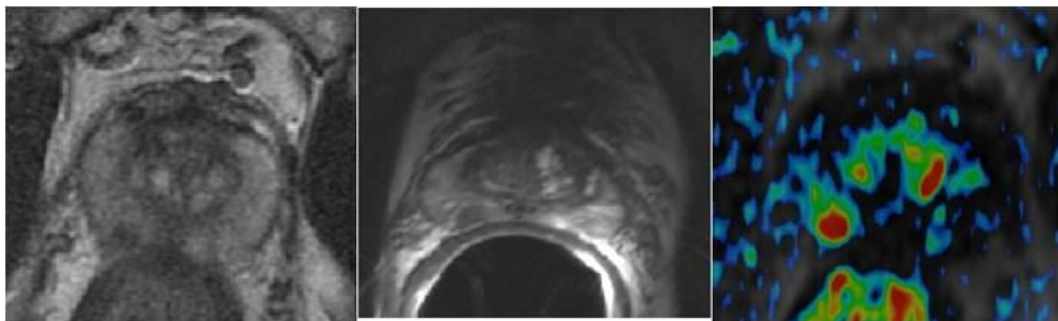


Figure 50. Suspicious area of low signal intensity seen in the right postero-medial PZ on T2 weighted imaging using PPA (left) and ER coils (middle). This correlates with an area (shown in red) of increased contrast uptake seen on DCE-MRI (right).

6.2.3. TRUS biopsy

This was performed within a week following the MRI. All biopsies were performed by a single experienced radiologist. Standard preparation was followed (quinilone and metronidazole antibiotic prophylaxis and enema administration). A Phillips ultrasound machine (Phillips iU22) with transrectal probe (C9.5 EC) was used. Patients were scanned in the left lateral decubitus position with knees and hips flexed to 90 degrees. Ultrasound

assessment of the prostate was done in both axial and sagittal planes [Figure 51]; biopsies were performed in the axial plane.

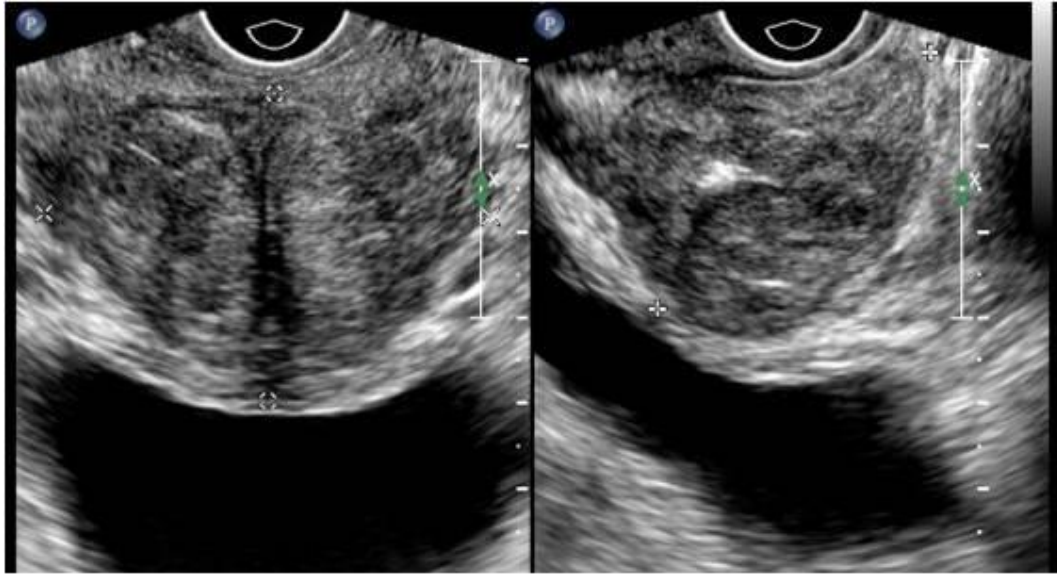


Figure 51. Trans-rectal ultrasound scan. Axial view on the left and sagittal view on the right. This allows measurement of the prostate gland in 3 dimensions to get the prostatic volume.

Local anaesthesia of the prostate was achieved using Lidocaine infiltration around the nerves bundles. Prostatic cores were obtained using an 18 gauge biopsy needle with a spring loaded biopsy gun (Manan gun, MANNAN Medical Products, Inc). A 12 core biopsy scheme was employed [Figure 52] including one targeted biopsy from the area that had suspicious changes on MR imaging.

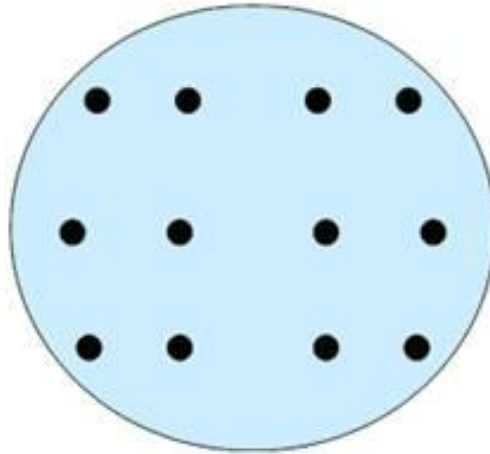


Figure 52. 12 core biopsy scheme. This was adjusted to include one biopsy from the suspicious area detected on MR imaging.

The number of biopsies remained the same (12 cores) as per routine clinical practice to prevent detection bias, as a higher number of biopsies will lead to a higher detection rate. The suspicious areas were identified by carefully evaluating the MR images while slicing the TRUS image from the prostate base to the apex axially and from the urethra to the left or right laterally [Figure 53]. The targeted biopsy was labelled and sent in a separate pot for histological examination.

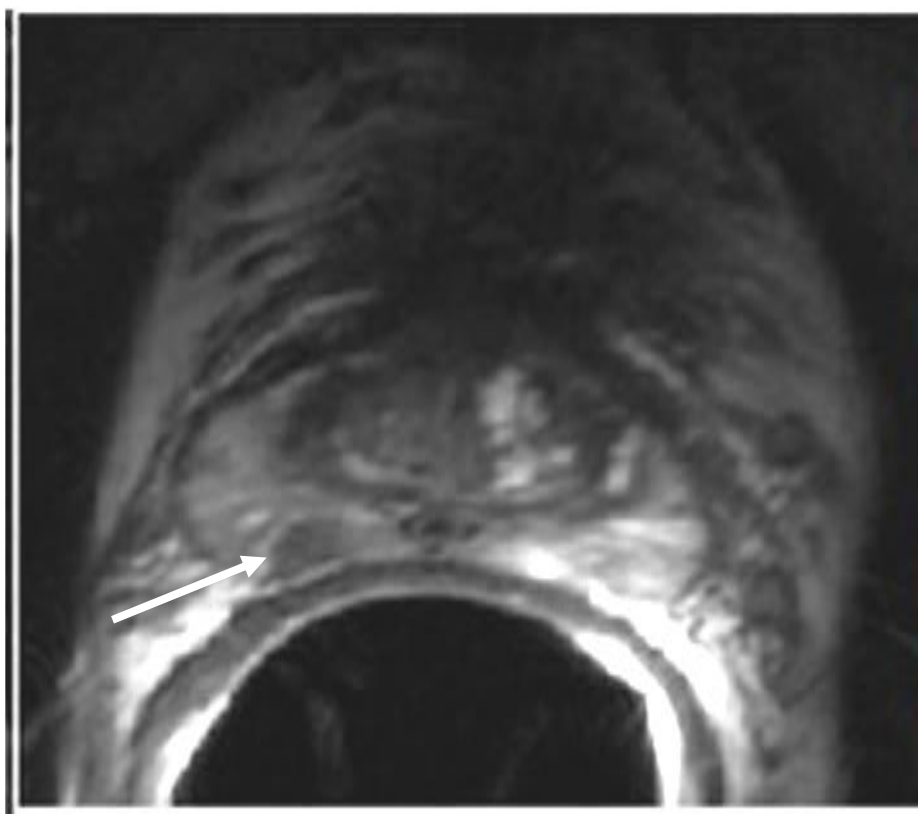
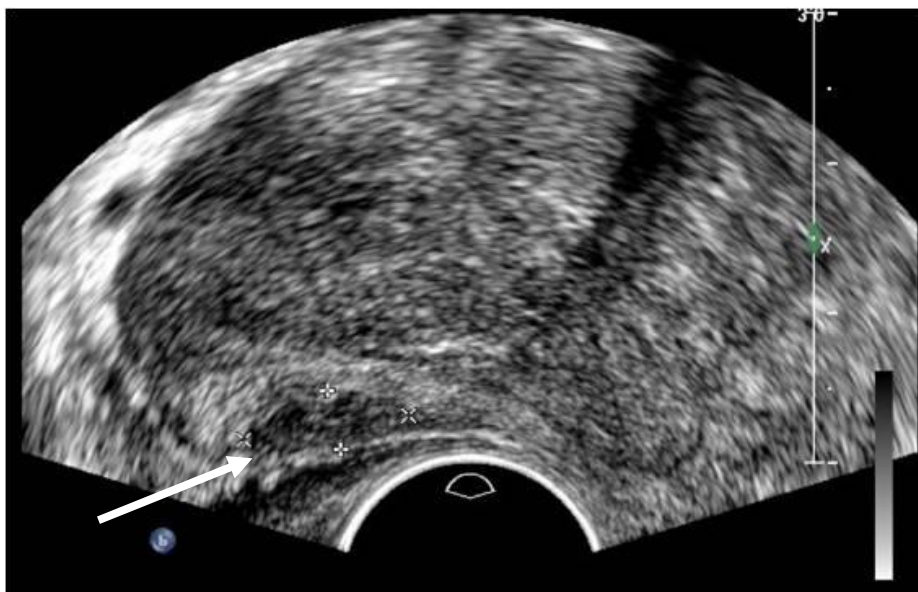


Figure 53. Hypoechoic lesion imaged during TRUS in an area highly suspicious of cancer on MRI (white arrow). Biopsy revealed adenocarcinoma.

6.3. Results

Seven (58.3%) prostate cancers were diagnosed in the 12 patients recruited (5 cases with Gleason score of 3+3=6, and 2 cases with Gleason score of 3+4=7. ASAP had previously been diagnosed in 4/7 of these patients. As shown in Table 30, MRI identified suspicious areas consistent with malignancy in 11 cases. Out of these cases, biopsy showed cancer presence in 7 cases. However, the site of positive biopsy correlated correctly with the exact area of suspicion on MRI in 3 cases (27.2%) only. For the remaining 4 cases, 3 cases showed cancer in the same side as the suspicious MRI findings, but in one case the cancer was on the side contra-lateral to the MRI lesion (patient number 1).

Patient number	Site of MRI lesion	Pathological evidence of cancer	Site of cancer on biopsy	Pathological features of MRI focus
1	Right	Positive	Left	Normal
2	Left	Negative	-	Normal
3	Left	Positive	Left	Cancer
4	Right	Positive	Right	Cancer
5	Right	Positive	Right	Inflammation
6	Left	Negative	-	Inflammation
7	Right	Negative	-	Inflammation
8	Left	Negative	-	Inflammation
9	Right	Positive	Right	Cancer
10	Negative	Negative	-	Normal
11	Right	Positive	Right	Normal
12	Left	Positive	Left	Normal

Table 30. This shows the site of suspicious lesion on MRI, if cancer was detected in this biopsy round, its site and pathological findings for the suspicious MRI focus for each patient.

Out of the 11 cases with suspicious MRI findings, 4 cases showed active, high degree of inflammation with several acini filled with neutrophil polymorphs and the formation of microabscesses within the targeted biopsies, but with no evidence of cancer in the gland.

Although the suspicious MRI site was shown to be pathologically normal in 4 cases, cancer was detected in other areas of the gland in 3 cases [Figure 54].

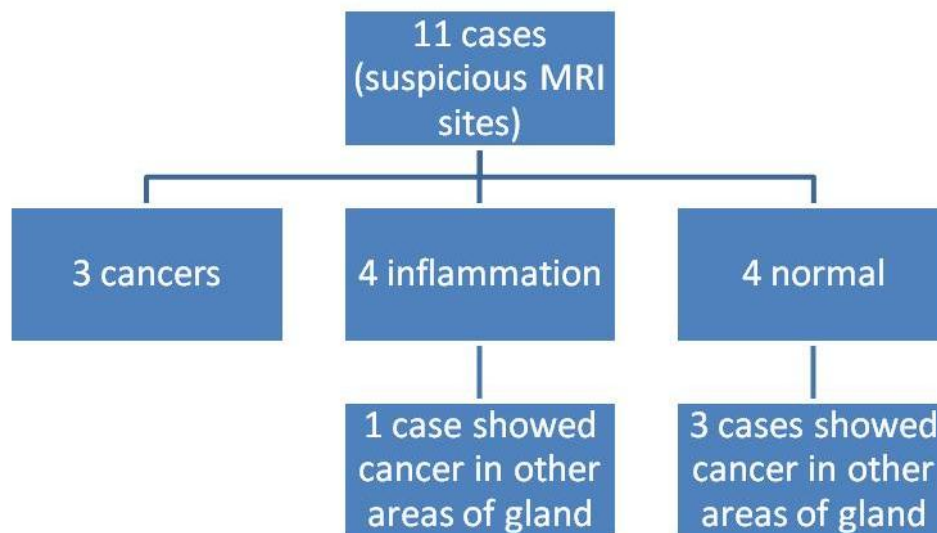


Figure 54. Organisation chart detailing all the pathological findings for the suspicious MR lesions.

6.4. Discussion

Despite the advances in our understanding of PSA and its use to indicate TRUS biopsy, the prostate cancer detection rate for sextant biopsy remains low [172]. Therefore, further biopsies are often indicated in cases of persistent elevation of PSA or in the presence of ASAP. Eight, twelve and even saturation biopsies have been performed to improve the detection rate.

The detection of ASAP on the initial biopsy warrants further investigations due to its strong association with prostate cancer [182]. Cancer is found on subsequent biopsies after the initial diagnosis of ASAP in 55% of cases [51], which indicates that a ASAP diagnosis mandates immediate re-biopsy.

Investigators have attempted to detect prostate cancer prior to biopsy using transrectal ultrasound scanning. Although cancer was detected in 30% of patients with a hypoechoic lesion, 18% of men with a normal TRUS had prostate cancer and as many cancers were isoechoic as were hypoechoic [183]. Consequently, researchers have studied the role of MRI in this group of patients to detect suspicious foci to be targeted for biopsy [176-181, 184]. The aim is to diagnose cancer earlier and prevent further unnecessary biopsies with their associated morbidity and complications.

In a study performed by Perotti et al [179], MR imaging with the use of an endorectal coil had encouraging results for the detection of tumour foci in patients who had elevated PSA levels and negative TRUS biopsy. In their study, endorectal MRI had 85.7% sensitivity and 65.4% specificity for detecting malignant lesions. The site of positive biopsy correlated correctly with the area of suspicion on MRI in 85.7% of cases.

In another study performed by Beyersdorff et al [178], combined endorectal and phased-array body coil technique was used. They achieved a similar sensitivity and specificity to Perotti et al. However, a site-by-site analysis

failed to show a significant correlation between MR imaging and individual biopsy site findings.

The use of MR spectroscopy has also been investigated in patients with prior negative biopsy in order to improve cancer detection rate on subsequent biopsy. In general, authors reported good and promising results to warrant the routine clinical use of MRI in this group of patients [Table 31].

	Pt No	SEN (%)	SPEC (%)	PPV (%)	NPV (%)	Acc (%)
Bhatia et al	21	100	84	40	100	86
Amsellem-Ouazana et al	42	73	96	92	87	88
Prando et al	42	100	44	55	100	67
Yuen et al	24	100	71	58	100	79

Table 31. A review of papers on the use of MR spectroscopy in patients with prior negative biopsy. (Patient number (Pt No), Sensitivity (SEN), Specificity (SPEC), Positive predictive value (PPV), Negative predictive value (NPV), Accuracy (ACC)).

In the Yuen et al study [180], MR spectroscopy increased the sensitivity and NPV of prostate cancer detection from 57% to 100% and from 83% to 100% respectively. However, the specificity and PPV decreased from 88% to 71% and 67% to 58% respectively.

The study described in this chapter is unique as it assesses the role of DCE-MRI for the detection of cancer foci in the prostate prior to repeat biopsy.

DCE-MRI has the potential to image the increased vascularity seen in cancers and hence improve localisation and detection based on the abnormal vascular morphology. It has been reported to increase the sensitivity and specificity for tumour detection compared to T2 weighted imaging [185].

This study showed that combined T2 weighted and DCE-MRI detected cancer within the same prostatic lobe in 7 out of 11 cases. However, there was a poor anatomical correlation between the area positive for malignancy on biopsy and the suspicious region on MRI (3 out of 11). A possible explanation for this finding is the difficulty in ensuring the accuracy of targeting of the TRUS guided biopsy to suspicious areas seen on MRI. The sampled area may not have correlated with the area intended for sampling. This spatial accuracy cannot be assessed unless all patients underwent radical prostatectomy to obtain whole mounted pathological correlates. In the studied cohort only two patients proceeded to radical prostatectomy (patients no 4 and 5 in table 30). The pathological assessment of these specimens confirmed the presence of cancer in the area corresponding to the suspicious lesion on MRI.

Another explanation is the presence of prostatitis. The inflammatory process can lead to hypervascularity similar to that seen in cancers. This gives the appearances of increased signal intensity on DCE-MRI mimicking a malignant lesion. This was the case in 4 patients in this study, where DCE-

MRI showed areas of increase contrast uptake, but biopsy of the suspicious site confirmed inflammatory activity only.

The results of this study should be interpreted cautiously due to the small sample size. The main limitation in this study that it was a pilot study which only assessed tumour in the peripheral zones where the MRI appearance and contrast uptake are characteristic. Central gland tumours were not assessed because of the limitation of DCE-MRI in detecting cancer foci due to the increased contrast uptake in the central gland secondary to benign prostatic hyperplasia. However, central gland tumours are much less common and biopsy of the central gland is not routinely performed.

It is unclear whether our diagnostic performance would improve the detection of prostate cancer. In the three cases where cancer was found at the same site of MR suspicious area, the rest of the 12 biopsies also detected cancer within the same prostatic lobe. This means that the diagnosis of prostate cancer will be made anyway regardless of the MRI findings and none of the cancer would have been missed if TRUS biopsy had not been directed at the abnormal areas detected by MRI.

6.5. Conclusion

My findings suggest that the role of DCE-MRI, in guiding TRUS biopsy in patients with prior negative biopsy, is still in its infancy. To validate this hypothesis, a larger number of patients must be studied and a better registration of MRI and TRUS images should be performed.

Chapter Seven

7. VISUALISATION OF PROSTATE CANCER FOCI AND PROSTATE CAPSULE USING ENDORECTAL COIL COMPARED TO PELVIC-PHASED ARRAY COIL AT 3 TESLA MRI

7.1. Introduction

The introduction of an endorectal coil (ERC) at 1.5T has improved the visualization of the prostate and its surrounding structures due to an increase in SNR. Hricak *et al* [170] reported superior staging results with the use of an integrated endorectal and PPA coil compared with PPA coil alone (68% vs 77% accuracy rates). However reports have quoted variable results with staging accuracy ranging from 60% to 80% for detecting extracapsular and seminal vesicle infiltration [127, 169, 186-195]. When readers achieve high specificity for extracapsular detection, their results suffer from considerable reduction in sensitivity [169, 186, 190, 191], as well as considerable inter-observer variability as discussed in chapter 3 [189, 191, 195]. The detection rate of tumour foci within the gland using ERC imaging at 1.5T has been reported to be 50-76% on T2w MR images with a false positive rate of 6-35% [190, 193, 196].

Since 3 Tesla whole body MR scanning has come into clinical practice, its image quality has been studied against endorectal coil at 1.5 Tesla imaging.

Sosna *et al* [197] qualitatively compared the image quality of phased-array body coil imaging of the prostate at 3Tesla with that of endorectal imaging at 1.5Tesla, and found them to be comparable.

It is a natural extension that the use of an ERC at 3T will further improve the image quality by allowing higher spatial resolution to be implemented with reduced slice thickness and smaller voxel size [100, 102]. This will potentially lead to better visualization of the prostate gland and the surrounding structures, revealing patho-anatomical details and subtle abnormalities not seen on either external pelvic phased array (PPA) coil alone at 3T or the combined external/endorectal coil at 1.5T [100, 198]. Preliminary results comparing 3T endorectal MRI with whole mounted histopathology results showed high staging accuracy mostly due to the improved detection of minimal capsular invasion [102].

The aim of this study is to evaluate the impact of endorectal MRI at 3T on visualisation of prostate zonal anatomy, identification of tumour extent and delineation of the capsule and peri-prostatic soft tissue and seminal vesicles.

7.2. Methods

7.2.1. Patient characteristics

56 patients (median age of 67 years with a range of 51 to 85 years) with biopsy proven prostate cancer were referred from the urology department for endorectal MR imaging. Median PSA was 8.4 ng/mL (range from 0.7 to 250 ng/mL) and median Gleason grade was 7 (range from 5 to 9). Exclusion

criteria were contraindications to MR imaging (e.g cardiac pacemakers, intra-orbital metal foreign bodies), and contraindications to endorectal coil insertion (e.g anorectal surgery, inflammatory bowel disease).

MR imaging was performed 3-4 weeks after prostate biopsy. The study protocol was approved by the institutional ethics board. Patient preparation was discussed in chapter 3.

7.2.2. MR technique

Endorectal and PPA MR imaging were performed with a 3T whole-body scanner (Signa HDx, GE Healthcare, Milwaukee, USA). The examination was performed with patients in the supine position. Bowel peristalsis was suppressed with an intravenous injection of 20 mg of hyoscine-N-butylbromide (Buscopan, Boehringer Ingelheim Limited) immediately before the start of the examination. Initially, high resolution T2 weighted images were obtained using an eight channel PPA coil (GE Healthcare). The following sequences were obtained: three plane localiser, low resolution axial T2w fast spin-echo (FSE) images, high resolution axial and coronal T2w FSE to assess the prostate gland and surrounding structures (TR/TE: 3100/97.3 ms, slice thickness: 3.0 mm with no gap, matrix 384 x 256, field of view 20 x 20 cm, number of slices 26 over 6:50 mins). The surface coil was then removed and a rigid ERC (Global Research Centre GRC, München, Germany) was inserted with the patient in the lateral decubitus position, provided there were no contraindications for its use. A three plane localiser was first obtained to confirm coil position and to select locations for the axial images.

Axial and coronal FSE T2w images were acquired (TR/TE: 5240/166.8 ms, slice thickness: 2.5 mm, no inter-slice gap, matrix: 256 x 224, field of view 14 x 14 cm, number of slices 22 obtained over 3:35 mins).

7.2.3. MR image evaluation

All MR images were archived and analysed using an Advantage Windows Workstation (GE Medical System) operating at 4.2-03 software level. MR images were independently evaluated by two readers who had different levels of experience in interpretation of MR findings. Reader A has more than 15 years of MR experience and reader B has one year of prostate MR experience. ER coil and PPA coil images were rated for overall quality as excellent, good, intermediate or poor (grade 1 to 4). The image quality was considered to be excellent if it showed fine anatomical details and no artefacts. It was considered to be poor if evaluation of the images was difficult due to unclear anatomic delineation.

In identifying the anatomical details, we assessed the visibility (graded from 1-4) of the peripheral zones (PZ) and their delineation separate from the central gland (CG) which implies both the transitional and central zones. Allowance was made for the presence of tumour invading the surgical capsule of the prostate and thus reducing differentiation of PZ and CG.

Hypointense areas on T2 weighted images were considered as suspicious of prostate cancer. The degree of suspicion of the presence of malignancy (graded from 1 = not seen, to 4 = highly suspicious) was assessed for both ER and PPA images.

Assessment of the prostatic capsule and the seminal vesicles was based on five specific features described in the literature as highly indicative of extracapsular extension (ECE) [127]. These features were discussed in Chapter 3. The likelihood of extracapsular extension was rated using a 3-point scale. A score of 1 indicated that extraprostatic disease was not present; a score of 2, that ECE was possible due to minor capsular irregularity and/or broad tumour contact; and a score of 3 indicated definite ECE with unequivocal findings in the peri-prostatic soft tissues.

7.2.4. Statistical analysis

The data were analysed using the statistical software package SPSS for Windows (version 13.0). Non parametric Sign test was used to determine if there was a statistically significant difference between the number of times the surface coil was rated superior to the ECR, versus the number of times the ERC was rated superior.

Kappa statistics were used to measure the inter-observer level of agreement. The following terms were used to describe the strength of agreement: = 0 - 0.20, poor agreement; = 0.21 – 0.40, fair agreement; = 0.41 – 0.60, moderate agreement; = 0.61 – 0.80, substantial agreement; and = 0.81 – 1.00, near perfect agreement [128].

7.3. Results:

The ERC was tolerated by all patients for the duration of the study which amounted to 7 minutes. The presence of motion artefacts was significantly higher using the ERC compared to surface coil (22 versus 11 cases); this was mainly due to patient movement or rectal peristalsis. However, motion artefact did not degrade the overall image quality which improved in 44% (25/56) of cases ($p < 0.001$). [Tables 32 & 33].

	Surface coil*	ERC*	<i>P value</i>
Discrimination between PZ and CG	2.95 (0.81)	3.34 (0.69)	<0.001
Visibility of PZ	2.84 (0.84)	3.34 (0.66)	<0.001
Degree of tumour identification	2.75 (1.10)	3.05 (0.96)	0.043
Overall image quality	2.96 (0.53)	3.30 (0.57)	<0.001

Table 32. Visual assessment of image quality by reader A according to specific criteria using PPA surface coil and ERC. (* Mean value of assessment on a scale 1 to 4 quoted with SD in parentheses.)

	Surface coil*	ERC*	P value
Discrimination between PZ and CG	2.89 (0.80)	3.32 (0.71)	<0.001
Visibility of PZ	2.70 (0.80)	3.21 (0.82)	<0.001
Degree of tumour identification	2.77 (1.02)	2.96 (0.97)	0.132
Overall image quality	2.88 (0.63)	3.16 (0.75)	0.004

Table 33. Visual assessment of image quality by reader B according to specific criteria using PPA surface coil and ERC. (* Mean value of assessment on a scale 1 to 4 quoted with SD in parentheses.)

There was a moderate agreement between the two readers for discriminating the PZ from the CG for both the PPA and ER coils ($k= 0.49, p< 0.001$ and $k= 0.54, p< 0.001$ respectively). Improvement in zonal discrimination was noted in 23/56 (41%) of scans for reader A ($p=0.001$), and 24/56 (42%) for reader B ($p<0.001$). [Table 34].

	Reader A		Reader B	
	Surface coil	ERC	Surface coil	ERC
Poor	2 (3.6%)	1 (1.8%)	1 (1.8%)	1 (1.8%)
Moderate	14 (25%)	4 (7.1%)	15 (32.1%)	5 (8.9%)
Good	25 (44.6%)	26 (46.4%)	23 (41.1%)	25 (44.6%)
Excellent	15 (26.8%)	25 (44.6%)	14 (25%)	25 (44.6%)

Table 34. Discrimination between PZ and CG. Number and percentage of patients in each category detailed for both readers.

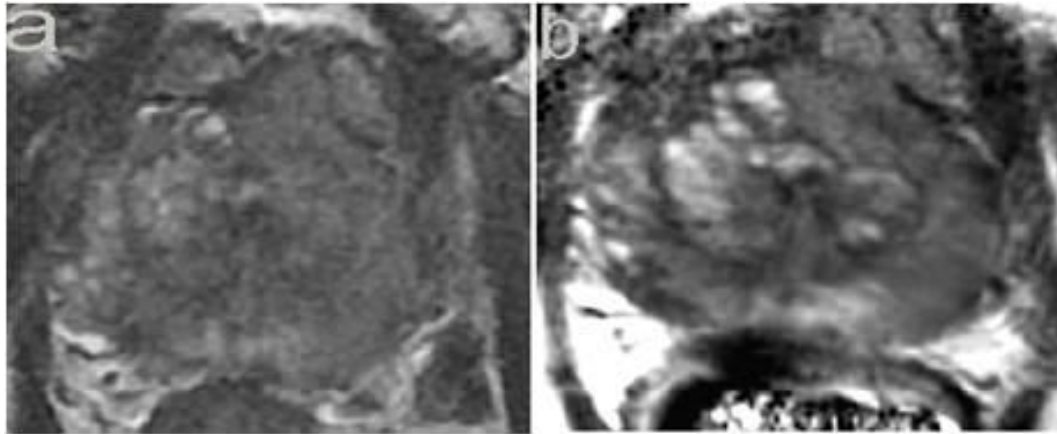


Figure 55. An example of PPA coil image (a) compared with ECR image (b). Noticeable improvement in CG and PZ discrimination by using ERC.

PZ and CG discrimination using an ERC was unchanged in 29 cases for both readers and worse in four and three cases for reader A and B respectively, mainly due to motion and flare artefacts.

In assessing the visibility of the PZ, there was again a moderate agreement between the two readers for both types of coils (PPA, $k= 0.46$, $p< 0.001$ and ERC, $k= 0.43$, $p< 0.001$). The visibility of the PZ on T2w FSE imaging improved in 53% (30/56) of patients for both readers ($p< 0.001$) [Table 35].

	Reader A		Reader B	
	Surface coil	ERC	Surface coil	ERC
Poor	3 (5.4%)	1 (1.8%)	5 (8.9%)	1 (1.8%)
Moderate	16 (28.6%)	3(5.4%)	14 (25%)	11 (19.6%)
Good	24 (42.9%)	28 (50%)	30 (53.6%)	19 (33.9%)
Excellent	13 (23.2%)	24 (42.9%)	7 (12.5%)	25 (44.6%)

Table 35. Visibility of PZ, the number and percentage of patients in each category for both readers.

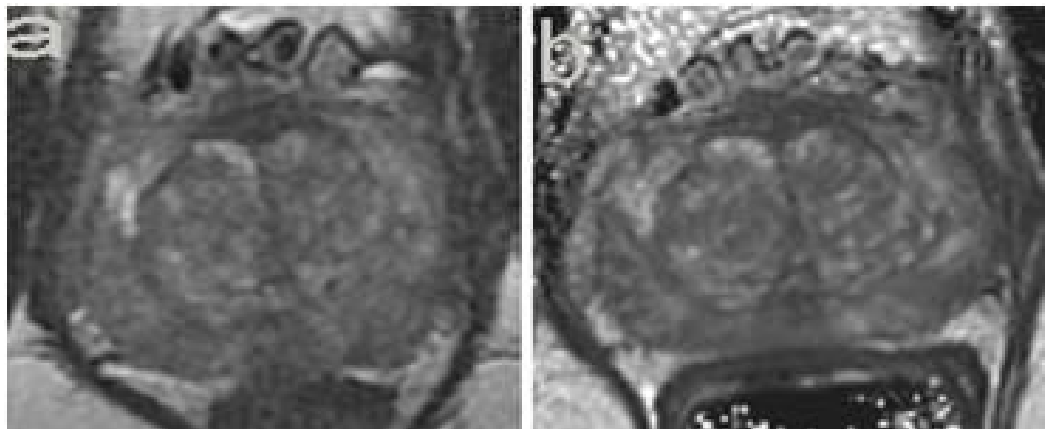


Figure 56. Better PZ visualization seen on ERC image (b) compared to PPA coil image (a).

The visibility of the PZ was worse in only five patients [Table 35]. This was due to significant movement artefact in four patients and coil malposition in one further case.

There was a moderate agreement between the two readers for the assessment of the degree of tumour identification on T2 weighted imaging using both the surface coil and ERC ($k= 0.53, p< 0.001$ and $k= 0.43, p< 0.001$). Tumour foci were better identified using the ERC in 29% and 32% for

readers A & B respectively [Table 36]. However, this was not statistically significant ($p=0.52$ $p=0.78$ for both readers).

	Reader A		Reader B	
	Surface coil	ERC	Surface coil	ERC
Poor	12 (21.4%)	7 (12.5%)	9 (16.1%)	7 (12.5%)
Moderate	6 (10.7%)	3 (5.4%)	10 (17.9%)	6 (10.7%)
Good	22 (39.3%)	26 (46.4%)	22 (39.3%)	25 (44.6%)
Excellent	16 (28.6%)	20 (35.7%)	15 (26.8%)	18 (32.1%)

Table 36. Degree of tumour identification according to reader.

More importantly, the use of the ERC allowed the identification of eight tumours by reader A and five tumours by reader B on T2w imaging which were not visualized with a similar sequence using the PPA coil [Figure 57].

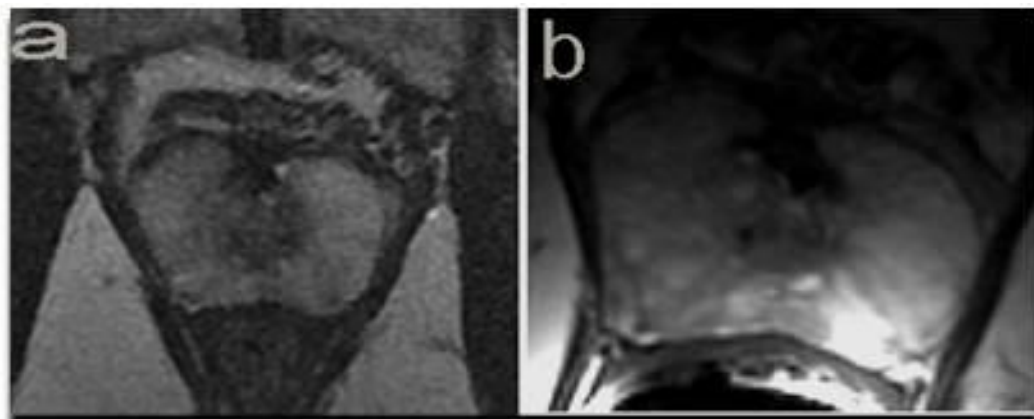


Figure 57. A 63 year old man with PSA of 8.0 and biopsy proven prostate cancer with Gleason score of 7. T2 weighted image using PPA (a) does not show any abnormalities. By using ERC (b) a low signal intensity area is seen in the right PZ.

Regarding staging of the disease [Table 37], there was a moderate agreement between readers in identifying definite or possible extracapsular extension ($k=0.53$, $p<0.001$), but near perfect agreement was achieved in staging assessment using the ERC ($k= 0.85$, $p<0.001$).

		ERC imaging			
		Organ-confined	Possible ECE	Definite ECE	Total
PPA coil Imaging	Organ-confined	32/26	2/3	3/3	37/32
	Possible ECE	2/7	1/2	0/1	3/10
	Definite ECE	5/4	1/0	10/10	16/14
	Total	39/37	4/5	13/14	56/56

Table 37. Extracapsular cancer extension as seen on T2w images (comparison between surface coil and ER coil imaging for reader A / reader B)

For the experienced reader, 37 cases showed an intact capsule on surface coil imaging, but five of the 37 patients (13.5%) were upstaged to definite (3 cases) or suspicious (2 cases) extracapsular disease using the ER coil [Figure 58].

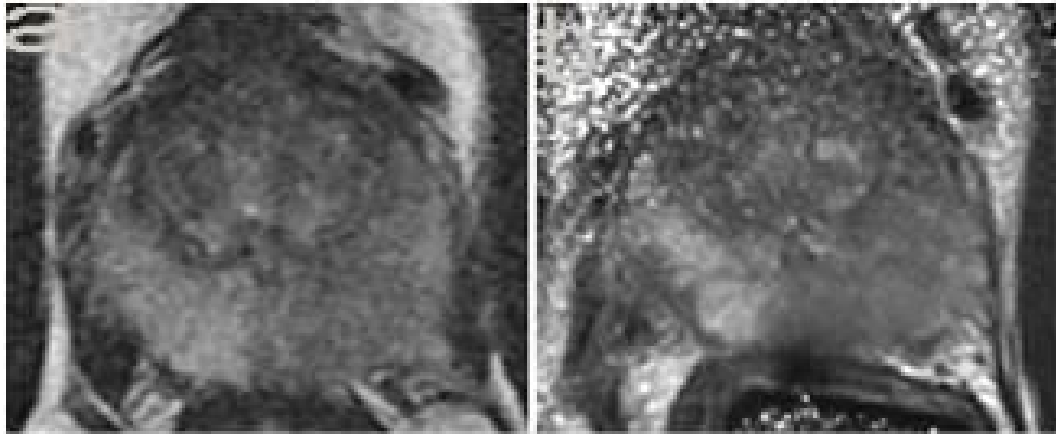


Figure 58. Low signal intensity area was seen in the left PZ and the cancer was staged as T2 (organ confined) on PPA coil image (a). ERC image shows the same low signal intensity area, causing irregularity of the prostatic capsule (b) suspicious of extraprostatic cancer extension (T3a).

On the other hand, five out of the sixteen patients (31%) who were thought to have definite extracapsular extension on surface coil imaging, were down-staged to organ confined disease after ERC imaging [Figure 48].

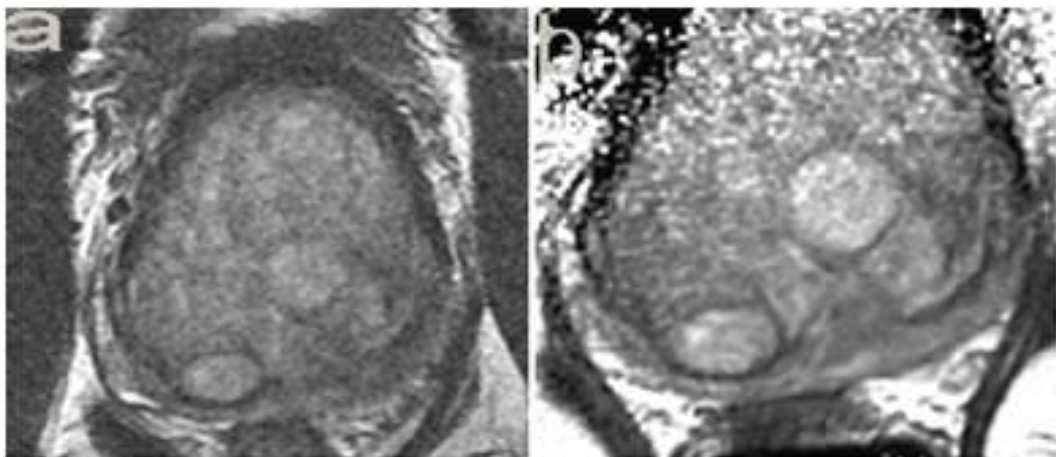


Figure 59. The prostatic capsule over the left PZ is not clearly seen using PPA coil (a). A better identification of the capsule allowed the reader to stage the disease as T2.

A noticeable alteration in identification of capsular penetration was found in the assessment by the less experienced reader B. There was a change in capsular staging in 17 cases. Seven cases suspicious of ECE and four cases of definite ECE were restaged as organ confined at ERC assessment. The remaining six cases with T2 disease at PPA evaluation were upstaged to either possible T3 (3 cases) or definite T3 (3 cases).

Readers A & B identified five and six cases respectively in which the presence of neurovascular bundle involvement on surface coil imaging was refuted using the ERC, due to better visualization of the recto-prostatic angle ($p=0.063$, $p=0.031$ for readers A & B).

Seminal vesicle assessment likewise improved for readers with 6/15 and 3/11 of cases of suspected SVI (readers A & B respectively) on PPA coil imaging, showing no significant abnormality on ERC imaging.

7.4. Discussion:

In this study, we evaluated T2 weighted MR images of the prostate looking at the zonal anatomy, cancer foci, prostatic capsule and the relationship of structures to each other, as well as to the neurovascular bundles and seminal vesicles, based on the spatial resolution and tissue contrast achievable at 3 T.

Previous studies have addressed the superiority of ERC MR imaging with regards to visualization of tumour foci and staging of the disease. Bloch *et al*

addressed the higher spatial resolution achieved at 3 T ERC and the reduction in voxel size to 0.35 mm^3 [100]. This allows an excellent visualization of anatomic details such as seminal ducts, intraprostatic urethra, pseudocapsule and small blood vessels. Heijmink *et al* [199] also achieved an improvement in spatial resolution and image quality, and substantial decrease in voxel size when ERC was used compared with PPA coil (0.16 mm^3 vs 0.73 mm^3).

In my study voxel sizes of 1.21 mm^3 and 0.84 mm^3 were achieved using PPA and ERC respectively. These relatively high voxel sizes, compared to previous reports, were due to low matrix size and large FOV with the advantage of reduction in scanning time and minimizing patient discomfort.

Better discrimination between the PZ and CG often lead to better identification of tumours that originate from the PZ and invade into the CG. The stromal layer which separates the PZ from the transitional zone seems to have a role as a barrier against tumour extension, keeping it confined to the zone in which it originated. However, 23% of prostate cancers involve both zones [200]. Identifying this stromal layer on MR imaging, can help in localising the tumour foci. This can be an additional advantage to guide modern focal ablation techniques, especially in cases where prostatic hypertrophy is present. Our study showed a 41% improvement in identifying the stromal layer and discriminating the PZ and CG when we used the ERC compared to surface coil T2w imaging. This improvement was noted

especially in the presence of CG hypertrophy which is common in this cohort of patients.

Better visibility of the PZ allows more accurate tumour identification for further analysis. This includes tumour volume measurement as well as comparing and registering data with other MR parameters such as dynamic contrast-enhanced and diffusion weighted imaging. In this study ERC imaging has more clearly delineated PZ tumour foci in 53% of cases, with better tumour identification in 29% and 32% for readers A and B respectively. Therefore, it is reasonable to say that ERC MR imaging should be an important component to prostate MRI for localisation and characterization of tumour foci.

With regards to capsule assessment and extra-prostatic tumour extension, this study demonstrated an alteration in staging (secondary to capsular tumour penetration, involvement of neurovascular bundles and seminal vesicle) in 12 and 18 cases for the experienced and less experienced readers respectively. These changes in staging can affect patients' management. Prostate cancer was down-staged on ERC MRI in 7 and 13 cases for readers A and B respectively, allowing potentially curative treatments such as surgery, brachytherapy or radiotherapy to be discussed with the patient. On the other hand upstaging the disease on ERC imaging (5 cases for both readers) would prompt discussion of alternative/ additional treatments such as hormonal or radio-therapy. In our centre patients with possible extracapsular extension (possible T3) on MRI, who are suitable for

radical prostatectomy, do proceed to surgery with a nerve scarifying procedure and regional lymphadenectomy at the side of suspected extracapsular extension. Adjuvant treatment is discussed following the pathology result.

ERC imaging is not without pitfalls as images can suffer from increased artefacts which can be due to different causes:

- 1) Signal shading, so a bright “flare” occurs in the posterior peripheral zones due to the proximity of the coil to the gland, and signal decreases in the anterior part of the gland [201]. Images can be corrected using a series of proton-density weighted (PD) images which can be noise filtered to demonstrate the sensitivity profile of the coil. Using this information T2-weighted images acquired in the same plane can be corrected for shading artefact [201]. This flare correction improves image uniformity and visualization of prostatic anatomy.

- 2) Good image quality, as well as flare correction, is only possible when there is no patient movement during the acquired sequence and between T2 weighted and PD sequences. Motion can be due to patient movement or rectal peristalsis. All patients received hyoscine-N-butylbromide intravenously to reduce bowel peristalsis and therefore reduce rectal motion artefact. When motion artefact was due to patient movement, the affected sequence was repeated for optimal results (in 4 cases).

- 3) Incorrect placement of the coil (ERC not parallel to the transverse plane of the gland). In this study I inflated the balloon with 60 ml of air to secure the coil in position following insertion, as well as applying gentle traction to the balloon during inflation to prevent coil migration.

Although significantly more artefacts were present at ERC MR imaging compared with PPA imaging at 3T (39% vs 19%), all other quality characteristics improved with ERC imaging.

7.5. Conclusion:

The use of ERC at 3T significantly improves the image quality and visualization of prostatic anatomical details which allow better identification of tumour foci. This Improvement in localisation and staging needs to be further evaluated against whole mounted pathology specimens.

We found that the patients who benefit most from the use of an ERC are those who are suitable for radical prostatectomy and who require optimal staging accuracy and those who are considered for focal treatments such as HIFU, photodynamic therapy or cryotherapy.

Future advances in MR technology such as 16 or 32 channels PPA coil may enhance spatial resolution and improve prostatic anatomical and pathological details. Until an improved surface coil is developed, patients who are referred for pre-treatment tumour staging and localisation at 3T need to undergo ERC imaging, either as a separate procedure or integrated with a PPA surface coil.

Chapter Eight

8. FUTURE APPLICATIONS OF PROSTATE MRI

Advances in MRI protocols employing a multi-parametric approach have succeeded in achieving reasonable accuracy for tumour localisation and staging. This has led to the greater use of MRI in PCa management. Moreover, recent studies demonstrated further utility of MRI in evaluating risk stratification, predicting tumour aggressiveness and cancer survival, and guiding interventions including prostate biopsy and ablation.

In this Chapter, I will discuss the potential future applications of prostate MRI and address some of the recent studies.

8.1. Predicting tumour aggressiveness and relation to Gleason score.

I have demonstrated in my research the differences in various MR parameters between cancer lesions and normal peripheral zone. These include ADC and DCE parameters. I have also shown a good correlation between ADC and tumour cellularity. This relationship between tumour features on MRI and histologic composition indicates a potential use of MRI to serve as an additional prognostic marker in assessing cancer aggressiveness and the need for treatment.

In this Chapter, I explore the recent research correlating various MR parameters with Gleason score, this being the most effective prognostic factor for survival, biochemical progression and recurrence.

8.1.1. Correlation between Gleason score and ADC values

Various recent studies have reported a significant negative correlation between Gleason score obtained from radical prostatectomy specimen and ADC values [202-204]. Verma et al [203], studied 110 patients with prostate cancer who underwent endorectal prostate MRI at 1.5 Tesla before radical prostatectomy. The author reported the ADC value in a total of 197 tumours to be negatively correlated with Gleason grades ($r = -0.39$). AT 3 Tesla endorectal MRI, Vargas et al [202], studied 51 patients and found that a low mean ADC value was significantly associated with a higher tumour Gleason score ($P = 0.017$).

Despite the statistically significant negative correlation between ADC and Gleason score, it was noted that there was considerable overlap in ADC values between Gleason score groups (low, intermediate and high risk groups), as well as variation of ADC values within the same group [204]. One of the reasons for the overlap in ADC values is the heterogeneity of prostate cancer and the presence of different Gleason grades within the same prostate [204].

Therefore, although there is a strong correlation between ADC and Gleason scores, it is currently insufficient for immediate diagnostic utility and further

investigation is needed to facilitate the noninvasive assessment of cellular density and thus Gleason score by the use of diffusion weighted imaging.

8.1.2. Assessment of cancer aggressiveness using spectroscopic prostate MR Imaging.

MR spectroscopic prostate imaging provides spatial mapping of the levels of various metabolites including citrate, choline and creatine in the prostate gland. PCa lesions are characterised by lower citrate levels and/or higher choline levels compared to normal tissue [205]. Therefore, the ratio of choline and creatine to citrate can be used as a marker for PCa.

Kobus et al [206] in a retrospective study involving 72 patients with PCa, validated the performance of spectroscopic MR imaging of the prostate at 3 Tesla with an endorectal coil. They assessed tumour aggressiveness based on choline + creatine / citrate and choline / creatine ratios, using the Gleason score from radical prostatectomy specimen as the gold standard. The author reported a good separation of low grade from high grade tumours based on the above measured parameters. The study also analysed the malignancy rating using a standardized threshold approach and achieved an AUC of 0.78 in discrimination between different aggressive classes. This preliminary study offers potential for noninvasive MR assessment of PCa aggressiveness.

Further confirmation of the above conclusion needs to be addressed in larger studies, including assessment of tumour arising in the central gland as well as in peripheral zones.

8.1.3. Assessment of cancer aggressiveness using DCE-MR

Imaging

Although there is good evidence that DCE-MRI parameters reflect angiogenesis and can discriminate between cancerous lesions and normal peripheral zone, up to date, there is no published data to suggest that DCE-MR parameters correlate with Gleason score or tumour aggressiveness. Previous studies [207, 208] examining the correlation between DCE-MRI parameters and various pathological features failed to show a correlation between tumour vascular permeability or maximum tumour gadolinium concentration and Gleason score or PSA.

However, recent MR studies on rectal tumours showed significant difference for K^{trans} with Duke's staging with moderate and promising correlation with TNM staging [209]. This implies that further in vivo DCE-MRI studies on organs with cancerous involvement are needed to address this issue. Future research should study the correlation between various DCE-MRI parameters and microvessel density which can be counted using various immunohistochemistry techniques including CD31 expression. The higher the microvessel density count, the more likely the tumour is to be aggressive with a greater risk of metastasis.

8.2. The role of prostate MRI in treatment selection for organ confined prostate cancer.

Various nomograms are available that combine clinical and biopsy findings to predict the probability of organ confined disease, classifying risks of prostate cancer, or predicting biochemical recurrence-free survival following surgery. With the advances of MRI as a noninvasive diagnostic imaging tool, recent studies have looked at incrementing the value of MRI in pre-operative nomograms. Wang *et al* [210], performed a retrospective study assessing data from 573 men with PCa who underwent pre-operative endorectal MRI and radical retropubic prostatectomy with pelvic lymphadenectomy. The Kattan pre-operative nomogram was used to estimate the risk of seminal vesicle involvement (SVI). The author found that the addition of endorectal MRI to the Kattan nomogram resulted in a valuable incremental improvement in its prediction for SVI. The area under the receiver operating characteristic curve was markedly greater for endorectal MRI plus the Kattan nomogram (0.87) than for either technique alone (0.80 and 0.76 for nomogram and MRI only respectively).

Other researchers developed tools using combined MRI variables, PSA level, and Gleason sum to predict 5 year biochemical recurrence after radical prostatectomy [211]. The authors found that the area under ROC of their new nomogram including MRI data was significantly greater than these of other

predictive tools including Kattan's nomogram (0.897 versus 0.737 respectively).

Shuckla-Dave *et al* [212] looked at incorporating MR imaging and spectroscopy in pre-operative nomogram for the prediction of insignificant prostate cancer. The probability of insignificant PCa on MRI/MRSI was recorded prospectively by two radiologists on a scale from 0 (definitely insignificant) to 3 (definitely significant PCa). Insignificant PCa was then defined on surgical pathology. The author concluded that MR models performed significantly better than the base clinical model (without biopsy data), and similar to a comprehensive clinical tool (with biopsy data). The authors also designed new nomogram models incorporating MRI results and clinical data without the need for detailed biopsy data.

Further research is needed to evaluate whether patients with insignificant cancer who have opted to have active surveillance should undergo annual MRI as part of their predictive tool for assessment of aggressiveness and risk of progression. In a recent review article, Ouzzane *et al* [213] summarised the role of MRI in the selection and monitoring of patients on active surveillance. The authors concluded that incorporation of MRI data into active surveillance selection criteria for patients with low-risk CaP provides a better baseline prognostic evaluation compared to the use of the clinical and histologic data only. This can reduce the number of patients reclassified as higher risk at subsequent follow-up biopsies. The routine application of MRI in decision making in this group of patients requires highly skilled MR

radiologists and advanced MRI technology and should be weighed against cost to justify its use.

8.3. MRI guided prostate biopsy

As mentioned in Chapter 6, the detection rate of prostate cancer in men with elevated and/or rising prostate specific antigen levels after negative TRUS biopsy is relatively poor. Targeting the suspicious areas on MRI, using USS, presents a significant problem with registering the two imaging modalities. Therefore, there is a strong present need for MRI-guided prostate biopsy as a tool to enhance detection rate, especially when multi-parametric MRI has considerable capability in finding cancerous lesions in the prostate.

Few recent studies have looked into the feasibility of performing real time MR guided prostate biopsy (MRGB). Beyersdorff *et al* [214] were the first to describe transrectal MRGB in a closed MR system by using anatomical T2-weighted MR images as part of a pre-biopsy planning. Hambrock *et al* [215] tested the feasibility of directing MR-guided biopsies by translating maps of suspicious areas of tumour in the prostate, identified from multiparametric 3T MRI data (including T2W MRI, DWI, and DCE-MRI), onto T2w MR images. This was performed using a 32-channel coil on a 3 Tesla MRI scanner. Results were analysed from 21 patients with elevated PSA levels and negative previous USS guided biopsy results. Tumour suspicious regions were identified, successfully translated on to T2w MR images and biopsied under MR guidance. 95% of patients had identifiable pathology using this technique.

In another study by the same group [216], the author analyzed the results of 68 patients who underwent multi-parametric 3T MR-guided biopsy and compared them with results from a matched population of patients who underwent multi-session TRUS-guided biopsy. The tumour detection rate for MR-guided biopsy was 59% using a median of four cores, which was significantly higher than that of TRUS-guided prostate biopsy (17%).

Krieger *et al* [217] described in detail the technique of MR-guided prostate biopsy including patient positioning, approach, guiding and tracking instruments, and the experiments in manual and robotic techniques. The transrectal approach was described by Futterer *et al* [218] as the preferable one, as it requires minimal anaesthetic and provides the shortest way to reach the prostate therefore reducing the potential for needle deflection. Other feasible approaches such as transperineal and transgluteal were also described [217].

The description of the procedure by the above authors can be summarised as follows:

- Patient position can be prone or supine depending on the device used. A needle guide filled with gadolinium is inserted rectally and the patient is positioned in the scanner bore with the pelvic phased array coil in place. Then multi-sequence MRI is performed with DWI, DCE and T2 weighted imaging to identify the region of interest (the suspicious prostatic area). These images are then translated to a T2 w

image using anatomical landmarks and 3 dimensional position estimation.

- The needle guide then can be advanced into the suspected lesion and biopsies are performed using an MR compatible biopsy gun. The procedure time is about 35 minutes.

In summary, MR-guided biopsies of the prostate are becoming more and more available. Both robotic and manual techniques have comparable results regarding accuracy and speed [219]. Although there is currently no consensus on the optimal technique, there is growing evidence that the use of MR-guided biopsy is highly useful in patient with high/ rising PSA but negative USS-guided biopsies, and widespread practice should be encouraged.

8.4. Summary

I believe that prostate MRI, using a high magnetic field with a multi sequences technique, has flourished in its role in prostate cancer diagnosis, management and prognostication.

In this research, each study was described in a separate chapter and had different cohort of patients. These were analysed in different time scale during the 2 ½ years of the research. Although there was some overlap of patient cohorts between each chapter and some patients' MR data were used in more than one study.

I have shown in my thesis that prostate MRI can achieve a diagnostic localisation accuracy of 80% using dynamic contrast enhancement, with a sensitivity of 79% and a specificity of 83%. The detection rate is particularly good in the peripheral zones where sensitivity reaches 90% and specificity 71%.

MRI also demonstrates high accuracy rate for prostate cancer staging especially with the use of an endorectal coil with an area under ROC curve of 0.93 given a sensitivity of 67% and specificity of 96%. There is leaning towards high specificity at the expense of moderate sensitivity to prevent overstaging of the disease, which may lead to potentially curative surgical treatment being withheld on the basis of false positive MR imaging.

These high accuracy rates using endorectal coil is mainly due to better tumour visualisation and identification, as in this study, the MR visibility of the PZ improved in 53% of cases following the use of ERC. Furthermore, the tumour foci were better identified in 29% of cases.

The above results cannot be achieved without an experienced radiologist who has completed a learning curve. I have demonstrated the difference in staging and localisation results between readers depending on their level of MR experience. The performance of the less experienced reader is greatly improved with the use of DCE-MRI and ERC compared with T2 weighted imaging alone.

In addition to the localisation and staging performance, I demonstrated in this study the role of MRI as a biomarker for prostate cancer. Based on diffusion weighted imaging, the ADC values were significantly lower ($p < 0.001$) in regions pathologically determined to be tumour ($1.45 \pm 0.26 \times 10^{-3} \text{ mm}^2/\text{s}$) compared to regions assigned as normal peripheral zone tissue ($1.90 \pm 0.33 \times 10^{-3} \text{ mm}^2/\text{s}$). The ADC correlates significantly with cell density ($r = -0.50$, $p < 0.0001$), leading to the belief that calculating ADC may reflect tumour aggressiveness as the average cell density is significantly higher in malignant tissues than normal prostatic tissues.

Moreover, DCE-MRI has also revealed significant separation between malignant and normal tissues based on enhancement parameters. I have produced enhancement data which has shown that malignant prostatic

lesions have a 56% higher MaxEI compared to normal PZ and take nearly half the time to reach that maximum. Similarly, the wash-in rate as represented by the initial slope was much higher in cancer lesions compared to normal PZ. As contrast enhancement is related to tumour angiogenesis, increased and rapid enhancement may be related to more aggressive tumour. However, this needs to be evaluated further in future studies.

In conclusion, I believe that this research has shone a light on the important role of MRI in prostate cancer management and the huge potential for further studies to enhance its role and benefit.

9. REFERENCES

- [1] UK CR. Cancer incidence for common cancers - UK statistics. 2008 [cited; Available from: <http://info.cancerresearchuk.org/cancerstats/incidence/commoncancers/>]
- [2] Ferlay J, Autier P, Boniol M, Heanue M, Colombet M, Boyle P. Estimates of the cancer incidence and mortality in Europe in 2006. *Ann Oncol*. 2007 Mar; **18**:581-92
- [3] Office for National Statistics CSr. Registrations of cancer diagnosed in 2008, England. In *Statistics N* ed. London, 2010
- [4] Breslow N, Chan CW, Dhom G, et al. Latent carcinoma of prostate at autopsy in seven areas. The International Agency for Research on Cancer, Lyons, France. *Int J Cancer*. 1977 Nov 15; **20**:680-8
- [5] Soos G, Tsakiris I, Szanto J, Turzo C, Haas PG, Dezso B. The Prevalence of Prostate Carcinoma and Its Precursor in Hungary: An Autopsy Study. *European Urology*. 2005; **48**:739-44
- [6] Murphy, Johnston, Whelan, Rider, Lloyd. Changing trends in prostatic cancer. *BJU International*. 1999; **83**:786-91
- [7] Brewster DH, Fraser LA, Harris V, Black RJ. Rising incidence of prostate cancer in Scotland: increased risk or increased detection? *BJU International*. 2000; **85**:463-73
- [8] Mettlin CJ, Murphy GP, Rosenthal DS, Menck HR. The National Cancer Data Base report on prostate carcinoma after the peak in incidence rates in the U.S. The American College of Surgeons Commission on Cancer and the American Cancer Society. *Cancer*. 1998 Oct 15; **83**:1679-84
- [9] Rohr LR. Incidental adenocarcinoma in transurethral resections of the prostate. Partial versus complete microscopic examination. *Am J Surg Pathol*. 1987 Jan; **11**:53-8
- [10] Gann PH. Interpreting recent trends in prostate cancer incidence and mortality. *Epidemiology*. 1997 Mar; **8**:117-20
- [11] Parker C, Muston D, Melia J, Moss S, Dearnaley D. A model of the natural history of screen-detected prostate cancer, and the effect of radical treatment on overall survival. *Br J Cancer*. 2006 May 22; **94**:1361-8

- [12] Barnes RW. Survival with conservative therapy. JAMA. 1969 Oct 13: **210**:331-2
- [13] Johansson JE, Andren O, Andersson SO, et al. Natural history of early, localised prostate cancer. JAMA. 2004 Jun 9: **291**:2713-9
- [14] Albertsen PC, Hanley JA, Fine J. 20-year outcomes following conservative management of clinically localised prostate cancer. JAMA. 2005 May 4: **293**:2095-101
- [15] Catalona WJ, Smith DS, Ratliff TL, et al. Measurement of prostate-specific antigen in serum as a screening test for prostate cancer. The New England journal of medicine. 1991 Apr 25: **324**:1156-61
- [16] Vickers AJ, Cronin AM, Bjork T, et al. Prostate specific antigen concentration at age 60 and death or metastasis from prostate cancer: case-control study. BMJ. 2010: **341**:c4521
- [17] Crawford ED, Thompson IM. Controversies regarding screening for prostate cancer. BJU Int Supp. 2007: **100**:5-7
- [18] Berger AP, Deibl M, Strasak A, et al. Large-scale study of clinical impact of PSA velocity: long-term PSA kinetics as method of differentiating men with from those without prostate cancer. Urology. 2007 Jan: **69**:134-8
- [19] Jesberger JA, Rafie N, Duerk J, et al. Model-free parameters from dynamic contrast-enhanced-MRI: Sensitivity to EES volume fraction and bolus timing. Journal of Magnetic Resonance Imaging. 2006: **24**:586-94
- [20] Pinsky PF, Andriole G, Crawford ED, et al. Prostate-specific antigen velocity and prostate cancer gleason grade and stage. Cancer. 2007 Apr 15: **109**:1689-95
- [21] Boccon-Gibod L, Djavan WB, Hammerer P, et al. Management of prostate-specific antigen relapse in prostate cancer: a European Consensus. Int J Clin Pract. 2004 Apr: **58**:382-90
- [22] Brawer MK. Prostate-specific antigen: current status. CA: a cancer journal for clinicians. 1999 Sep-Oct: **49**:264-81
- [23] Freedland SJ, Kane CJ, Presti JC, Jr., et al. Comparison of preoperative prostate specific antigen density and prostate specific antigen for predicting recurrence after radical prostatectomy: results from the search data base. The Journal of urology. 2003 Mar: **169**:969-73

- [24] Tosoian JJ, Trock BJ, Landis P, et al. Active surveillance program for prostate cancer: an update of the Johns Hopkins experience. *J Clin Oncol*. 2011 Jun 1: **29**:2185-90
- [25] Stenman UH, Leinonen J, Alfthan H, Rannikko S, Tuhkanen K, Alfthan O. A complex between prostate-specific antigen and alpha 1-antichymotrypsin is the major form of prostate-specific antigen in serum of patients with prostatic cancer: assay of the complex improves clinical sensitivity for cancer. *Cancer research*. 1991 Jan 1: **51**:222-6
- [26] Elabbady AA, Khedr MM. Free/total PSA ratio can help in the prediction of high gleason score prostate cancer in men with total serum prostate specific antigen (PSA) of 3-10 ng/ml. *International urology and nephrology*. 2006: **38**:553-7
- [27] Andriole GL, Crawford ED, Grubb RL, 3rd, et al. Mortality results from a randomized prostate-cancer screening trial. *N Engl J Med*. 2009 Mar 26: **360**:1310-9
- [28] Schroder FH, Hugosson J, Roobol MJ, et al. Screening and prostate-cancer mortality in a randomized European study. *N Engl J Med*. 2009 Mar 26: **360**:1320-8
- [29] Stamey TA. Making the most out of six systematic sextant biopsies. *Urology*. 1995 Jan: **45**:2-12
- [30] Elabbady AA, Khedr MM. Extended 12-core prostate biopsy increases both the detection of prostate cancer and the accuracy of Gleason score. *European urology*. 2006 Jan: **49**:49-53; discussion
- [31] Walz J, Graefen M, Chun FK, et al. High incidence of prostate cancer detected by saturation biopsy after previous negative biopsy series. *European urology*. 2006 Sep: **50**:498-505
- [32] Scattoni V, Zlotta A, Montironi R, Schulman C, Rigatti P, Montorsi F. Extended and saturation prostatic biopsy in the diagnosis and characterisation of prostate cancer: a critical analysis of the literature. *European urology*. 2007 Nov: **52**:1309-22
- [33] Sommer FG, Nghiem HV, Herfkens R, McNeal J. Gadolinium-enhanced MRI of the abnormal prostate. *Magnetic Resonance Imaging*. 1993: **11**:941-8
- [34] Ishidoya S, Endoh M, Nakagawa H, Saito S, Arai Y. Novel anatomical findings of the prostatic gland and the surrounding capsular structures in the normal prostate. *Tohoku J Exp Med*. 2007 May: **212**:55-62

- [35] Srigley JR. Key issues in handling and reporting radical prostatectomy specimens. *Archives of pathology & laboratory medicine*. 2006 Mar: **130**:303-17
- [36] Reiner WG, Walsh PC. An anatomical approach to the surgical management of the dorsal vein and Santorini's plexus during radical retropubic surgery. *J Urol*. 1979 Feb: **121**:198-200
- [37] Byar DP, Mostofi FK. Carcinoma of the prostate: prognostic evaluation of certain pathologic features in 208 radical prostatectomies. Examined by the step-section technique. *Cancer*. 1972 Jul: **30**:5-13
- [38] Shinichiro Shimizu JKYETUSKTTMK. Frequency and number of neuroendocrine tumor cells in prostate cancer: No difference between radical prostatectomy specimens from patients with and without neoadjuvant hormonal therapy. *The Prostate*. 2007: **67**:645-52
- [39] Bostwick DG, Brawer MK. Prostatic intra-epithelial neoplasia and early invasion in prostate cancer. *Cancer*. 1987 Feb 15: **59**:788-94
- [40] Brawer MK. Prostatic intraepithelial neoplasia: an overview. *Reviews in urology*. 2005: **7 Suppl 3**:S11-8
- [41] Akhavan A, Keith JD, Bastacky SI, Cai C, Wang Y, Nelson JB. The proportion of cores with high-grade prostatic intraepithelial neoplasia on extended-pattern needle biopsy is significantly associated with prostate cancer on site-directed repeat biopsy. *BJU international*. 2007 Apr: **99**:765-9
- [42] Gokden N, Roehl KA, Catalona WJ, Humphrey PA. High-grade prostatic intraepithelial neoplasia in needle biopsy as risk factor for detection of adenocarcinoma: current level of risk in screening population. *Urology*. 2005 Mar: **65**:538-42
- [43] Langer JE, Rovner ES, Coleman BG, et al. Strategy for repeat biopsy of patients with prostatic intraepithelial neoplasia detected by prostate needle biopsy. *The Journal of urology*. 1996 Jan: **155**:228-31
- [44] Lefkowitz GK, Taneja SS, Brown J, Melamed J, Lepor H. Followup interval prostate biopsy 3 years after diagnosis of high grade prostatic intraepithelial neoplasia is associated with high likelihood of prostate cancer, independent of change in prostate specific antigen levels. *The Journal of urology*. 2002 Oct: **168**:1415-8
- [45] Kronz JD, Allan CH, Shaikh AA, Epstein JI. Predicting cancer following a diagnosis of high-grade prostatic intraepithelial neoplasia on needle biopsy: data on men with more than one follow-up biopsy. *The American journal of surgical pathology*. 2001 Aug: **25**:1079-85

- [46] Epstein JI, Herawi M. Prostate needle biopsies containing prostatic intraepithelial neoplasia or atypical foci suspicious for carcinoma: implications for patient care. *The Journal of urology*. 2006 Mar: **175**:820-34
- [47] Loeb S, Roehl KA, Yu X, Han M, Catalona WJ. Use of prostate-specific antigen velocity to follow up patients with isolated high-grade prostatic intraepithelial neoplasia on prostate biopsy. *Urology*. 2007 Jan: **69**:108-12
- [48] Bostwick DG, Srigley J, Grignon D, et al. Atypical adenomatous hyperplasia of the prostate: morphologic criteria for its distinction from well-differentiated carcinoma. *Human pathology*. 1993 Aug: **24**:819-32
- [49] Iczkowski KA, Bostwick DG. Criteria for biopsy diagnosis of minimal volume prostatic adenocarcinoma: analytic comparison with nondiagnostic but suspicious atypical small acinar proliferation. *Archives of pathology & laboratory medicine*. 2000 Jan: **124**:98-107
- [50] Cheville JC, Reznicek MJ, Bostwick DG. The focus of "atypical glands, suspicious for malignancy" in prostatic needle biopsy specimens: incidence, histologic features, and clinical follow-up of cases diagnosed in a community practice. *American journal of clinical pathology*. 1997 Dec: **108**:633-40
- [51] Mancuso PA, Chabert C, Chin P, et al. Prostate cancer detection in men with an initial diagnosis of atypical small acinar proliferation. *BJU international*. 2007 Jan: **99**:49-52
- [52] Girasole CR, Cookson MS, Putzi MJ, et al. Significance of atypical and suspicious small acinar proliferations, and high grade prostatic intraepithelial neoplasia on prostate biopsy: implications for cancer detection and biopsy strategy. *The Journal of urology*. 2006 Mar: **175**:929-33; discussion 33
- [53] Montironi R, Scattoni V, Mazzucchelli R, Lopez-Beltran A, Bostwick DG, Montorsi F. Atypical foci suspicious but not diagnostic of malignancy in prostate needle biopsies (also referred to as "atypical small acinar proliferation suspicious for but not diagnostic of malignancy"). *Eur Urol*. 2006 Oct: **50**:666-74
- [54] Gleason DF, Mellinger GT. Prediction of prognosis for prostatic adenocarcinoma by combined histological grading and clinical staging. *The Journal of urology*. 1974 Jan: **111**:58-64
- [55] Epstein JI, Amin M, Boccon-Gibod L, et al. Prognostic factors and reporting of prostate carcinoma in radical prostatectomy and pelvic lymphadenectomy specimens. *Scandinavian journal of urology and nephrology*. 2005 May:34-63

- [56] Koh H, Kattan MW, Scardino PT, et al. A nomogram to predict seminal vesicle invasion by the extent and location of cancer in systematic biopsy results. *The Journal of urology*. 2003 Oct: **170**:1203-8
- [57] Saad F, Clarke N, Colombel M. Natural History and Treatment of Bone Complications in Prostate Cancer. *European Urology*. 2006: **49**:429-40
- [58] Kwanchanit Tantivejkul LMKKJP. Dynamic process of prostate cancer metastasis to bone. *Journal of Cellular Biochemistry*. 2004: **91**:706-17
- [59] Kenneth S. Koeneman FYLWKC. Osteomimetic properties of prostate cancer cells: A hypothesis supporting the predilection of prostate cancer metastasis and growth in the bone environment. *The Prostate*. 1999: **39**:246-61
- [60] Nadiminty N, Lou W, Lee SO, et al. Prostate-specific antigen modulates genes involved in bone remodeling and induces osteoblast differentiation of human osteosarcoma cell line SaOS-2. *Clin Cancer Res*. 2006 Mar 1: **12**:1420-30
- [61] Greene, Page, Fleming. *AJCC cancer staging manual*. 6th edn, New York: Springer-Verlag, 2002
- [62] Schroder FH, van der Maas P, Beemsterboer P, et al. Evaluation of the digital rectal examination as a screening test for prostate cancer. Rotterdam section of the European Randomized Study of Screening for Prostate Cancer. *Journal of the National Cancer Institute*. 1998 Dec 2: **90**:1817-23
- [63] Philip J, Dutta Roy S, Ballal M, Foster CS, Javle P. Is a digital rectal examination necessary in the diagnosis and clinical staging of early prostate cancer? *BJU international*. 2005 May: **95**:969-71
- [64] Heidenreich A, Aus G, Abbou CC, et al. Guidelines on Prostate Cancer. *European Association of Urology Guidelines European Association of Urology*, 2007
- [65] Lange PH, Ercole CJ, Lightner DJ, Fraley EE, Vessella R. The value of serum prostate specific antigen determinations before and after radical prostatectomy. *The Journal of urology*. 1989 Apr: **141**:873-9
- [66] Partin AW, Mangold LA, Lamm DM, Walsh PC, Epstein JI, Pearson JD. Contemporary update of prostate cancer staging nomograms (Partin Tables) for the new millennium. *Urology*. 2001 Dec: **58**:843-8
- [67] Augustin H, Eggert T, Wenske S, et al. Comparison of accuracy between the Partin tables of 1997 and 2001 to predict final pathological stage

in clinically localised prostate cancer. The Journal of urology. 2004 Jan: **171**:177-81

[68] Mullerad M, Hricak H, Wang L, Chen HN, Kattan MW, Scardino PT. Prostate cancer: detection of extracapsular extension by genitourinary and general body radiologists at MR imaging. Radiology. 2004 Jul: **232**:140-6

[69] D'Amico AV. Combined-modality staging for localised adenocarcinoma of the prostate. Oncology (Williston Park, NY. 2001 Aug: **15**:1049-59; discussion 60-2, 64-5, 69-70,73-5

[70] D'Amico AV, Whittington R, Malkowicz SB, et al. Biochemical outcome after radical prostatectomy, external beam radiation therapy, or interstitial radiation therapy for clinically localised prostate cancer. Jama. 1998 Sep 16: **280**:969-74

[71] Tsuzuki T, Hernandez DJ, Aydin H, Trock B, Walsh PC, Epstein JI. Prediction of extraprostatic extension in the neurovascular bundle based on prostate needle biopsy pathology, serum prostate specific antigen and digital rectal examination. The Journal of urology. 2005 Feb: **173**:450-3

[72] Bill-Axelson A, Holmberg L, Ruutu M, et al. Radical prostatectomy versus watchful waiting in early prostate cancer. The New England journal of medicine. 2005 May 12: **352**:1977-84

[73] Bill-Axelson A, Holmberg L, Ruutu M, et al. Radical prostatectomy versus watchful waiting in early prostate cancer. The New England journal of medicine. 2011 May 5: **364**:1708-17

[74] Gerber GS, Thisted RA, Chodak GW, et al. Results of radical prostatectomy in men with locally advanced prostate cancer: multi-institutional pooled analysis. European urology. 1997: **32**:385-90

[75] Hull GW, Rabbani F, Abbas F, Wheeler TM, Kattan MW, Scardino PT. Cancer control with radical prostatectomy alone in 1,000 consecutive patients. The Journal of urology. 2002 Feb: **167**:528-34

[76] Ward JF, Moul JW. Biochemical recurrence after definitive prostate cancer therapy. Part I: defining and localizing biochemical recurrence of prostate cancer. Curr Opin Urol. 2005 May: **15**:181-6

[77] Kupelian P, Katcher J, Levin H, et al. External beam radiotherapy versus radical prostatectomy for clinical stage T1-2 prostate cancer: therapeutic implications of stratification by pretreatment PSA levels and biopsy Gleason scores. The cancer journal from Scientific American. 1997 Mar-Apr: **3**:78-87

- [78] Martinez AA, Gonzalez JA, Chung AK, et al. A comparison of external beam radiation therapy versus radical prostatectomy for patients with low risk prostate carcinoma diagnosed, staged, and treated at a single institution. *Cancer*. 2000 Jan 15: **88**:425-32
- [79] Wilt TJ, Brawer MK, Jones KM, et al. Radical prostatectomy versus observation for localised prostate cancer. *The New England journal of medicine*. 2012 Jul 19: **367**:203-13
- [80] Hsu CY, Joniau S, Oyen R, Roskams T, Van Poppel H. Outcome of surgery for clinical unilateral T3a prostate cancer: a single-institution experience. *European urology*. 2007 Jan: **51**:121-8; discussion 8-9
- [81] Joniau S, Hsu CY, Lerut E, et al. A pretreatment table for the prediction of final histopathology after radical prostatectomy in clinical unilateral T3a prostate cancer. *European urology*. 2007 Feb: **51**:388-94; discussion 95-6
- [82] Bostwick DG, Montironi R. Evaluating radical prostatectomy specimens: therapeutic and prognostic importance. *Virchows Arch*. 1997 Jan: **430**:1-16
- [83] Epstein JI, Partin AW, Sauvageot J, Walsh PC. Prediction of progression following radical prostatectomy. A multivariate analysis of 721 men with long-term follow-up. *The American journal of surgical pathology*. 1996 Mar: **20**:286-92
- [84] Thuraiaraja R, Osborn J, McFarlane J, Bahl A, Persad R. Radical prostatectomy with positive surgical margins: how are patients managed? *BJU international*. 2006 Mar: **97**:445-50
- [85] Choo R, Hruby G, Hong J, et al. Positive resection margin and/or pathologic T3 adenocarcinoma of prostate with undetectable postoperative prostate-specific antigen after radical prostatectomy: to irradiate or not? *International journal of radiation oncology, biology, physics*. 2002 Mar 1: **52**:674-80
- [86] Bolla M, van Poppel H, Collette L, et al. Postoperative radiotherapy after radical prostatectomy: a randomised controlled trial (EORTC trial 22911). *Lancet*. 2005 Aug 13-19: **366**:572-8
- [87] Abu-Yousef MM, Narayana AS. Prostatic carcinoma: detection and staging using suprapubic US. *Radiology*. 1985 Jul: **156**:175-80
- [88] Watanabe H, Kato H, Kato T, Morita M, Tanaka M. [Diagnostic application of ultrasonotomography to the prostate]. *Nippon Hinyokika Gakkai zasshi*. 1968 Apr: **59**:273-9

- [89] Kuligowska E, Barish MA, Fenlon HM, Blake M. Predictors of prostate carcinoma: accuracy of gray-scale and color Doppler US and serum markers. *Radiology*. 2001 Sep: **220**:757-64
- [90] Tang J, Li X, Wang N, et al. Correlation between hypoechoic nodules on ultrasonography and benign hyperplasia in the prostatic outer gland. *J Ultrasound Med*. 2005 Apr: **24**:483-8
- [91] Hsu CY, Joniau S, Oyen R, Roskams T, Van Poppel H. Detection of clinical unilateral T3a prostate cancer - by digital rectal examination or transrectal ultrasonography? *BJU international*. 2006 Nov: **98**:982-5
- [92] Engeler CE, Wasserman NF, Zhang G. Preoperative assessment of prostatic carcinoma by computerized tomography. Weaknesses and new perspectives. *Urology*. 1992 Oct: **40**:346-50
- [93] Farsad M, Schiavina R, Castellucci P, et al. Detection and localisation of prostate cancer: correlation of (11)C-choline PET/CT with histopathologic step-section analysis. *J Nucl Med*. 2005 Oct: **46**:1642-9
- [94] Heenan SD. Magnetic resonance imaging in prostate cancer. *Prostate cancer and prostatic diseases*. 2004: **7**:282-8
- [95] Rouviere O, Hartman RP, Lyonnet D. Prostate MR imaging at high-field strength: evolution or revolution? *European radiology*. 2006 Feb: **16**:276-84
- [96] Sonnad SS, Langlotz CP, Schwartz JS. Accuracy of MR imaging for staging prostate cancer: a meta-analysis to examine the effect of technologic change. *Acad Radiol*. 2001 Feb: **8**:149-57
- [97] Jager GJ, Severens JL, Thornbury JR, de La Rosette JJ, Ruijs SH, Barentsz JO. Prostate cancer staging: should MR imaging be used?--A decision analytic approach. *Radiology*. 2000 May: **215**:445-51
- [98] Okafuji T, Yabuuchi H, Sakai S, et al. MR imaging features of pure mucinous carcinoma of the breast. *European Journal of Radiology*. 2006: **60**:405-13
- [99] Muramoto S, Uematsu H, Sadato N, et al. H-2 (15)O positron emission tomography validation of semiquantitative prostate blood flow determined by double-echo dynamic MRI: A preliminary study. *Journal of Computer Assisted Tomography*. 2002: **26**:510-4
- [100] Bloch BN, Rofsky NM, Baroni RH, Marquis RP, Pedrosa I, Lenkinski RE. 3 Tesla magnetic resonance imaging of the prostate with combined

pelvic phased-array and endorectal coils; Initial experience(1). Academic radiology. 2004 Aug: **11**:863-7

[101] Kim CK, Park BK, Kim B. Localisation of prostate cancer using 3T MRI: comparison of T2-weighted and dynamic contrast-enhanced imaging. Journal of computer assisted tomography. 2006 Jan-Feb: **30**:7-11

[102] Futterer JJ, Heijmink SW, Scheenen TW, et al. Prostate cancer: local staging at 3-T endorectal MR imaging--early experience. Radiology. 2006 Jan: **238**:184-91

[103] Liney G. MRI from A to Z: A Definitive Guide for Medical Professionals: Springer, 2007

[104] Heywang SH, Hahn D, Schmidt H, et al. MR imaging of the breast using gadolinium-DTPA. Journal of computer assisted tomography. 1986 Mar-Apr: **10**:199-204

[105] Caravan P, Ellison JJ, McMurry TJ, Lauffer RB. Gadolinium(III) Chelates as MRI Contrast Agents: Structure, Dynamics, and Applications. Chemical reviews. 1999 Sep 8: **99**:2293-352

[106] Kaiser WA, Zeitler E. MR imaging of the breast: fast imaging sequences with and without Gd-DTPA. Preliminary observations. Radiology. 1989 Mar: **170**:681-6

[107] Kuhl CK, Mielcareck P, Klaschik S, et al. Dynamic Breast MR Imaging: Are Signal Intensity Time Course Data Useful for Differential Diagnosis of Enhancing Lesions? Radiology. 1999 April 1, 1999: **211**:101-10

[108] Buckley DL, Kerlake RW, Blackband SJ, Horsman A. Quantitative analysis of multi-slice Gd-DTPA enhanced dynamic MR images using an automated simplex minimization procedure. Magn Reson Med. 1994 Nov: **32**:646-51

[109] Buckley DL, Roberts C, Parker GJM, Logue JP, Hutchinson CE. Prostate cancer: Evaluation of vascular characteristics with dynamic contrast-enhanced T1-weighted MR imaging - Initial experience. Radiology. 2004: **233**:709-15

[110] Schlemmer HP, Merkle J, Grobholz R, et al. Can pre-operative contrast-enhanced dynamic MR imaging for prostate cancer predict microvessel density in prostatectomy specimens? European Radiology. 2004: **14**:309-17

- [111] Preziosi P, Orlacchio A, Di Giambattista G, et al. Enhancement patterns of prostate cancer in dynamic MRI. *Eur Radiol.* 2003 May: **13**:925-30
- [112] Kim JK, Hong SS, Choi YJ, et al. Wash-in rate on the basis of dynamic contrast-enhanced MRI: usefulness for prostate cancer detection and localisation. *J Magn Reson Imaging.* 2005 Nov: **22**:639-46
- [113] Stejskal EO, Tanner JE. Spin diffusion measurements: spin echoes in the presence of a time-dependent field gradient. *J Chem Phys* 1965: **42**:288-92
- [114] Moseley ME, Cohen Y, Mintorovitch J, et al. Early detection of regional cerebral ischemia in cats: comparison of diffusion- and T2-weighted MRI and spectroscopy. *Magn Reson Med.* 1990 May: **14**:330-46
- [115] Pickles MD, Gibbs P, Lowry M, Turnbull LW. Diffusion changes precede size reduction in neoadjuvant treatment of breast cancer. *Magnetic resonance imaging.* 2006 Sep: **24**:843-7
- [116] Guo Y, Cai YQ, Cai ZL, et al. Differentiation of clinically benign and malignant breast lesions using diffusion-weighted imaging. *J Magn Reson Imaging.* 2002 Aug: **16**:172-8
- [117] Pickles MD, Gibbs P, Sreenivas M, Turnbull LW. Diffusion-weighted imaging of normal and malignant prostate tissue at 3.0T. *J Magn Reson Imaging.* 2006 Feb: **23**:130-4
- [118] Gibbs P, Pickles MD, Turnbull LW. Diffusion imaging of the prostate at 3.0 tesla. *Invest Radiol.* 2006 Feb: **41**:185-8
- [119] desouza NM, Reinsberg SA, Scurr ED, Brewster JM, Payne GS. Magnetic resonance imaging in prostate cancer: the value of apparent diffusion coefficients for identifying malignant nodules. *The British journal of radiology.* 2007 Feb: **80**:90-5
- [120] Kim CK, Park BK, Han JJ, Kang TW, Lee HM. Diffusion-weighted imaging of the prostate at 3 T for differentiation of malignant and benign tissue in transition and peripheral zones: preliminary results. *Journal of computer assisted tomography.* 2007 May-Jun: **31**:449-54
- [121] Miao H, Fukatsu H, Ishigaki T. Prostate cancer detection with 3-T MRI: comparison of diffusion-weighted and T2-weighted imaging. *European journal of radiology.* 2007 Feb: **61**:297-302

- [122] Haider MA, van der Kwast TH, Tanguay J, et al. Combined T2-weighted and diffusion-weighted MRI for localisation of prostate cancer. *Ajr*. 2007 Aug; **189**:323-8
- [123] Shimofusa R, Fujimoto H, Akamata H, et al. Diffusion-weighted imaging of prostate cancer. *Journal of computer assisted tomography*. 2005 Mar-Apr; **29**:149-53
- [124] Mazaheri Y, Shukla-Dave A, Hricak H, et al. Prostate cancer: identification with combined diffusion-weighted MR imaging and 3D 1H MR spectroscopic imaging--correlation with pathologic findings. *Radiology*. 2008 Feb; **246**:480-8
- [125] Kozlowski P, Chang SD, Goldenberg SL. Diffusion-weighted MRI in prostate cancer - comparison between single-shot fast spin echo and echo planar imaging sequences. *Magnetic resonance imaging*. 2007 Jun 11:
- [126] Issa B. In vivo measurement of the apparent diffusion coefficient in normal and malignant prostatic tissues using echo-planar imaging. *J Magn Reson Imaging*. 2002 Aug; **16**:196-200
- [127] Outwater EK, Petersen RO, Siegelman ES, Gomella LG, Chernesky CE, Mitchell DG. Prostate carcinoma: assessment of diagnostic criteria for capsular penetration on endorectal coil MR images. *Radiology*. 1994 Nov; **193**:333-9
- [128] Landis JR, Koch GG. The measurement of observer agreement for categorical data. *Biometrics*. 1977 Mar; **33**:159-74
- [129] Augustin H, Fritz GA, Ehammer T, Auprich M, Pummer K. Accuracy of 3-Tesla magnetic resonance imaging for the staging of prostate cancer in comparison to the Partin tables. *Acta Radiol*. 2009 Jun; **50**:562-9
- [130] Rouviere O, Hartman RP, Lyonnet D. Prostate MR imaging at high-field strength: evolution or revolution? *European Radiology*. 2006; **16**:276-84
- [131] Heidenreich A, Aus G, Bolla M, et al. EAU guidelines on prostate cancer. *Eur Urol*. 2008 Jan; **53**:68-80
- [132] Kim B, Breau RH, Papadatos D, et al. Diagnostic accuracy of surface coil magnetic resonance imaging at 1.5 T for local staging of elevated risk prostate cancer. *Can Urol Assoc J*. 2010 Aug; **4**:257-62
- [133] Roethke MC, Lichy MP, Kniess M, et al. Accuracy of preoperative endorectal MRI in predicting extracapsular extension and influence on neurovascular bundle sparing in radical prostatectomy. *World J Urol*. 2012 Jan 17:

- [134] Ruprecht O, Weisser P, Bodelle B, Ackermann H, Vogl TJ. MRI of the prostate: Interobserver agreement compared with histopathologic outcome after radical prostatectomy. *Eur J Radiol.* 2012 Mar: **81**:456-60
- [135] Dickinson L, Ahmed HU, Allen C, et al. Magnetic resonance imaging for the detection, localisation, and characterisation of prostate cancer: recommendations from a European consensus meeting. *European urology.* 2011 Apr: **59**:477-94
- [136] Chenevert TL, McKeever PE, Ross BD. Monitoring early response of experimental brain tumors to therapy using diffusion magnetic resonance imaging. *Clin Cancer Res.* 1997 Sep: **3**:1457-66
- [137] Lee KC, Sud S, Meyer CR, et al. An imaging biomarker of early treatment response in prostate cancer that has metastasized to the bone. *Cancer research.* 2007 Apr 15: **67**:3524-8
- [138] Kuwano H, Miyazaki T, Tsutsumi S, et al. Cell density modulates the metastatic aggressiveness of a mouse colon cancer cell line, colon 26. *Oncology.* 2004: **67**:441-9
- [139] Tworek JA, Appelman HD, Singleton TP, Greenson JK. Stromal tumors of the jejunum and ileum. *Mod Pathol.* 1997 Mar: **10**:200-9
- [140] Sugahara T, Korogi Y, Kochi M, et al. Usefulness of diffusion-weighted MRI with echo-planar technique in the evaluation of cellularity in gliomas. *J Magn Reson Imaging.* 1999 Jan: **9**:53-60
- [141] Hayashida Y, Hirai T, Morishita S, et al. Diffusion-weighted imaging of metastatic brain tumors: comparison with histologic type and tumor cellularity. *Ajnr.* 2006 Aug: **27**:1419-25
- [142] Lyng H, Haraldseth O, Rofstad EK. Measurement of cell density and necrotic fraction in human melanoma xenografts by diffusion weighted magnetic resonance imaging. *Magn Reson Med.* 2000 Jun: **43**:828-36
- [143] Gibbs P, Tozer DJ, Liney GP, Turnbull LW. Comparison of quantitative T2 mapping and diffusion-weighted imaging in the normal and pathologic prostate. *Magn Reson Med.* 2001 Dec: **46**:1054-8
- [144] Sato C, Naganawa S, Nakamura T, et al. Differentiation of noncancerous tissue and cancer lesions by apparent diffusion coefficient values in transition and peripheral zones of the prostate. *J Magn Reson Imaging.* 2005 Mar: **21**:258-62

- [145] Ren J, Huan Y, Wang H, et al. Diffusion-weighted imaging in normal prostate and differential diagnosis of prostate diseases. *Abdominal imaging*. 2008 Jan 25:
- [146] Morgan VA, Kyriazi S, Ashley SE, DeSouza NM. Evaluation of the potential of diffusion-weighted imaging in prostate cancer detection. *Acta Radiol*. 2007 Jul: **48**:695-703
- [147] Gibbs P, Pickles MD, Turnbull LW. Repeatability of echo-planar-based diffusion measurements of the human prostate at 3 T. *Magn Reson Imaging*. 2007 Dec: **25**:1423-9
- [148] Kumar V, Jagannathan NR, Kumar R, et al. Apparent diffusion coefficient of the prostate in men prior to biopsy: determination of a cut-off value to predict malignancy of the peripheral zone. *NMR in biomedicine*. 2007 Aug: **20**:505-11
- [149] Campbell SC. Advances in angiogenesis research: relevance to urological oncology. *The Journal of urology*. 1997: **158**:1663-74
- [150] Brawer MK. Quantitative microvessel density. A staging and prognostic marker for human prostatic carcinoma. *Cancer*. 1996 Jul 15: **78**:345-9
- [151] Weidner N, Carroll PR, Flax J, Blumenfeld W, Folkman J. Tumor angiogenesis correlates with metastasis in invasive prostate carcinoma. *The American journal of pathology*. 1993 Aug: **143**:401-9
- [152] Bettencourt MC, Bauer JJ, Sesterhenn IA, Mostofi FK, McLeod DG, Moul JW. Ki-67 expression is a prognostic marker of prostate cancer recurrence after radical prostatectomy. *The Journal of urology*. 1996 Sep: **156**:1064-8
- [153] Alonzi R, Padhani AR, Allen C. Dynamic contrast enhanced MRI in prostate cancer. *European Journal of Radiology*. 2007: **63**:335-50
- [154] Villers A, Puech P, Leroy X, Biserte J, Fantoni JC, Lemaitre L. Dynamic contrast-enhanced MRI for preoperative identification of localised prostate cancer. *European Urology Supplements*. 2007: **6**:525-32
- [155] Hara N, Okuizumi M, Koike H, Kawaguchi M, Bilim V. Dynamic contrast-enhanced magnetic resonance imaging (DCE-MRI) is a useful modality for the precise detection and staging of early prostate cancer. *Prostate*. 2005: **62**:140-7

- [156] Ocak I, Bernardo M, Metzger G, et al. Dynamic contrast-enhanced MRI of prostate cancer at 3 T: A study of pharmacokinetic parameters. *American Journal of Roentgenology*. 2007: **189**:W192-W201
- [157] Kiessling F, Lichy M, Grobholz R, et al. Detection of prostate carcinomas with T1-weighted dynamic contrast-enhance MRI. Value of two-compartment model. *Radiologe*. 2003: **43**:474-80
- [158] van Dorsten FA, van der Graaf M, Engelbrecht MRW, et al. Combined quantitative dynamic contrast-enhanced MR imaging and H-1 MR spectroscopic imaging of human prostate cancer. *Journal of Magnetic Resonance Imaging*. 2004: **20**:279-87
- [159] Gardner M, J, Altman D G. *Statistics With Confidence*. British Medical Journal. 1989:28-33
- [160] Jager GJ, Ruijter ET, van de Kaa CA, et al. Dynamic TurboFLASH subtraction technique for contrast-enhanced MR imaging of the prostate: correlation with histopathologic results. *Radiology*. 1997 Jun: **203**:645-52
- [161] Kim JK, Hong SS, Choi YJ, et al. Wash-in rate on the basis of dynamic contrast-enhanced MRI: Usefulness for prostate cancer detection and localisation. *Journal of Magnetic Resonance Imaging*. 2005: **22**:639-46
- [162] Rouviere O, Raudrant A, Ecochard R, et al. Characterization of time-enhancement curves of benign and malignant prostate tissue at dynamic MR imaging. *Eur Radiol*. 2003 May: **13**:931-42
- [163] Liney GP, Turnbull LW, Knowles AJ. In vivo magnetic resonance spectroscopy and dynamic contrast enhanced imaging of the prostate gland. *Nmr in Biomedicine*. 1999: **12**:39-44
- [164] Padhani AR, Gapinski CJ, Macvicar DA, et al. Dynamic contrast enhanced MRI of prostate cancer: Correlation with morphology and tumour stage, histological grade and PSA. *Clinical Radiology*. 2000: **55**:99-109
- [165] Kiessling F, Lichy M, Grobholz R, et al. Simple models improve the discrimination of prostate cancers from the peripheral gland by T1-weighted dynamic MRI. *European Radiology*. 2004: **14**:1793-801
- [166] Noworolski SM, Henry RG, Vigneron DB, Kurhanewicz J. Dynamic contrast-enhanced MRI in normal and abnormal prostate tissues as defined by biopsy, MRI, and 3D MRSI. *Magn Reson Med*. 2005 Feb: **53**:249-55
- [167] Turnbull LW, Buckley DL, Turnbull LS, Liney GP, Knowles AJ. Differentiation of prostatic carcinoma and benign prostatic hyperplasia:

Correlation between dynamic Gd-DTPA-enhanced MR imaging and histopathology. *Journal of Magnetic Resonance Imaging*. 1999; **9**:311-6

[168] Padhani AR, MacVicar AD, Gapinski CJ, et al. Effects of androgen deprivation on prostatic morphology and vascular permeability evaluated with mr imaging. *Radiology*. 2001 Feb: **218**:365-74

[169] Ikonen S, Kivisaari L, Vehmas T, et al. Optimal timing of post-biopsy MR imaging of the prostate. *Acta Radiol*. 2001 Jan: **42**:70-3

[170] White S, Hricak H, Forstner R, et al. Prostate cancer: effect of postbiopsy hemorrhage on interpretation of MR images. *Radiology*. 1995 May: **195**:385-90

[171] Brawer MK, Deering RE, Brown M, Preston SD, Bigler SA. Predictors of pathologic stage in prostatic carcinoma. The role of neovascularity. *Cancer*. 1994 Feb 1: **73**:678-87

[172] Djavan B, Ravery V, Zlotta A, et al. Prospective evaluation of prostate cancer detected on biopsies 1, 2, 3 and 4: when should we stop? *The Journal of urology*. 2001 Nov: **166**:1679-83

[173] Roehrborn CG, Pickens GJ, Sanders JS. Diagnostic yield of repeated transrectal ultrasound-guided biopsies stratified by specific histopathologic diagnoses and prostate specific antigen levels. *Urology*. 1996 Mar: **47**:347-52

[174] Perachino M, di Ciolo L, Barbetti V, et al. Results of rebiopsy for suspected prostate cancer in symptomatic men with elevated PSA levels. *European urology*. 1997: **32**:155-9

[175] Stewart CS, Leibovich BC, Weaver AL, Lieber MM. Prostate cancer diagnosis using a saturation needle biopsy technique after previous negative sextant biopsies. *The Journal of urology*. 2001 Jul: **166**:86-91; discussion -2

[176] Pal RP, Elmussareh M, Chanawani M, Khan MA. The role of a standardized 36 core template-assisted transperineal prostate biopsy technique in patients with previously negative transrectal ultrasonography-guided prostate biopsies. *BJU Int*. 2012 Feb: **109**:367-71

[177] Amsellem-Ouazana D, Younes P, Conquy S, et al. Negative prostatic biopsies in patients with a high risk of prostate cancer. Is the combination of endorectal MRI and magnetic resonance spectroscopy imaging (MRSI) a useful tool? A preliminary study. *European urology*. 2005 May: **47**:582-6

[178] Beyersdorff D, Taupitz M, Winkelmann B, et al. Patients with a history of elevated prostate-specific antigen levels and negative transrectal US-

guided quadrant or sextant biopsy results: value of MR imaging. *Radiology*. 2002 Sep: **224**:701-6

[179] Perrotti M, Han KR, Epstein RE, et al. Prospective evaluation of endorectal magnetic resonance imaging to detect tumor foci in men with prior negative prostatic biopsy: a pilot study. *The Journal of urology*. 1999 Oct: **162**:1314-7

[180] Yuen JS, Thng CH, Tan PH, et al. Endorectal magnetic resonance imaging and spectroscopy for the detection of tumor foci in men with prior negative transrectal ultrasound prostate biopsy. *The Journal of urology*. 2004 Apr: **171**:1482-6

[181] Bhatia C, Phongkitkarun S, Booranapitaksonti D, Kochakarn W, Chaleumsanyakorn P. Diagnostic accuracy of MRI/MRSI for patients with persistently high PSA levels and negative TRUS-guided biopsy results. *Journal of the Medical Association of Thailand = Chotmaihet thangphaet*. 2007 Jul: **90**:1391-9

[182] Lopez JI. Prostate adenocarcinoma detected after high-grade prostatic intraepithelial neoplasia or atypical small acinar proliferation. *BJU international*. 2007 Dec: **100**:1272-6

[183] Melchior SW, Brawer MK. Role of transrectal ultrasound and prostate biopsy. *J Clin Ultrasound*. 1996 Oct: **24**:463-71

[184] Prando A, Kurhanewicz J, Borges AP, Oliveira EM, Jr., Figueiredo E. Prostatic biopsy directed with endorectal MR spectroscopic imaging findings in patients with elevated prostate specific antigen levels and prior negative biopsy findings: early experience. *Radiology*. 2005 Sep: **236**:903-10

[185] Kim CK, Park BK, Kim B. Localisation of prostate cancer using 3T MRI - Comparison of T2-weighted and dynamic contrast-enhanced imaging. *Journal of Computer Assisted Tomography*. 2006: **30**:7-11

[186] Bates TS, Gillatt DA, Cavanagh PM, Speakman M. A comparison of endorectal magnetic resonance imaging and transrectal ultrasonography in the local staging of prostate cancer with histopathological correlation. *Br J Urol*. 1997 Jun: **79**:927-32

[187] Chelsky MJ, Schnall MD, Seidmon EJ, Pollack HM. Use of endorectal surface coil magnetic resonance imaging for local staging of prostate cancer. *J Urol*. 1993 Aug: **150**:391-5

[188] Belin X, Cornud F, Fromont G, et al. MRI of cancers of the prostate with T1-weighted sequences using fat-suppression and gadolinium injections. *Journal de Radiologie*. 1994: **75**:159-67

- [189] Harris RD, Schned AR, Heaney JA. Staging of prostate cancer with endorectal MR imaging: lessons from a learning curve. *Radiographics*. 1995 Jul; **15**:813-29; discussion 29-32
- [190] Jager GJ, Ruijter ET, van de Kaa CA, et al. Local staging of prostate cancer with endorectal MR imaging: correlation with histopathology. *AJR Am J Roentgenol*. 1996 Apr; **166**:845-52
- [191] Perrotti M, Kaufman RP, Jr., Jennings TA, et al. Endo-rectal coil magnetic resonance imaging in clinically localised prostate cancer: is it accurate? *J Urol*. 1996 Jul; **156**:106-9
- [192] Presti JC, Jr., Hricak H, Narayan PA, Shinohara K, White S, Carroll PR. Local staging of prostatic carcinoma: comparison of transrectal sonography and endorectal MR imaging. *AJR Am J Roentgenol*. 1996 Jan; **166**:103-8
- [193] Quinn SF, Franzini DA, Demlow TA, et al. MR imaging of prostate cancer with an endorectal surface coil technique: correlation with whole-mount specimens. *Radiology*. 1994 Feb; **190**:323-7
- [194] Yu KK, Hricak H, Alagappan R, Chernoff DM, Bacchetti P, Zaloudek CJ. Detection of extracapsular extension of prostate carcinoma with endorectal and phased-array coil MR imaging: multivariate feature analysis. *Radiology*. 1997 Mar; **202**:697-702
- [195] Yu KK, Scheidler J, Hricak H, et al. Prostate cancer: prediction of extracapsular extension with endorectal MR imaging and three-dimensional proton MR spectroscopic imaging. *Radiology*. 1999 Nov; **213**:481-8
- [196] Kurhanewicz J, vigneron d, Carroll P, Coakley F. Multiparametric magnetic resonance imaging in prostate cancer: present and future. *Current Opinion in Urology*. 2008; **18**:71-7
- [197] Sosna J, Pedrosa I, Dewolf WC, Mahallati H, Lenkinski RE, Rofsky NM. MR imaging of the prostate at 3 Tesla: comparison of an external phased-array coil to imaging with an endorectal coil at 1.5 Tesla. *Acad Radiol*. 2004 Aug; **11**:857-62
- [198] Futterer JJ, Scheenen TWJ, Huisman HJ, et al. Initial experience of 3 tesla endorectal coil magnetic resonance imaging and H-1-spectroscopic imaging of the prostate. *Investigative Radiology*. 2004; **39**:671-80
- [199] Futerer JJ, Heijmink SWTP, Scheenen TWJ, et al. Prostate cancer localisation with dynamic contrast-enhanced MR imaging and proton MR spectroscopic imaging. *Radiology*. 2006; **241**:449-58

- [200] Erbersdobler A, Augustin H, Schlomm T, Henke RP. Prostate cancers in the transition zone: Part 1; pathological aspects. *BJU Int.* 2004 Dec: **94**:1221-5
- [201] Liney GP, Turnbull LW, Knowles AJ. A simple method for the correction of endorectal surface coil inhomogeneity in prostate imaging. *J Magn Reson Imaging.* 1998 Jul-Aug: **8**:994-7
- [202] Vargas HA, Akin O, Franiel T, et al. Diffusion-weighted endorectal MR imaging at 3 T for prostate cancer: tumor detection and assessment of aggressiveness. *Radiology.* 2011 Jun: **259**:775-84
- [203] Verma S, Rajesh A, Morales H, et al. Assessment of aggressiveness of prostate cancer: correlation of apparent diffusion coefficient with histologic grade after radical prostatectomy. *AJR Am J Roentgenol.* 2011 Feb: **196**:374-81
- [204] Itou Y, Nakanishi K, Narumi Y, Nishizawa Y, Tsukuma H. Clinical utility of apparent diffusion coefficient (ADC) values in patients with prostate cancer: can ADC values contribute to assess the aggressiveness of prostate cancer? *J Magn Reson Imaging.* 2011 Jan: **33**:167-72
- [205] Kurhanewicz J, Vigneron DB, Hricak H, Narayan P, Carroll P, Nelson SJ. Three-dimensional H-1 MR spectroscopic imaging of the in situ human prostate with high (0.24-0.7-cm³) spatial resolution. *Radiology.* 1996 Mar: **198**:795-805
- [206] Kobus T, Hambrock T, Hulsbergen-van de Kaa CA, et al. In vivo assessment of prostate cancer aggressiveness using magnetic resonance spectroscopic imaging at 3 T with an endorectal coil. *Eur Urol.* 2011 Nov: **60**:1074-80
- [207] Padhani AR, Gapinski CJ, Macvicar DA, et al. Dynamic contrast enhanced MRI of prostate cancer: correlation with morphology and tumour stage, histological grade and PSA. *Clin Radiol.* 2000 Feb: **55**:99-109
- [208] Turnbull LW, Buckley DL, Turnbull LS, Liney GP, Knowles AJ. Differentiation of prostatic carcinoma and benign prostatic hyperplasia: correlation between dynamic Gd-DTPA-enhanced MR imaging and histopathology. *J Magn Reson Imaging.* 1999 Feb: **9**:311-6
- [209] Yao WW, Zhang H, Ding B, et al. Rectal cancer: 3D dynamic contrast-enhanced MRI; correlation with microvascular density and clinicopathological features. *Radiol Med.* 2011 Apr: **116**:366-74

- [210] Wang L, Hricak H, Kattan MW, et al. Prediction of seminal vesicle invasion in prostate cancer: incremental value of adding endorectal MR imaging to the Kattan nomogram. *Radiology*. 2007 Jan: **242**:182-8
- [211] Poulakis V, Witzsch U, de Vries R, et al. Preoperative neural network using combined magnetic resonance imaging variables, prostate-specific antigen, and gleason score for predicting prostate cancer biochemical recurrence after radical prostatectomy. *Urology*. 2004 Dec: **64**:1165-70
- [212] Shukla-Dave A, Hricak H, Akin O, et al. Preoperative nomograms incorporating magnetic resonance imaging and spectroscopy for prediction of insignificant prostate cancer. *BJU Int*. 2011 Sep 20:
- [213] Ouzzane A, Puech P, Villers A. MRI and surveillance. *Curr Opin Urol*. 2012 May: **22**:231-6
- [214] Beyersdorff D, Winkel A, Hamm B, Lenk S, Loening SA, Taupitz M. MR imaging-guided prostate biopsy with a closed MR unit at 1.5 T: initial results. *Radiology*. 2005 Feb: **234**:576-81
- [215] Hambrock T, Futterer JJ, Huisman HJ, et al. Thirty-two-channel coil 3T magnetic resonance-guided biopsies of prostate tumor suspicious regions identified on multimodality 3T magnetic resonance imaging: technique and feasibility. *Invest Radiol*. 2008 Oct: **43**:686-94
- [216] Hambrock T, Somford DM, Hoeks C, et al. Magnetic resonance imaging guided prostate biopsy in men with repeat negative biopsies and increased prostate specific antigen. *J Urol*. 2010 Feb: **183**:520-7
- [217] Krieger A, Iordachita, II, Guion P, et al. An MRI-compatible robotic system with hybrid tracking for MRI-guided prostate intervention. *IEEE Trans Biomed Eng*. 2011 Nov: **58**:3049-60
- [218] Futterer JJ, Verma S, Hambrock T, Yakar D, Barentsz JO. High-risk prostate cancer: value of multi-modality 3T MRI-guided biopsies after previous negative biopsies. *Abdom Imaging*. 2011 Oct 29:
- [219] Schouten MG, Bomers JG, Yakar D, et al. Evaluation of a robotic technique for transrectal MRI-guided prostate biopsies. *Eur Radiol*. 2012 Feb: **22**:476-83